Solution- Processed Hybrid Hosts: A Way to Explore High Triplet Energy with Admirable Current and Power Efficiency Devoiding Outcoupling Mode for Phosphorescent OLED

Diksha Thakur,‖ Deepak Kumar Dubey,‖ Rohit Ashok Kumar Yadav, Mangili Venkateswarulu, Subrata Banik, Jwo-Huei Jou*, Subrata Ghosh*

Diksha Thakur, Mangili Venkateswarulu, Dr Subrata Ghosh

School of Basic Sciences, IIT Mandi, Himachal Pradesh, India, 175005

Email: subrata@iitmandi.ac.in

Subrata Banik

Department of Chemistry and Chemical Sciences

Central University of Jammu, Jammu 181143, J&K, India

Deepak Kumar Dubey, Rohit Ashok Kumar Yadav, Prof. Jwo-Huei Jou

Department of Materials Science and Engineering,

National Tsing Hua University

No. 101, Sec. 2, Guangfu Road, Hsinchu 30013, Taiwan, R.O.C.

E-mail: jjou@mx.nthu.edu.tw

‖ *Both authors have equal contribution*

General: ^{1}H and ^{13}C NMR spectra were recorded on Jeol ECX NMR spectrometer.HRMS-ESI spectra were recorded on Bruker Maxis Impact HD instrument.Theoretical mass values were calculated from compass isotope pattern software. UV–vis and fluorescence spectra were recorded on Simadzu UV-2450 and perkin Elmer LS55 respectively. All the spectral studies were performed at 5 micromolar concentration. Solvents and chemicals were purchased from commercial resources and used without further purification. Spectroscopic grade solvents were used for photophysical studies. Thermogravimetric analysis (TGA) and DSC was recorded on a Perkin Elmer Pyris 1 and NETZSCH STA449 F1 JUPITER instrument under nitrogen atmosphere at a heating rate of 10 °C/min. The temperature of

degradation (Td) was correlated to a 5% weight loss. Cyclic voltammetry (CV) was carried out in nitrogen-purged dichloromethane (oxidation scan) and dmf at room temperature on Metrohm Autolab electrochemical workstation. Tetrabutylammonium hexafluorophosphate (TBAPF6) (0.1 M) was used as the supporting electrolyte. The conventional three-electrode configuration consists of a platinum disc working electrode, a platinum wire auxiliary electrode, and Ag/AgCl as reference electrode with ferrocenium–ferrocene (Fc+/Fc) as the external standard. Cyclic voltammograms were obtained at scan rate of 100 mV s-1 in dichloromethane solutions. Diffraction studies were performed on Agilent Technologies X-ray diffractometer.Phosphorescence spectra were recorded on an F-7000 fluorescence spectrophotometer.

Computational Details: The ground state (S_0) geometries were optimized at B3LYP/6-311G(d,p) level. The little difference between optimized geometries and experimental outcomes may be due to the fact that theoretical studies were calculated in gaseous state and experimental studies were done in different solvents. The absorption transition were calculated using TD-DFT level of theory on same level.

Detailed synthetic procedures and Characterization

4-(diphenylamino)benzaldehyde (DT301): DT301 was prepared according to reported procedure.[1]

General Procedure for the synthesis of DT309, DT313, DT316, DT320, DT321.

A mixture of4-(diphenylamino)benzaldehyde(1 mmol),Benzil (1 mmol), corresponding amine (5 mmol) and ammonium acetate (4 mmol) was refluxed in acetic acid (15 mL) under nitrogen atmosphere. After 14h, reaction mixture was quenched with addition of water and extracted in ethyl acetate. The organic layer was then washed with water (2×25 ml) and dried over sodium sulphate. The organic layer was dried over rota evaporator and solid was washed with hexane 3-4 times followed by washing with methanol.

DT309: ^{1}HNMR (500MHz, $CDCl_3$, δ): 7.59-7.58 (m, 2H), 7.30 (d, 2H, J = 8.95 Hz), 7.25-7.21 (m, 9H), 7.18-7.16 (m, 1H), 7.14-7.12(m, 2H), 7.07 (d, 4H, J = 7.55 Hz), 7.03-6.98 (m, 4H), 6.91 (d, 2H, J = 8.95 Hz), 6.77-6.75 (m, 2H), 3.76 (s, 3H) ^{13}C- NMR (125 MHz, $CDCl_3$, δ): 159.03, 147.65, 147.31, 146.90, 137.86, 134.55, 131.11, 130.82, 129.99, 129.50, 129.46, 129.23, 128.28, 128.08, 127.76, 127.31, 126.43, 124.80, 124.07, 123.19, 122.17, 114.13, 55.31.HRMS (ESI): Calculated for $C_{40}H_{31}N_3O$ [M+H$^+$]: 570.2539; Found: 570.2537

DT313: ^{1}HNMR (500MHz, $CDCl_3$, δ): 7.59-7.58 (m, 2H), 7.31-7.29(m, 2H), 7.26-7.21(m, 10H), 7.14-7.12(m, 2H), 7.07(d, 4H, J = 7.55 Hz), 7.03-7.00 (m, 2H), 6.98-6.96 (m, 2H), 6.92-6.91 (m, 2H), 6.76-6.74 (m, 2H), 3.89 (t, 2H, J = 6.85 Hz), 1.74 (q, 2H, J = 7.55 Hz), 1.47 (q, 2H, J = 7.55 Hz), 0.96 (t, 3H, J = 7.55 Hz) ^{13}C- NMR (125 MHz, $CDCl_3$, δ): 158.68, 147.62, 147.33, 146.89, 137.85, 134.58, 131.12, 130.83, 129.75, 129.50, 129.40, 129.23, 128.27, 128.09, 127.74, 127.31, 126.42, 124.79, 124.13, 123.17, 122.21, 114.61, 67.81, 31.21, 19.20, 13.88.HRMS (ESI): Calculated for $C_{43}H_{37}N_3O$ [M+H$^+$]: 612.3009; Found: 612.3006

DT316: ^{1}HNMR (500MHz,DMSO, δ): 9.76 (s, 1H), 7.47-7.45 (m, 2H), 7.32-7.28 (m, 9H), 7.23-7.20 (m, 4H), 7.16-7.14 (m, 1H), 7.09-7.01 (m, 8H), 6.81-6.80 (m, 2H), 6.67-6.65 (m, 2H) ^{13}C- NMR (125 MHz, $CDCl_3$, δ): 157.31, 147.07, 146.65, 145.83, 136.37, 134.60, 131.32, 131.11, 130.68, 129.83, 129.67, 128.98, 128.39, 128.21, 128.11, 127.91, 126.28, 124.64, 123.96, 123.68, 121.21, 115.61. HRMS (ESI): Calculated for $C_{39}H_{29}N_3O$ [M+H$^+$]: 556.2383; Found: 556.2384

DT320:^{1}HNMR (500MHz, $CDCl_3$, δ): 7.59 (d, 2H, J = 6.85 Hz), 7.31 (d, 2H, J = 8.25 Hz), 7.26-7.16(m, 11H), 7.13-7.11(m, 2H), 7.08 (d, 4H, J = 7.60 Hz), 7.04- 7.01 (m, 2H), 6.99-6.96 (m, 2H), 6.91 (d, 2H, J = 8.25 Hz), 6.77- 6.74 (m, 2H), 3.97 (q, 2H, J = 6.9 Hz), 1.39 (t, 3H, J = 7.55 Hz) ^{13}C- NMR (125 MHz, $CDCl_3$, δ): 158.52, 147.74, 147.27, 146.84, 131.11, 130.79, 129.55, 129.43, 129.25, 128.28, 128.10, 127.80, 127.36, 126.50, 124.84, 123.23,

122.08, 114.60, 63.56, 14.70.HRMS (ESI): Calculated for $C_{41}H_{33}N_3O$ [M+H$^+$]: 584.2696; Found: 584.2696

DT321: ^{1}HNMR (500MHz ,$CDCl_3$, δ): 7.59 (d, 2H, J = 7.55 Hz), 7.31 (d, 2H, J = 8.25 Hz), 7.25-7.17 (m, 10H), 7.13-7.12 (m, 2H), 7.07 (d, 4H, J = 7.55 Hz), 7.03- 7.00 (m, 2H), 6.98-6.96 (m, 2H), 6.91 (d, 2H, J = 8.95 Hz), 6.75 (d, 2H, J = 8.90 Hz), 3.85 (t, 2H, J = 6.85 Hz), 1.78 (q, 2H, J = 6.90 Hz), 1.02 (t, 3H, J = 7.55 Hz) ^{13}C- NMR (125 MHz, $CDCl_3$, δ): 158.68, 147.66, 147.31, 146.88, 137.79, 134.51, 131.12, 130.81, 129.73, 129.52, 129.40, 129.23, 128.27, 128.08, 127.76, 127.33, 126.44, 124.81, 124.02, 123.19, 122.16, 114.62, 69.56, 22.49, 10.48.. HRMS (ESI): Calculated for $C_{42}H_{35}N_3O$ [M+H$^+$]: 598.2852; Found: 598.2852

Synthesis Scheme

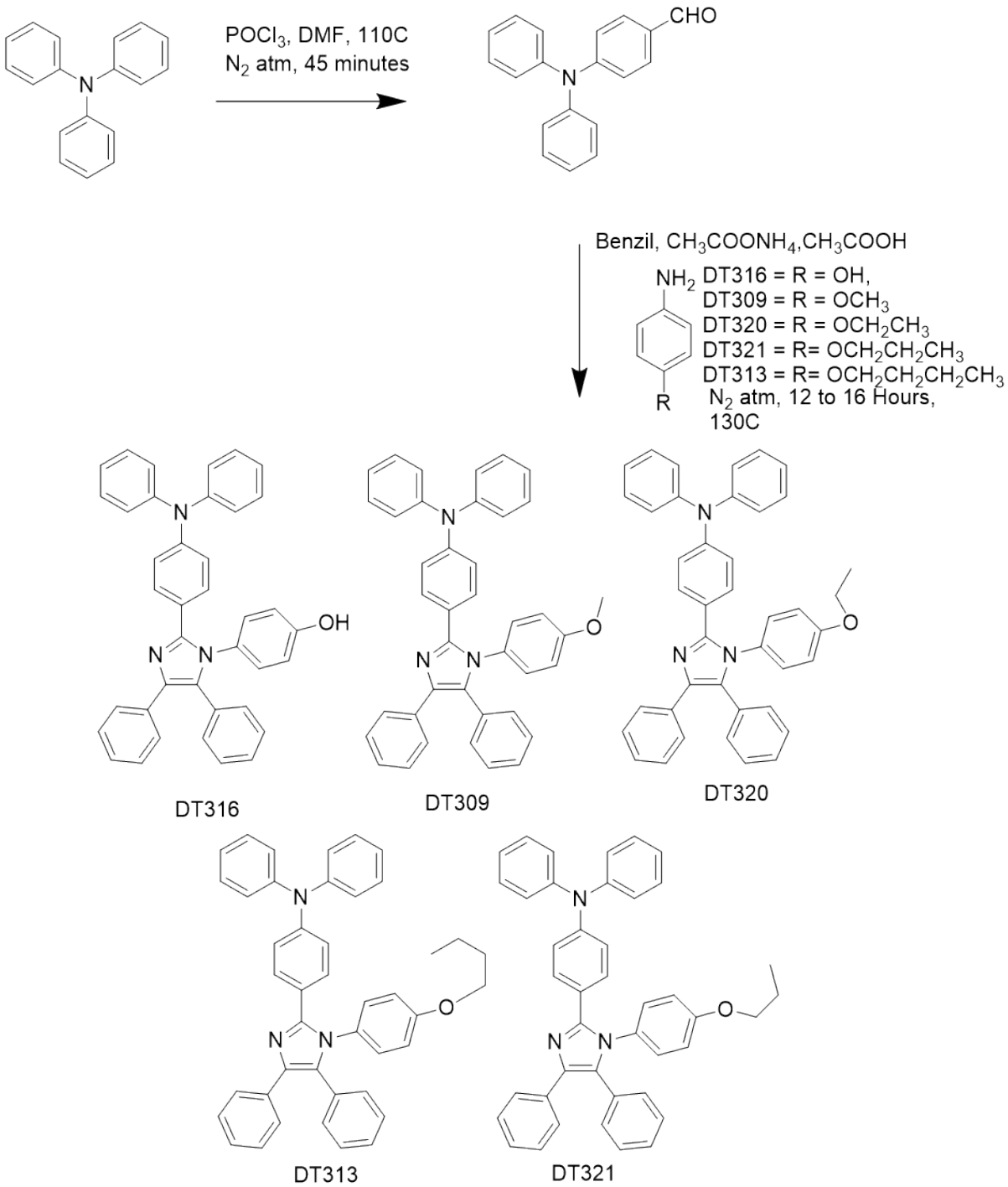

Figure S1. Synthesis scheme for **DT316, DT309, DT320, DT321,** and **DT313.**

OLED Device Fabrication and Performance Measurements

All the solution processed OLED devices were fabricated on a glass substrate with a patterned ITO, which is 125 nm thick. After cleaning with detergents solution, the ITO glasses were cleaned for 30 min sequentially in acetone and isopropanol by ultrasonic bath at a temperatute of 50°C and 60°C, respectively. The hole injection layer (HIL) of PEDOT:PSS was spin-coated on preclened and UV-O_3 treated (20 min) ITO substrate at a speed of 4000 rpm for 20s and annealed at 120 °C for 15 min. On top of the HIL layer, a emissive layer of either host:Ir(ppy)$_3$ (S_1= 2.84 eV, T_1= 2.42 eV)[2,3] or host:Ir(2-phq)$_3$ (S_1= 2.30 eV, T_1= 2.10 eV),[2,4] which was prepared in tetrahydrofuran (THF) solvent with a concentration of 5 mg/mL, was spin-coated at a speed of 2500 rpm for 20s and annealed for at 100°C for 15 min. After the spin-coating process, an eletron transporting layer of TPBi (35 nm, 1.4-1.8 Å/s), an electron injection layer of lithium fluoride (1 nm, 0.1-0.2 Å/s) and a cathode of aluminum (120 nm, 12-16 Å/s) were sequentially deposited under high vacuum (~10^{-6} Pa).

For device measurements, the luminance, CIE chromatic coordinates and the EL spectrum of the resultant OLEDs were measured by using a programmable source meter (Keithley 2400), luminance meter (Minolta CS-100), and a spectrophotometer (Spectrascan PR655, Photo Research). The emission area of the devices was 9 mm^2, and only the luminance in the forward direction was measured.

Single Carrier Device Fabrication and Measurements:

Single carrier devices, namely, hole only device (HOD) and electron only device (EOD), were fabracted by following the aforementioned approach as for OLED device fabrication. In HOD and EOD, hole and electron transporting materials TAPC and TPBi were spin coated on HIL (PEDOT:PSS) and precleaned glass substract, respectively, followed by a 20 nm layer of synthesised host materials either **DT-316, DT-309, DT-320, DT-321** or **DT-313** was spin-coated over on it. All these layers spin coated at a speed of 2500 rpm for 20 s and baked

at 100°C for 15 min to remove the residual solvent. Before the spin coating, the solution were prepared by dissolving all the materials TAPC, TPBi and hosts in the THF solvent with a concentration of 10 mg/mL. After the spin-coating process, a 35 nm layer of hole and eletron transporting materials, TAPC and TPBi, were deposited under high vaccum with a rate of 1.4-1.8 Å/s, respectively, for HOD and EOD; followed by a 1 nm layer of electron injecting material lithium fluoride and a 120 nm layer aluminium as a cathode were deposited sequentially under same condition with a rate of 0.1-0.2 Å/s and 12-16 Å/s, respevtively.

The I-V characteristics of all the fabricated devices were performed by using a programmable source meter Keithley 2400.

Photophysical Data

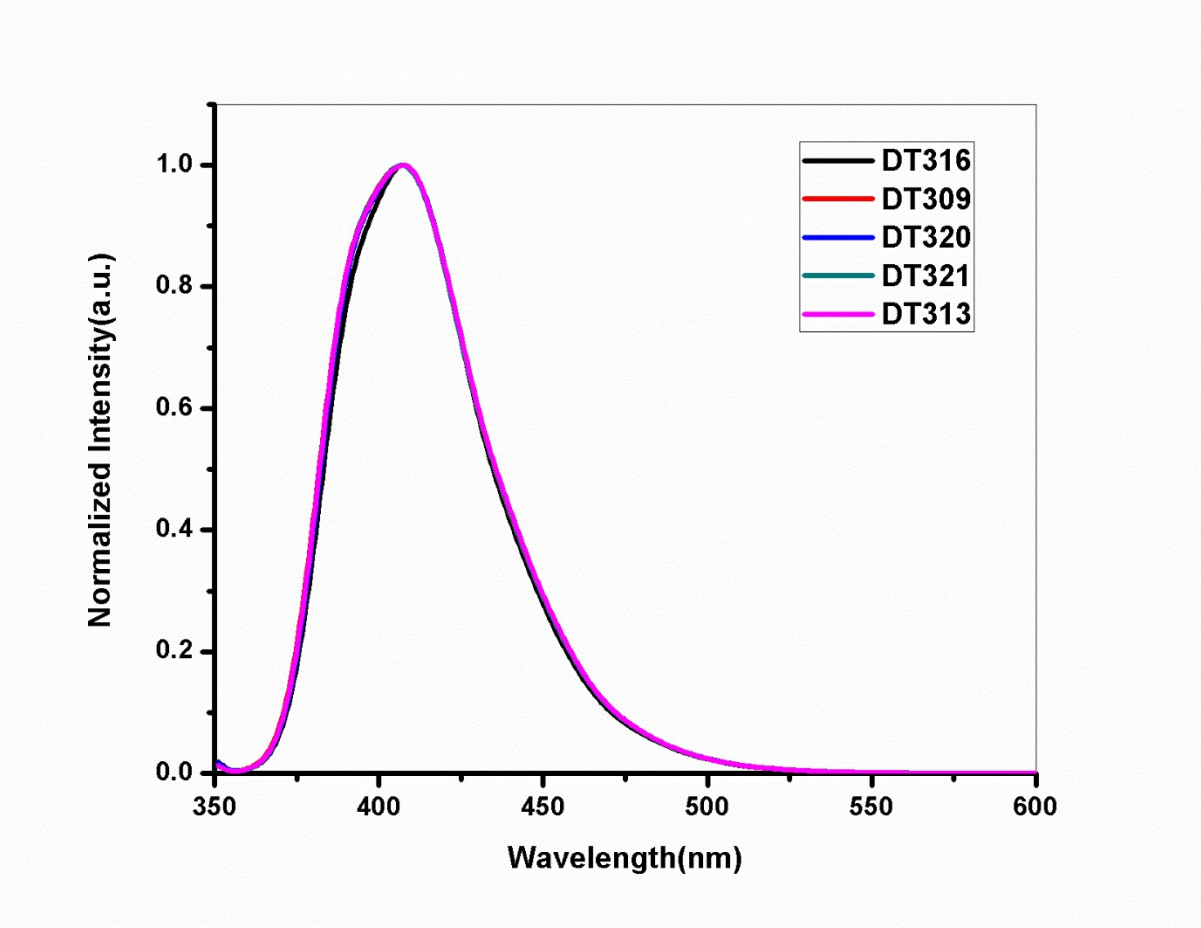

Figure S2. Photoluminiscence emission spectra for **DT316, DT309. DT320, DT321,** and **DT313.**

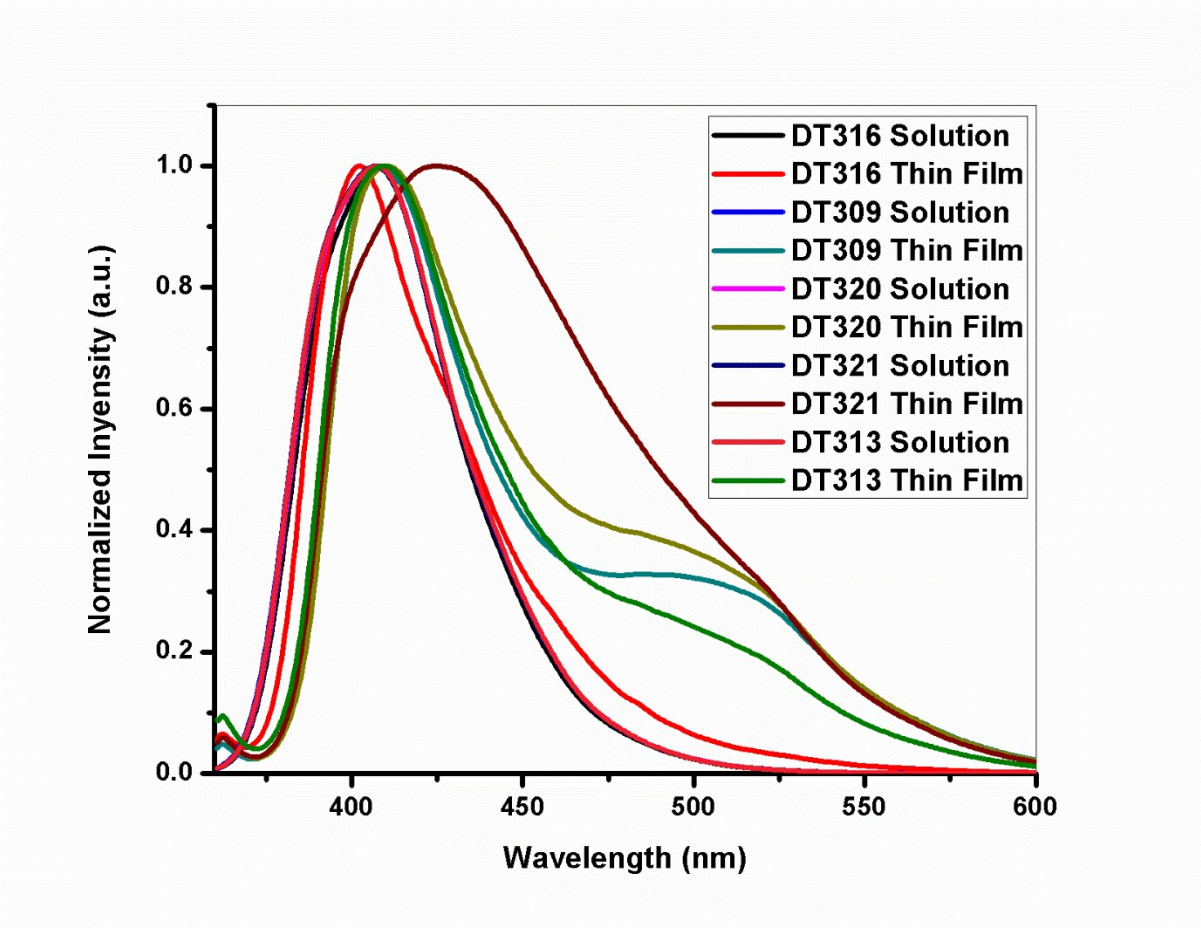

Figure S3. Comparision of photoluminiscence emission spectra for **DT316, DT309, DT320, DT321** and **DT313** in solution and thin film.

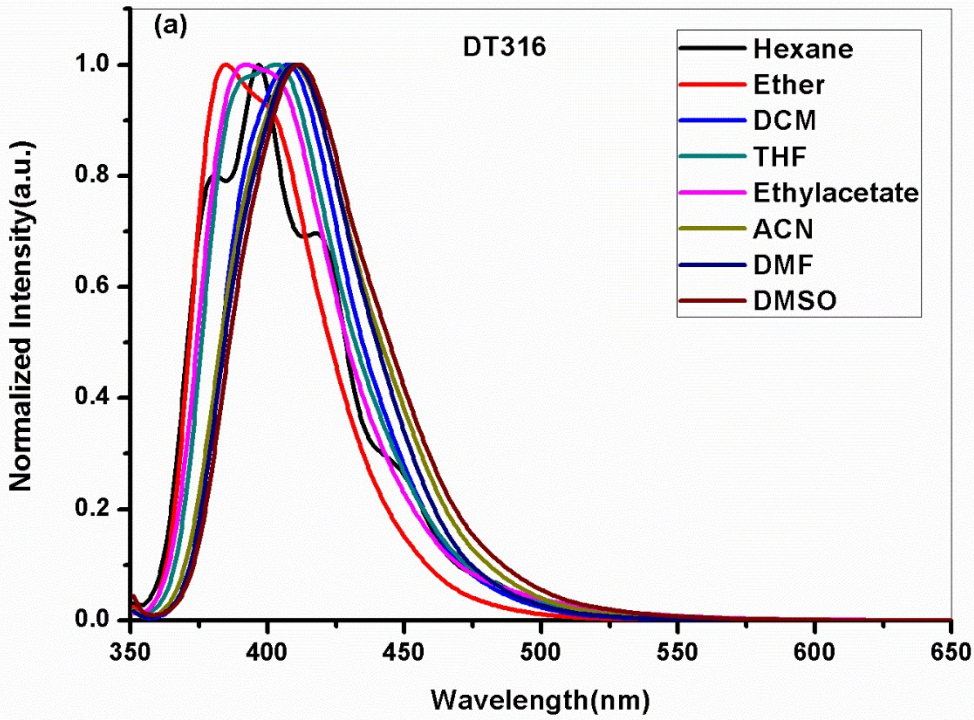
(a)
DT316
Hexane
Ether
DCM
THF
Ethylacetate
ACN
DMF
DMSO
Normalized Intensity(a.u.)
1.0
0.8
0.6
0.4
0.2
0.0
350
400
450
500
550
600
650
Wavelength(nm)

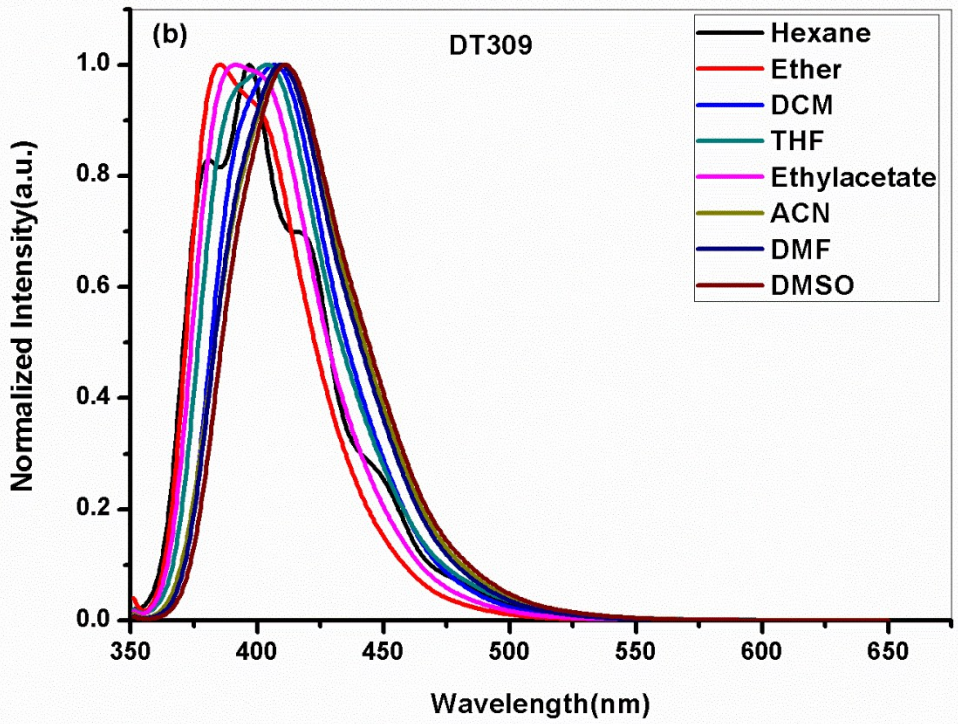
(b)
DT309
Hexane
Ether
DCM
THF
Ethylacetate
ACN
DMF
DMSO
Normalized Intensity(a.u.)
Wavelength(nm)
0.0
0.2
0.4
0.6
0.8
1.0
350
400
450
500
550
600
650

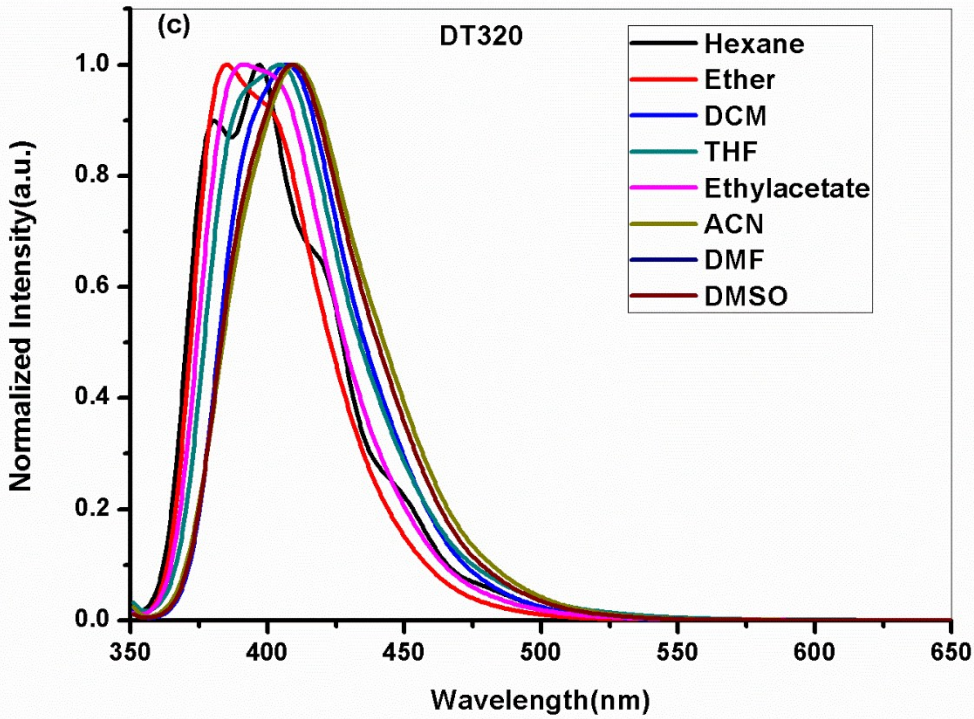
(c)
DT320
Hexane
Ether
DCM
THF
Ethylacetate
ACN
DMF
DMSO
Normalized Intensity(a.u.)
Wavelength(nm)
0.0
0.2
0.4
0.6
0.8
1.0
350
400
450
500
550
600
650

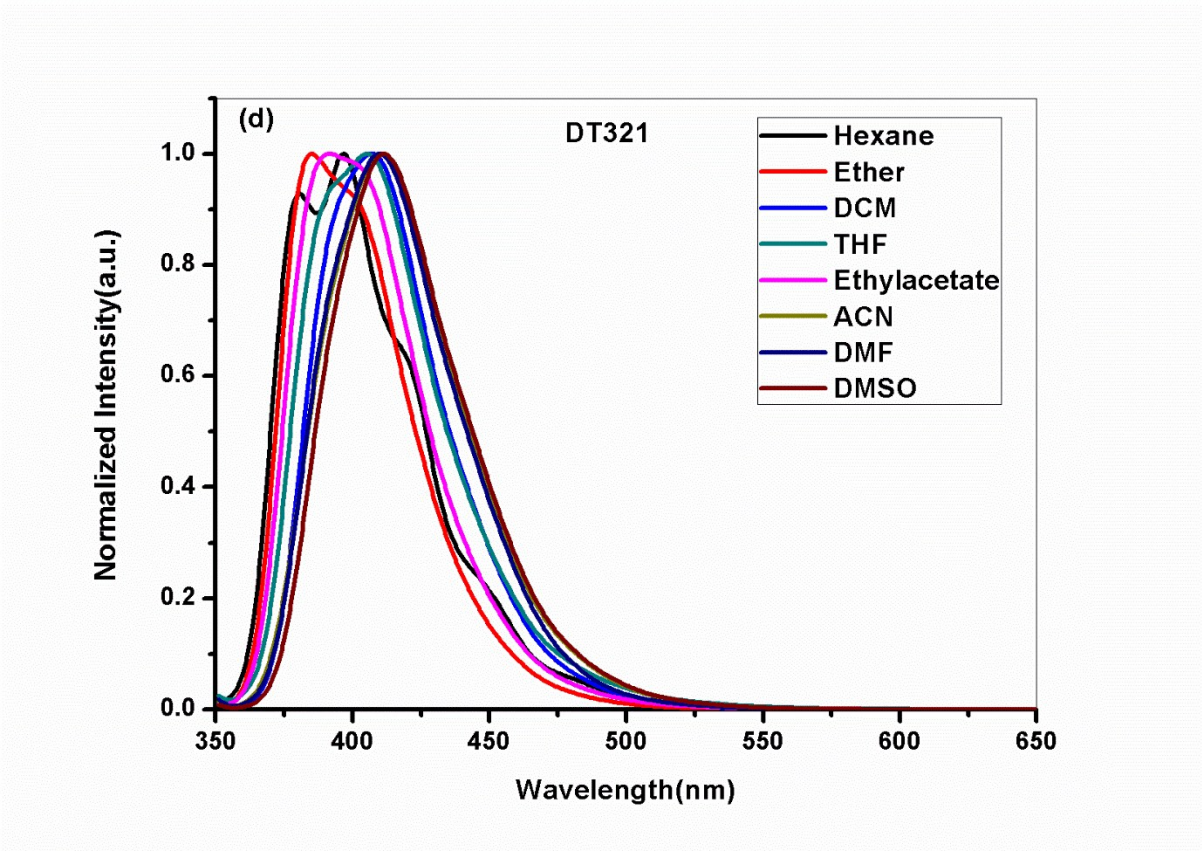

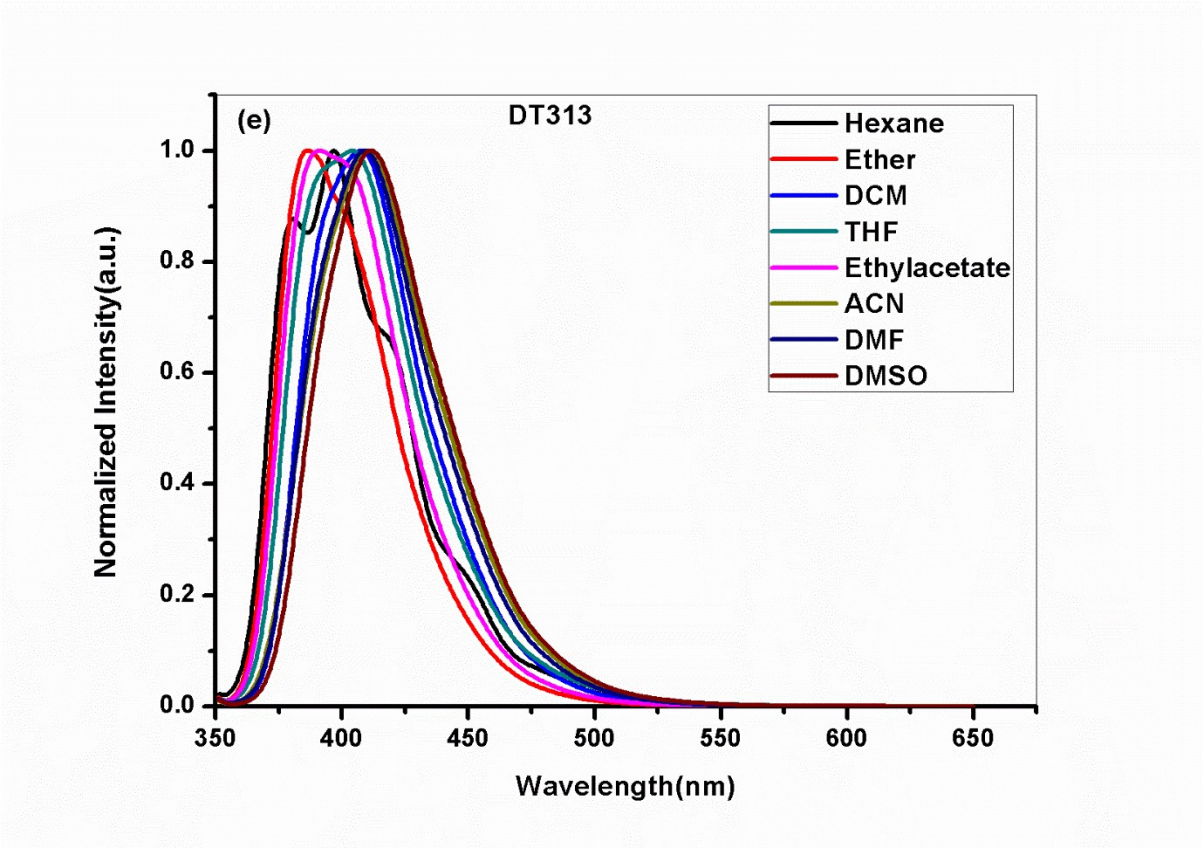

Figure S4. Solvatochromic emission behavior of compound **(a) DT316, (b) DT309, (c) DT320, (d) DT321,** and **(e) DT313** in different solvents.

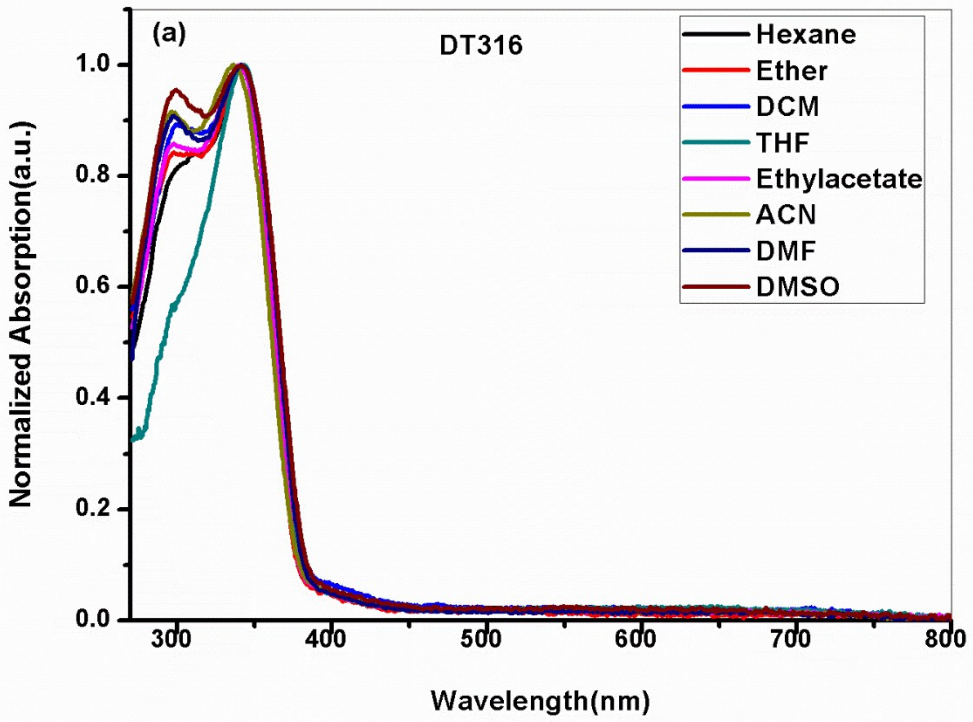
(a)
DT316
Hexane
Ether
DCM
THF
Ethylacetate
ACN
DMF
DMSO
Normalized Absorption(a.u.)
Wavelength(nm)
0.0
0.2
0.4
0.6
0.8
1.0
300
400
500
600
700
800

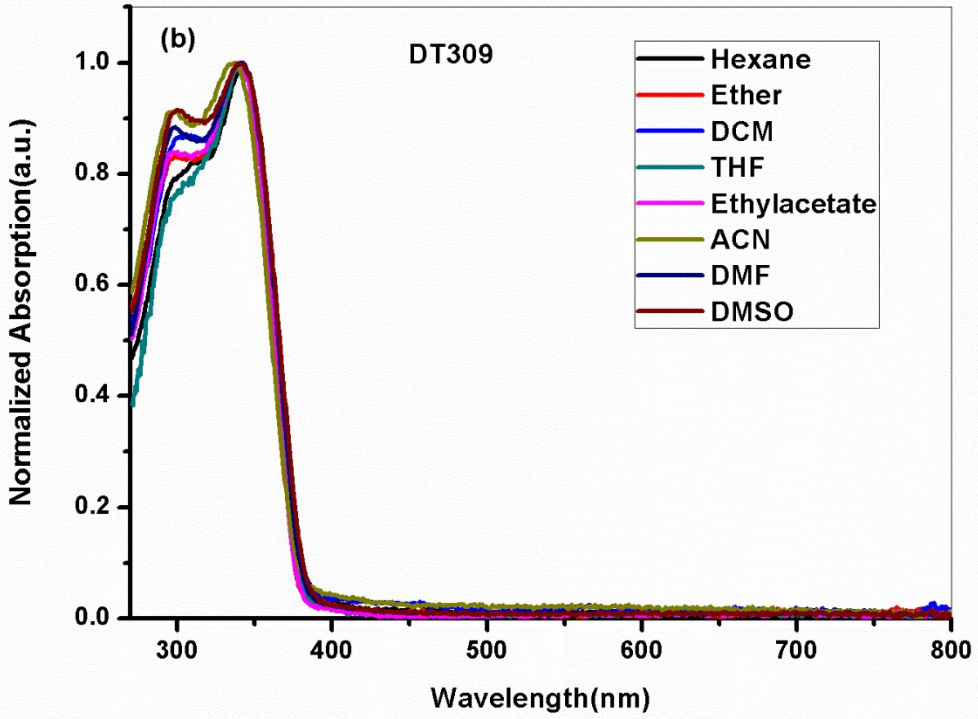
(b)
DT309
Hexane
Ether
DCM
THF
Ethylacetate
ACN
DMF
DMSO
Normalized Absorption(a.u.)
Wavelength(nm)
0.0
0.2
0.4
0.6
0.8
1.0
300
400
500
600
700
800

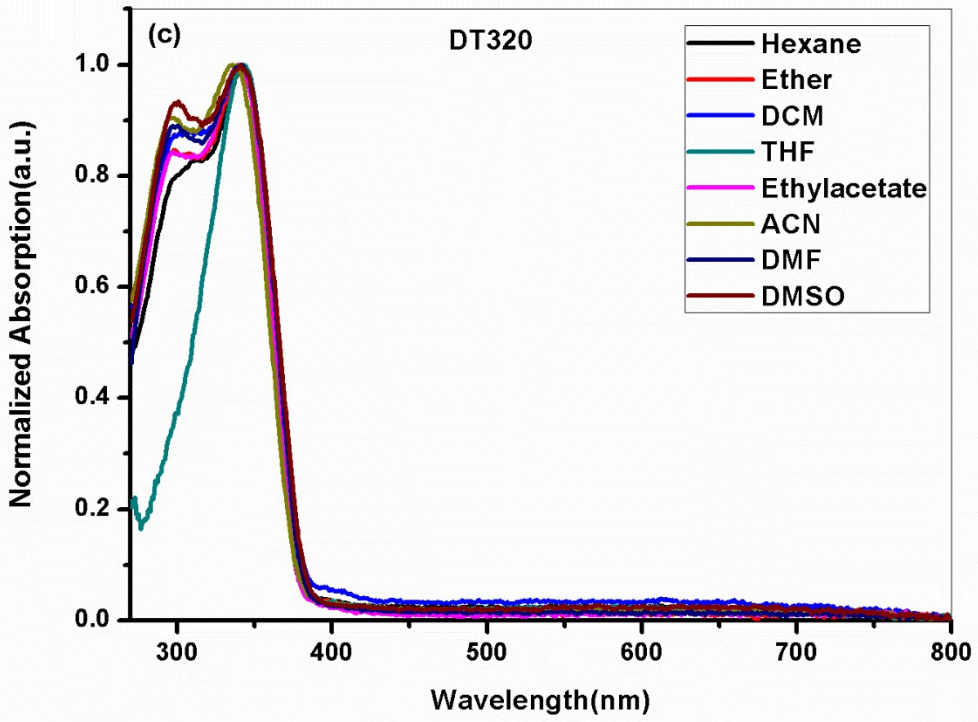
(c)
DT320
Hexane
Ether
DCM
THF
Ethylacetate
ACN
DMF
DMSO
Normalized Absorption(a.u.)
Wavelength(nm)
0.0
0.2
0.4
0.6
0.8
1.0
300
400
500
600
700
800

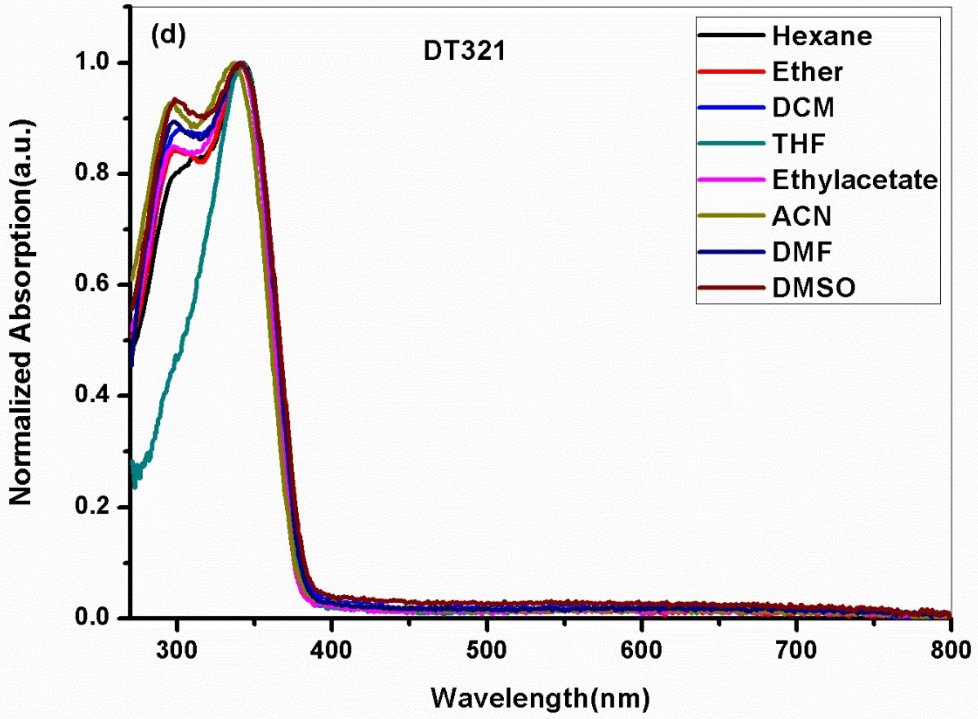
(d)
DT321
Hexane
Ether
DCM
THF
Ethylacetate
ACN
DMF
DMSO
Normalized Absorption(a.u.)
Wavelength(nm)
0.0
0.2
0.4
0.6
0.8
1.0
300
400
500
600
700
800

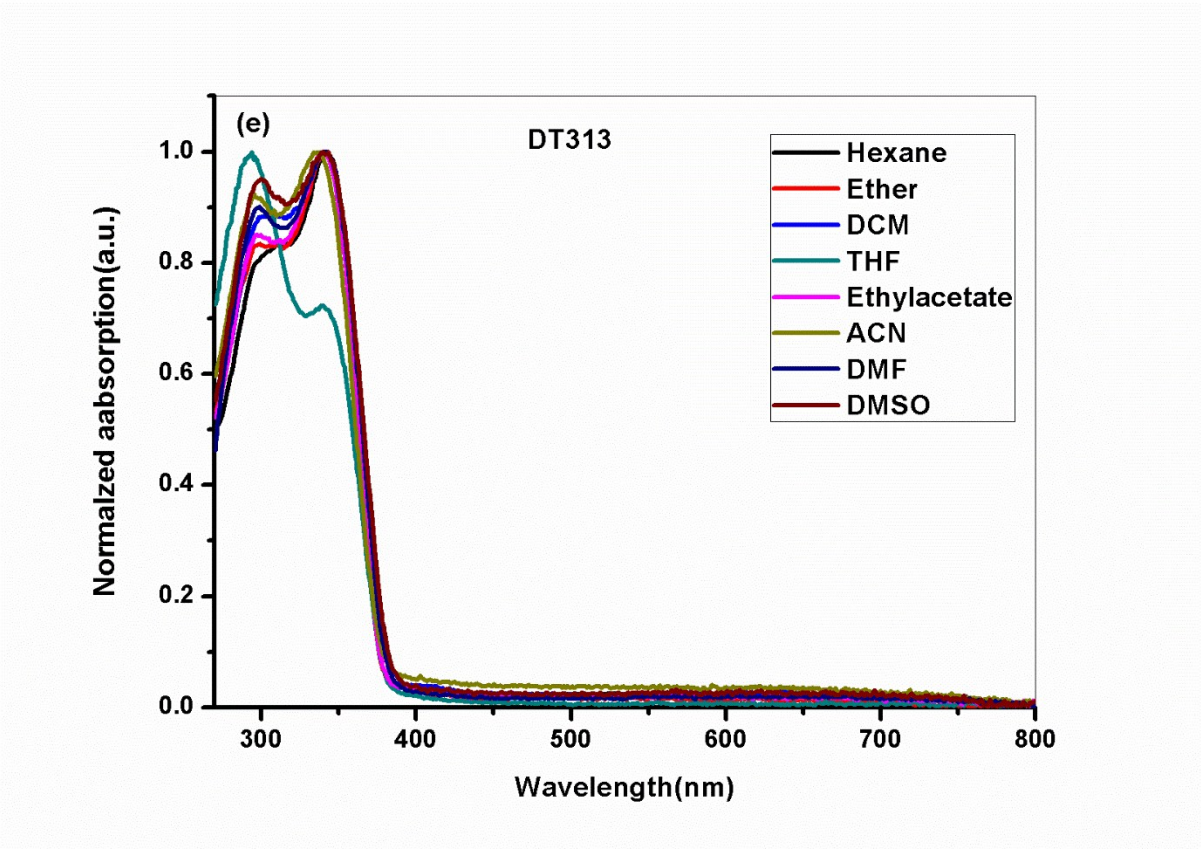

Figure S5. Solvatochromic UV-vis absorption behavior of compound **(a) DT316, (b) DT309, (c) DT320, (d) DT321,** and **(e) DT313** in different solvents.

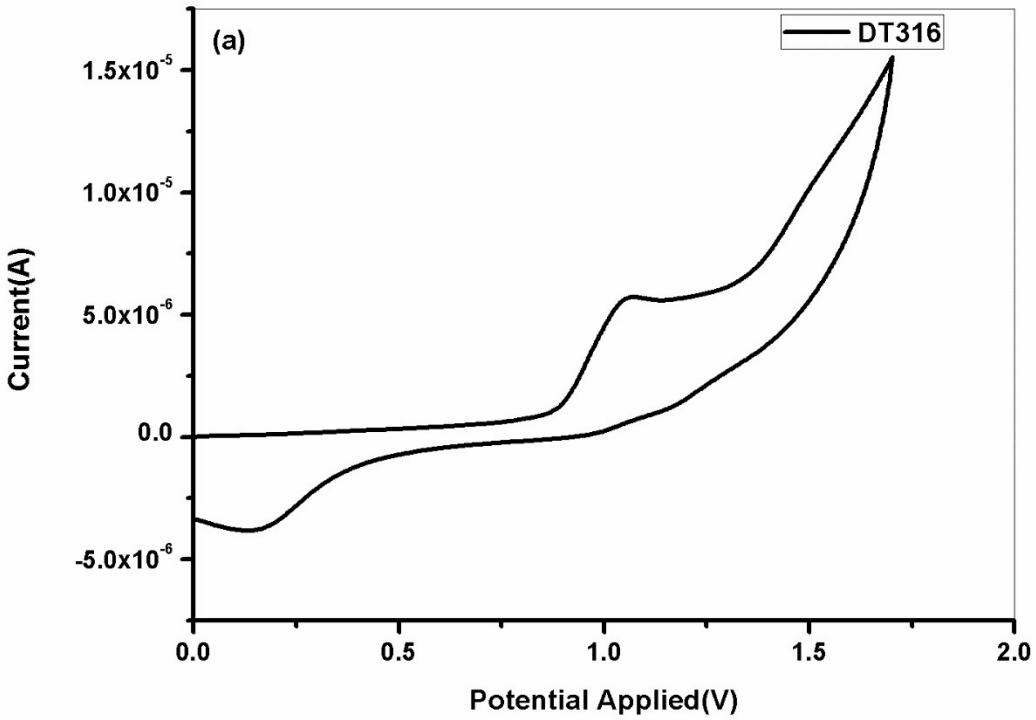
(a)
DT316
1.5x10-5
1.0x10-5
5.0x10-6
0.0
-5.0x10-6
Current(A)
0.0
0.5
1.0
1.5
2.0
Potential Applied(V)

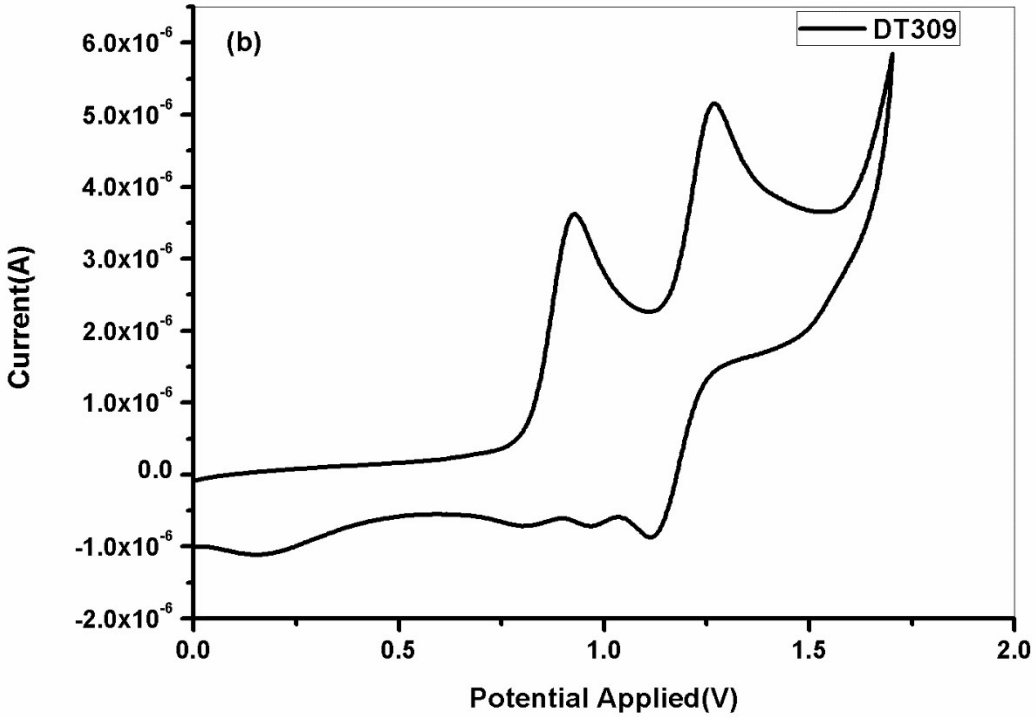
(b)
DT309
6.0x10-6
5.0x10-6
4.0x10-6
3.0x10-6
2.0x10-6
1.0x10-6
0.0
-1.0x10-6
-2.0x10-6
Current(A)
0.0
0.5
1.0
1.5
2.0
Potential Applied(V)

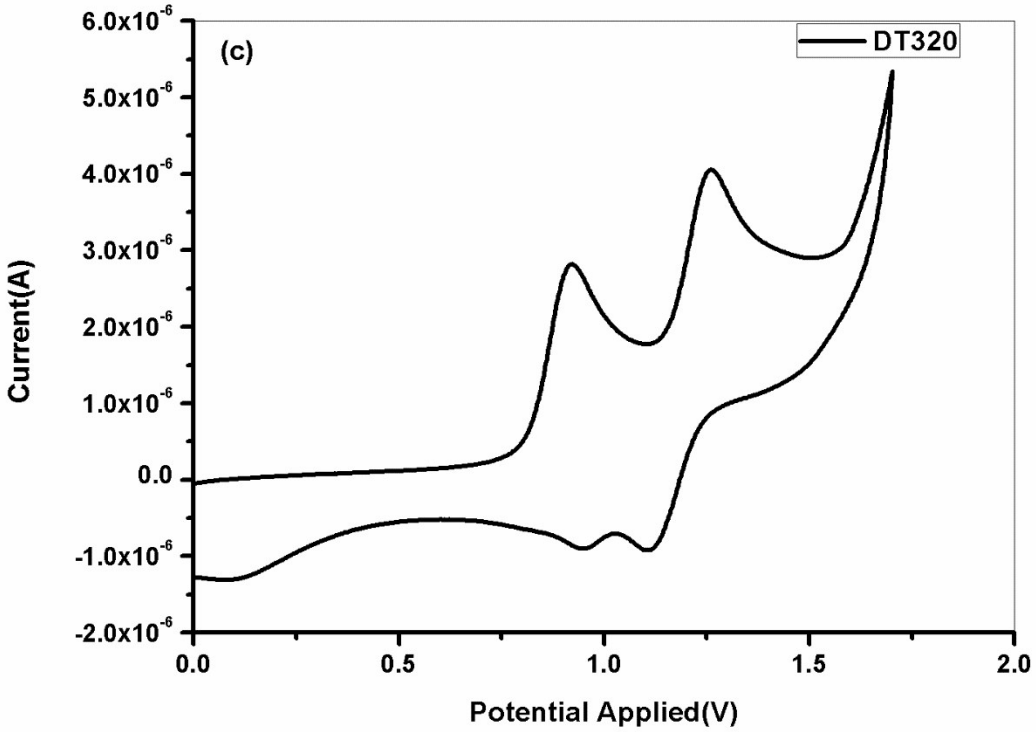
(c)
DT320
6.0x10^-6
5.0x10^-6
4.0x10^-6
3.0x10^-6
2.0x10^-6
1.0x10^-6
0.0
-1.0x10^-6
-2.0x10^-6
Current(A)
0.0
0.5
1.0
1.5
2.0
Potential Applied(V)

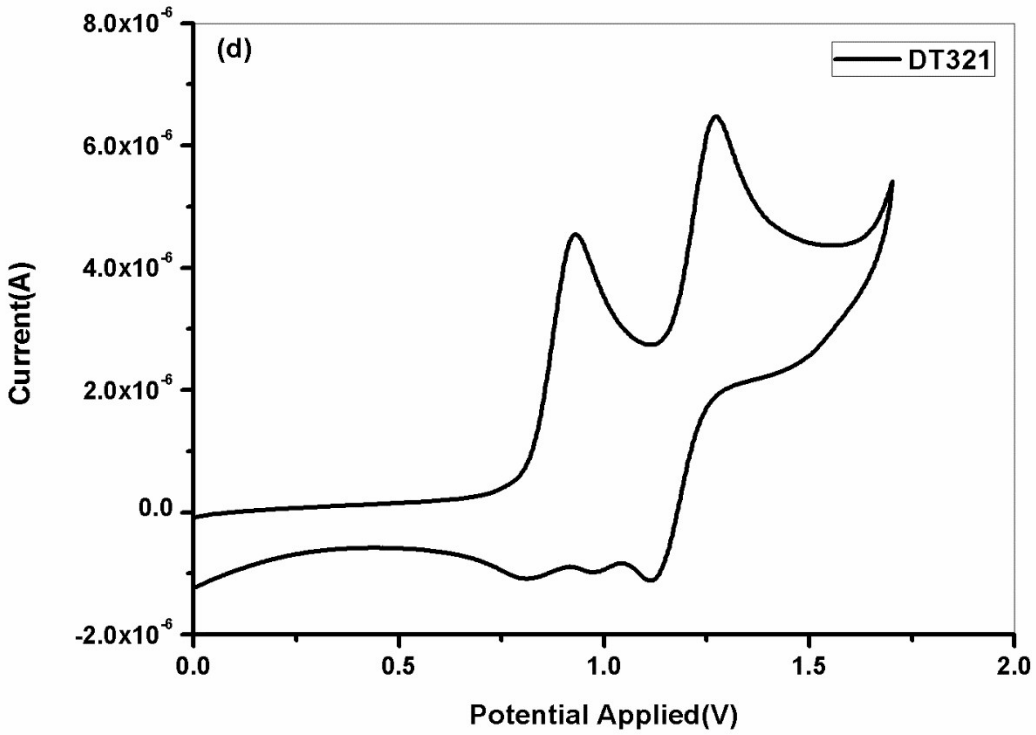
(d)
DT321
8.0x10^-6
6.0x10^-6
4.0x10^-6
2.0x10^-6
0.0
-2.0x10^-6
Current(A)
0.0
0.5
1.0
1.5
2.0
Potential Applied(V)

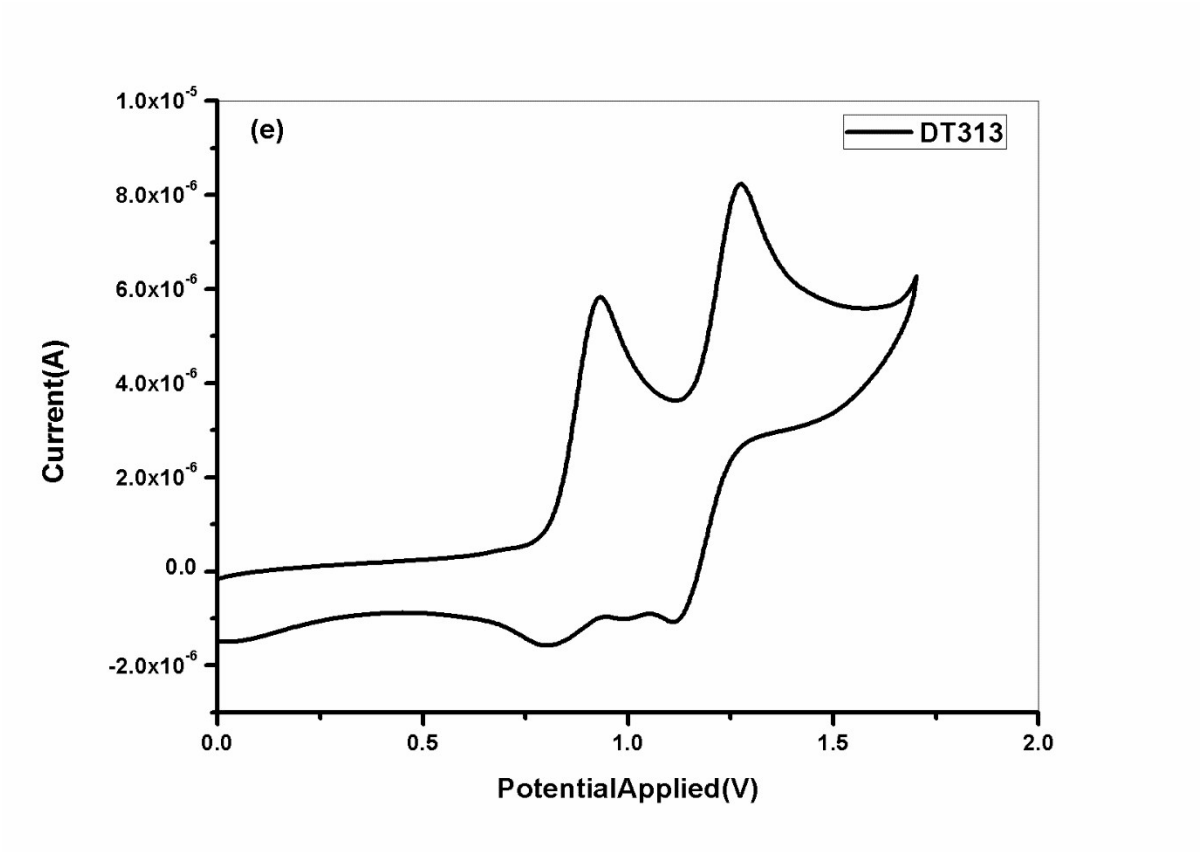

Figure S6. Cyclic voltamogramms of **(a) DT316, (b) DT309, (c) DT320, (d) DT321** and **(e) DT313.**

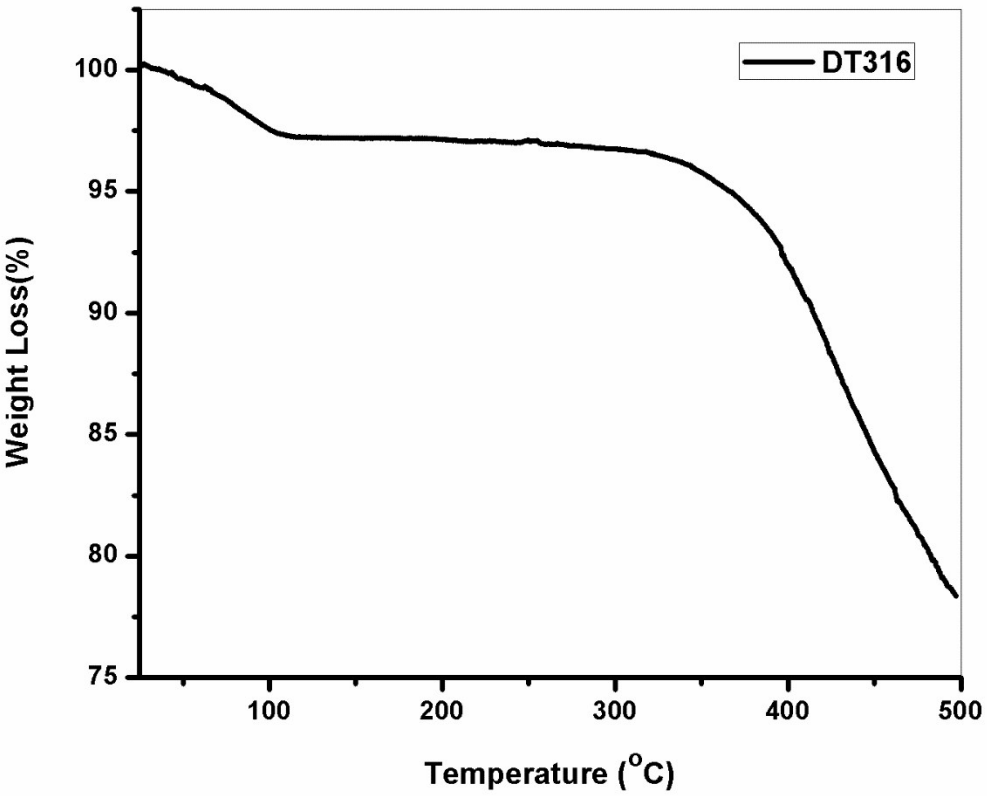
DT316
Weight Loss(%)
100
95
90
85
80
75
100
200
300
400
500
Temperature (°C)

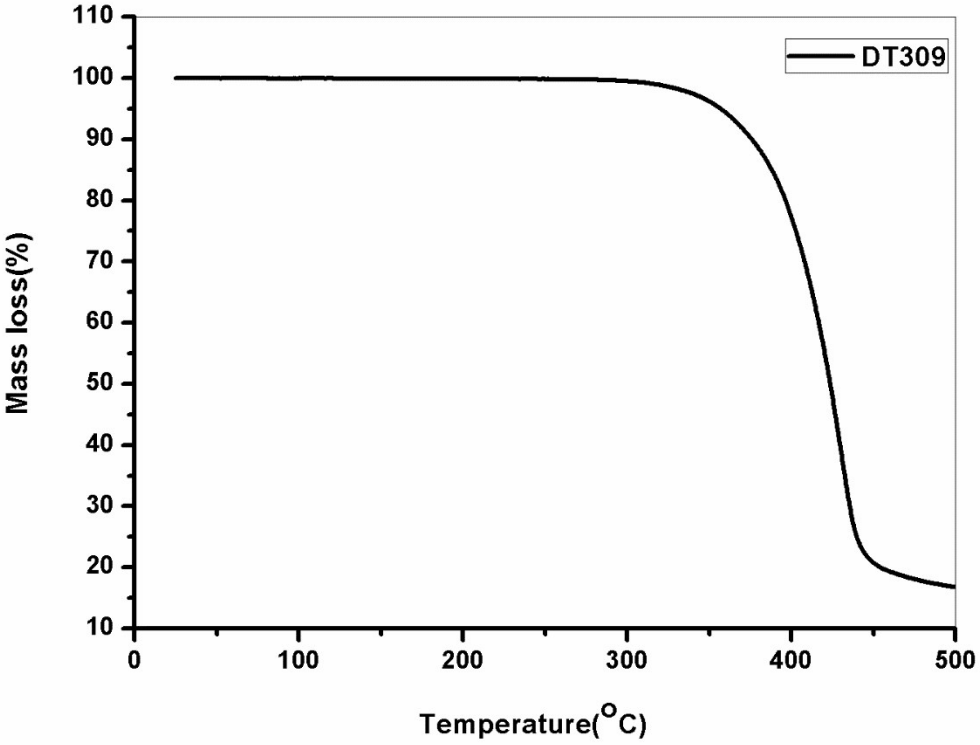
DT309
Mass loss(%)
110
100
90
80
70
60
50
40
30
20
10
0
100
200
300
400
500
Temperature(°C)

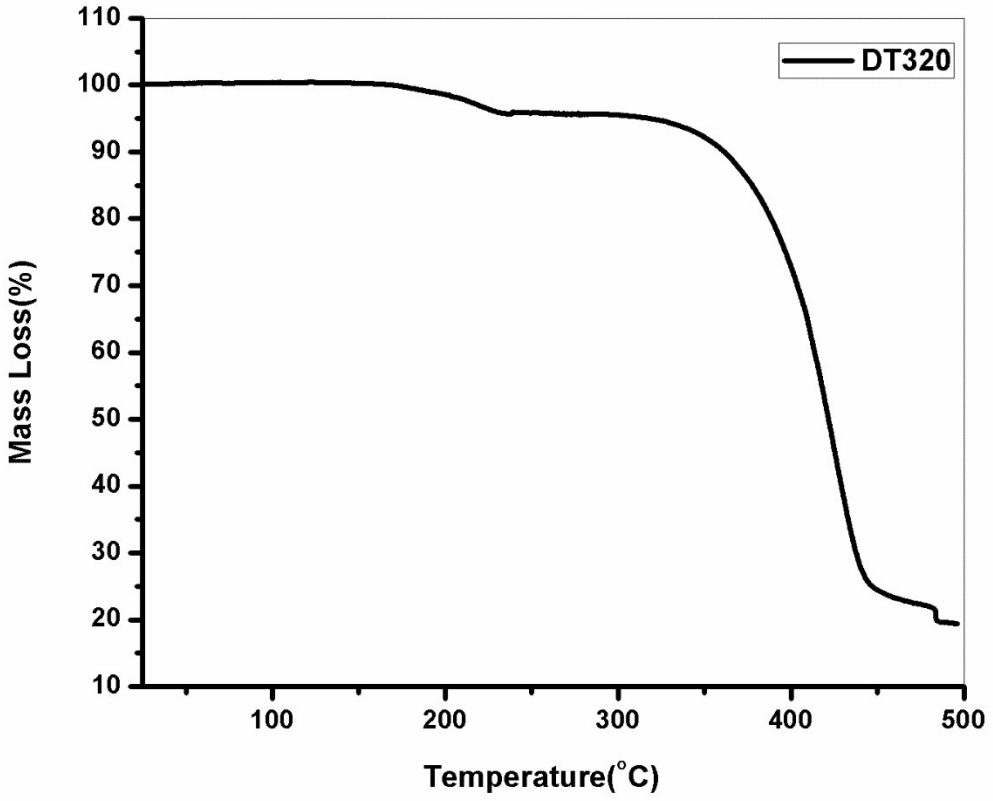
DT320
Mass Loss(%)
110
100
90
80
70
60
50
40
30
20
10
100
200
300
400
500
Temperature(°C)

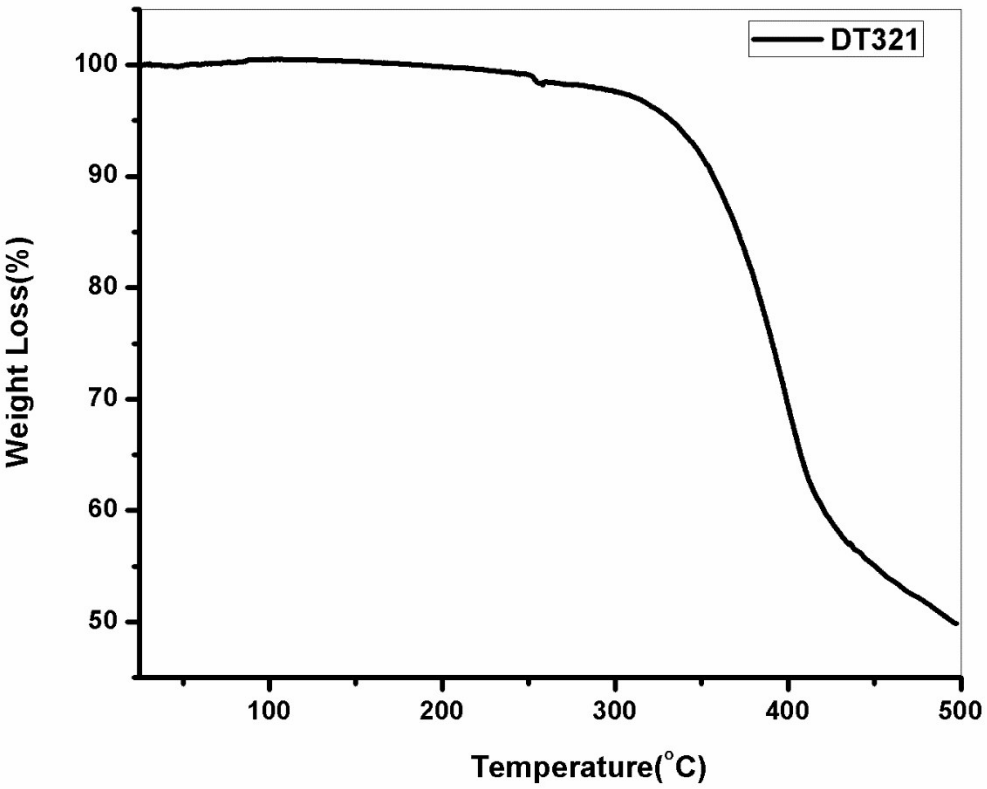
DT321
Weight Loss(%)
100
90
80
70
60
50
100
200
300
400
500
Temperature(°C)

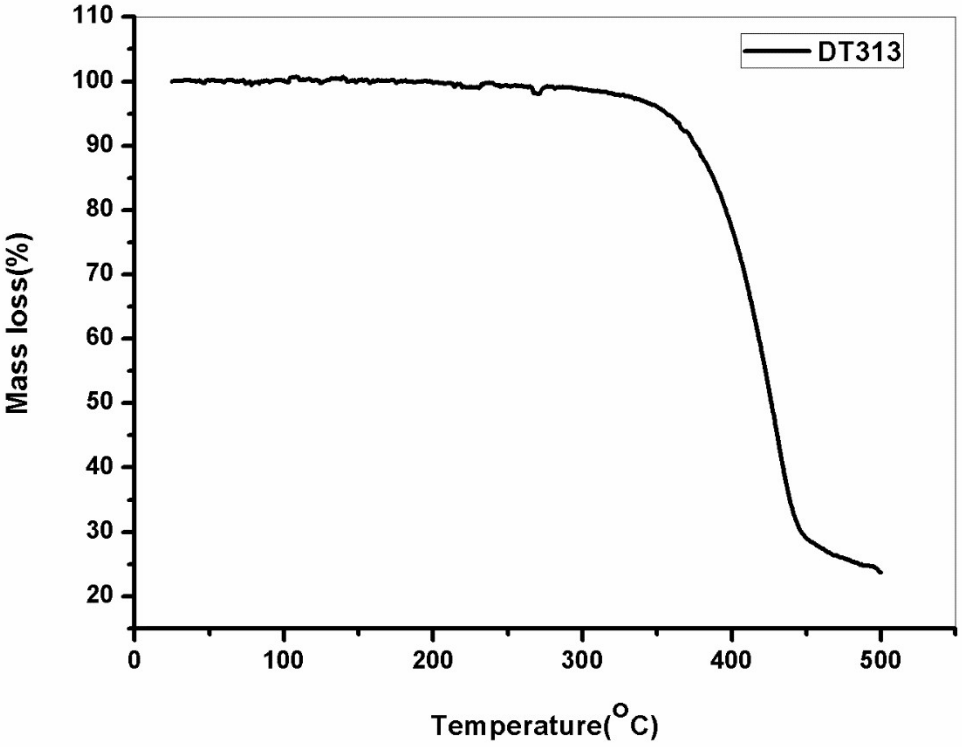
DT313
Mass loss(%)
110
100
90
80
70
60
50
40
30
20
0
100
200
300
400
500
Temperature(°C)

Figure S7. TGA (Thermogravimetric analysis) graphs of **DT316, DT309, DT320, DT321,** and **DT313**.

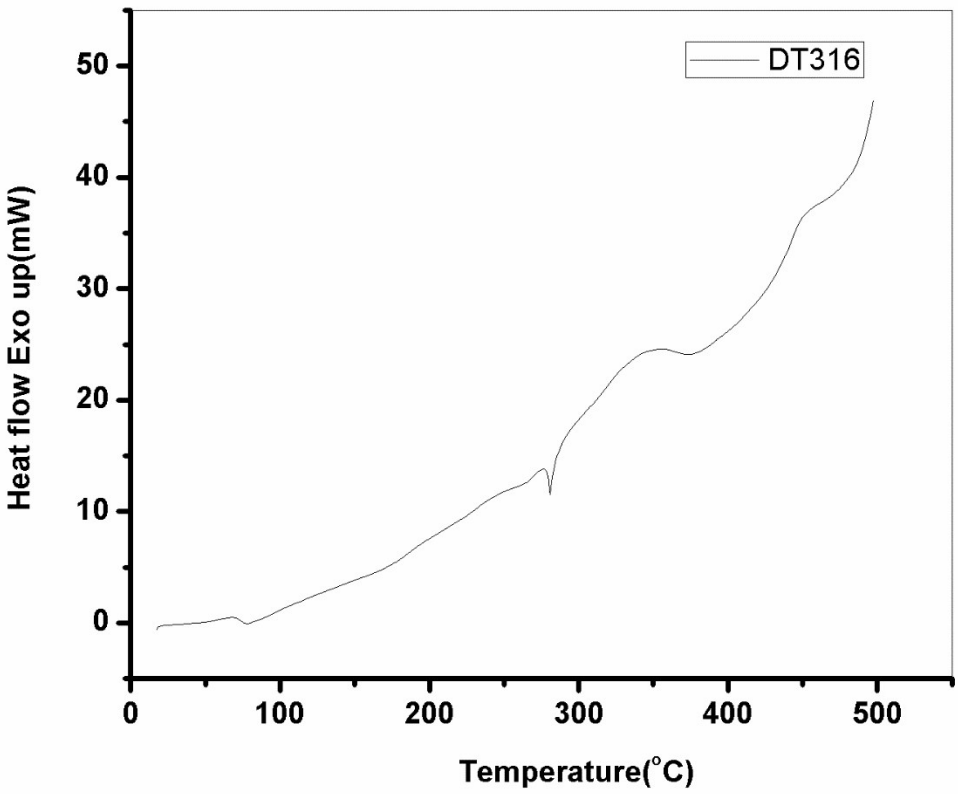

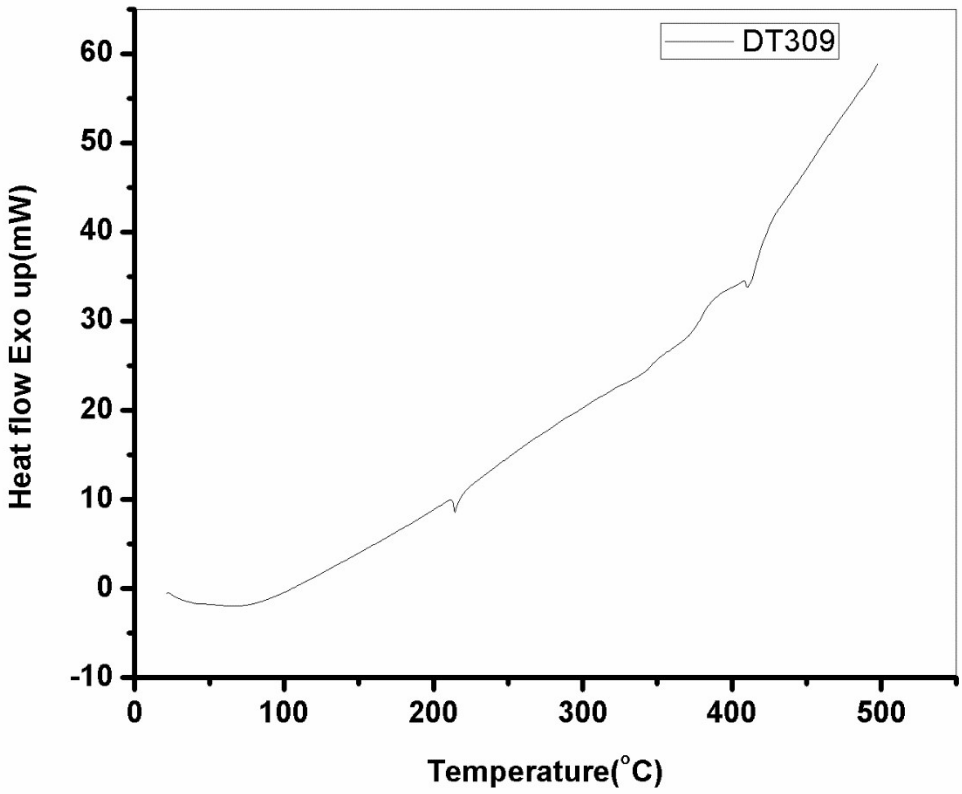
DT309
Heat flow Exo up(mW)
60
50
40
30
20
10
0
-10
0
100
200
300
400
500
Temperature(°C)

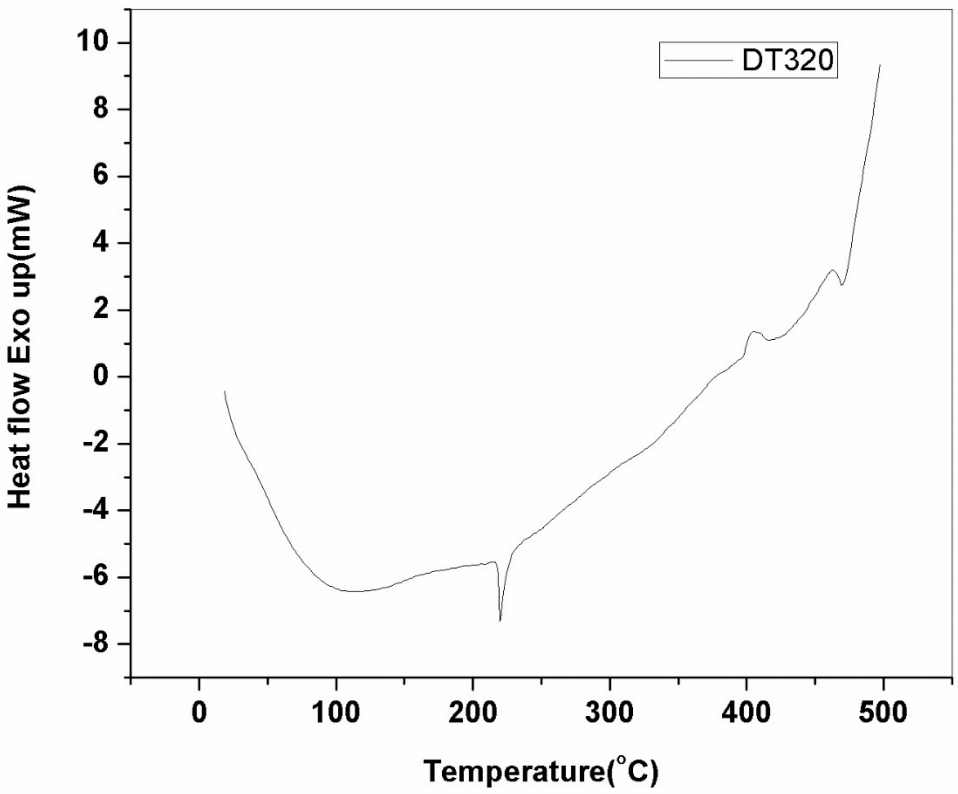
DT320
Heat flow Exo up(mW)
10
8
6
4
2
0
-2
-4
-6
-8
0
100
200
300
400
500
Temperature(°C)

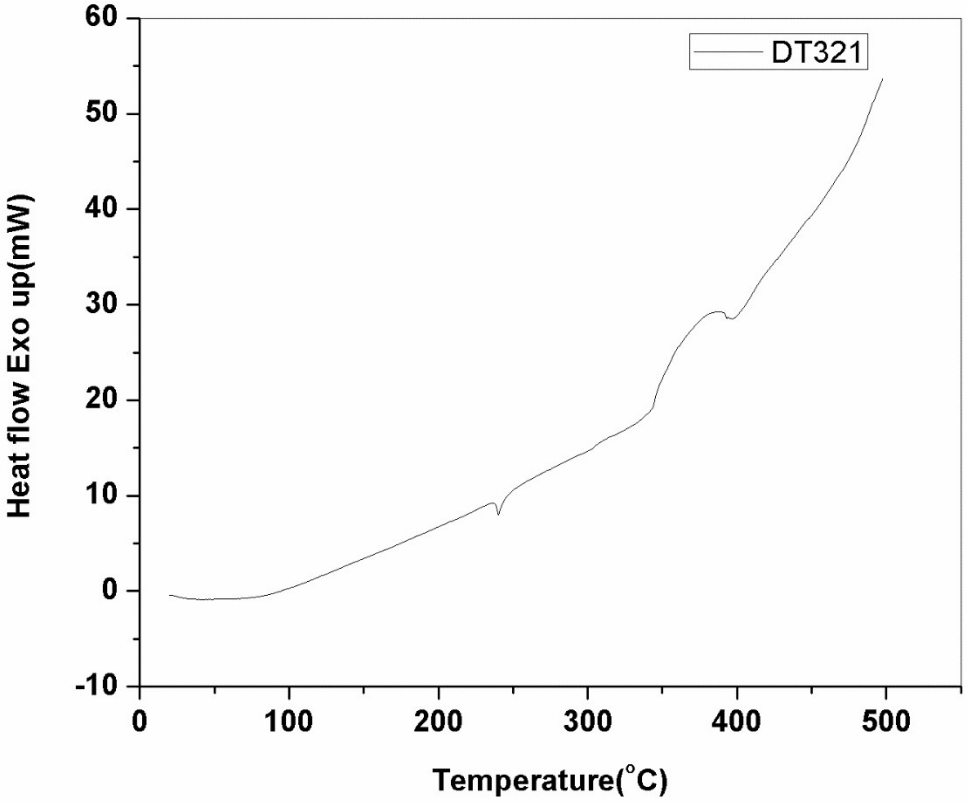
DT321
Heat flow Exo up(mW)
Temperature(°C)
60
50
40
30
20
10
0
-10
0
100
200
300
400
500

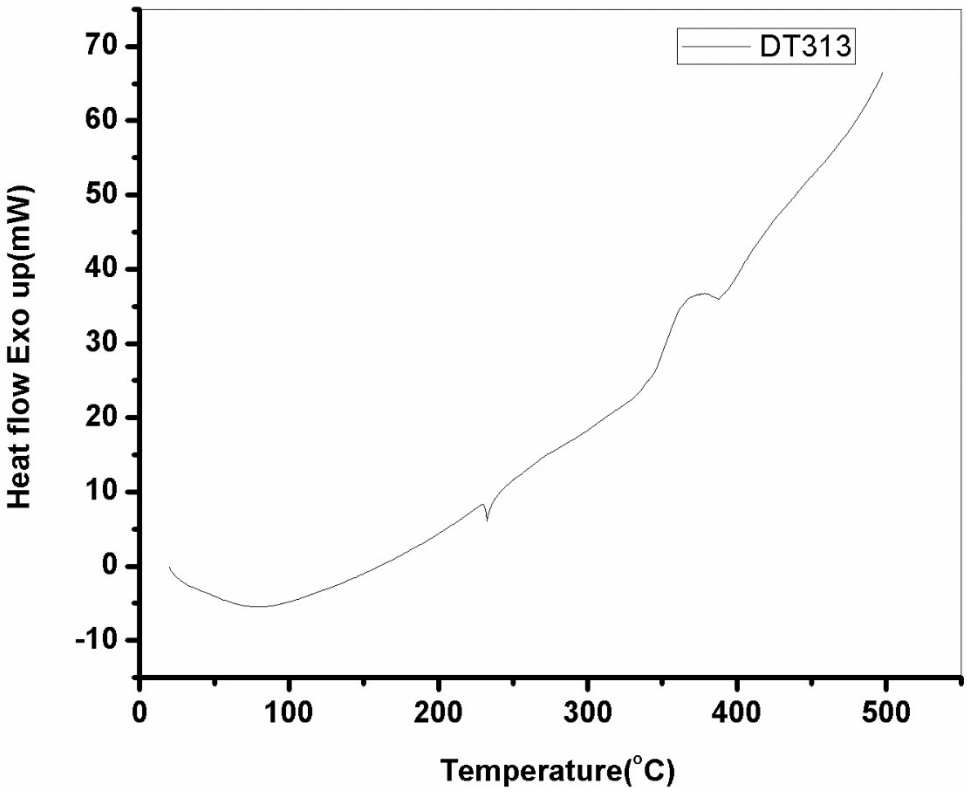

Figure S8. DSC graphs of **DT316, DT309, DT320, DT321,** and **DT313**.

Single crystal X-Ray Diffraction data analysis

Table S1. Crystal data and structure refinement for DT309_LT_CU.

Identification code	DT309_LT_CU
Empirical formula	$C_{40}H_{31}N_3O$
Formula weight	569.68
Temperature/K	149.99(10)
Crystal system	triclinic
Space group	P-1
a/Å	9.6216(9)
b/Å	13.1484(11)
c/Å	14.1763(9)

α/°	107.143(6)
β/°	98.785(7)
γ/°	109.218(8)
Volume/Å^3	1555.0(2)
Z	2
ρ_{calc}g/cm^3	1.217
μ/mm^{-1}	0.571
F(000)	600.0
Crystal size/mm^3	0.185 × 0.148 × 0.106
Radiation	CuKα (λ = 1.54184)
2Θ range for data collection/°	8.14 to 134.92
Index ranges	$-11 \leq h \leq 11$, $-15 \leq k \leq 15$, $-16 \leq l \leq 13$
Reflections collected	9288
Independent reflections	5439 [R_{int} = 0.0434, R_{sigma} = 0.0478]
Data/restraints/parameters	5439/0/398
Goodness-of-fit on F^2	1.124
Final R indexes [I>=2σ (I)]	R_1 = 0.0550, wR_2 = 0.1623
Final R indexes [all data]	R_1 = 0.0664, wR_2 = 0.1882
Largest diff. peak/hole / e Å^{-3}	0.32/-0.34

Table S2. Crystal data and structure refinement for DT320_LT_CU.

Identification code	DT320_LT_CU
Empirical formula	$C_{41}H_{33}N_3O$
Formula weight	583.70
Temperature/K	149.99(10)
Crystal system	monoclinic
Space group	$P2_1/n$
a/Å	14.2266(9)
b/Å	12.6251(7)
c/Å	18.0008(12)
α/°	90.00
β/°	109.736(8)
γ/°	90.00
Volume/Å^3	3043.2(3)
Z	4
ρ_{calc}g/cm^3	1.274
μ/mm^{-1}	0.595
F(000)	1232.0
Crystal size/mm^3	0.24 × 0.12 × 0.096
Radiation	CuKα (λ = 1.54184)
2Θ range for data collection/°	6.9 to 133.82

Index ranges	$-13 \leq h \leq 16$, $-15 \leq k \leq 8$, $-21 \leq l \leq 20$
Reflections collected	9821
Independent reflections	5319 [R_{int} = 0.0535, R_{sigma} = 0.0557]
Data/restraints/parameters	5319/0/407
Goodness-of-fit on F^2	1.057
Final R indexes [I>=2σ (I)]	R_1 = 0.0728, wR_2 = 0.2117
Final R indexes [all data]	R_1 = 0.0866, wR_2 = 0.2553
Largest diff. peak/hole / e $Å^{-3}$	0.56/-0.51

Table S3. Crystal data and structure refinement for DT321_LT_CU.

Identification code	DT321_LT_CU
Empirical formula	$C_{42}H_{35}N_3O$
Formula weight	597.73
Temperature/K	149.99(10)
Crystal system	triclinic
Space group	P-1
a/Å	10.1569(7)
b/Å	12.0507(10)
c/Å	15.4796(7)
α/°	69.073(6)
β/°	75.218(5)
γ/°	65.857(7)
Volume/$Å^3$	1601.61(18)
Z	2
ρ_{calc}g/cm^3	1.239
μ/mm^{-1}	0.577
F(000)	632.0
Crystal size/mm^3	0.301 × 0.16 × 0.098
Radiation	CuKα (λ = 1.54184)
2Θ range for data collection/°	8.4 to 133.78
Index ranges	$-11 \leq h \leq 12$, $-14 \leq k \leq 14$, $-13 \leq l \leq 18$
Reflections collected	9551
Independent reflections	5503 [R_{int} = 0.0437, R_{sigma} = 0.0489]
Data/restraints/parameters	5503/0/416
Goodness-of-fit on F^2	1.110
Final R indexes [I>=2σ (I)]	R_1 = 0.0646, wR_2 = 0.1854
Final R indexes [all data]	R_1 = 0.0835, wR_2 = 0.2591
Largest diff. peak/hole / e $Å^{-3}$	0.45/-0.47

Table S4. Crystal data and structure refinement for DT313_RT_CU.

Identification code	DT313_RT_CU
Empirical formula	$C_{43}H_{37}N_3O$
Formula weight	611.76
Temperature/K	293(2)
Crystal system	triclinic
Space group	P-1
a/Å	10.1410(7)
b/Å	12.4994(8)
c/Å	15.4396(10)
α/°	95.664(5)
β/°	103.464(6)
γ/°	112.004(6)
Volume/Å^3	1726.7(2)
Z	2
ρ_{calc}g/cm^3	1.177
μ/mm^{-1}	0.546
F(000)	648.0
Crystal size/mm^3	0.473 × 0.074 × 0.052
Radiation	CuKα (λ = 1.54184)
2Θ range for data collection/°	6.02 to 133.72
Index ranges	$-12 \leq h \leq 10$, $-14 \leq k \leq 12$, $-17 \leq l \leq 18$
Reflections collected	10480
Independent reflections	6057 [R_{int} = 0.0235, R_{sigma} = 0.0355]
Data/restraints/parameters	6057/0/425
Goodness-of-fit on F^2	1.051
Final R indexes [I>=2σ (I)]	R_1 = 0.0579, wR_2 = 0.1592
Final R indexes [all data]	R_1 = 0.0723, wR_2 = 0.1757
Largest diff. peak/hole / e Å^{-3}	0.42/-0.23

Table S5. CCDC No. of crystals.

Compound	**Molecular Formula**	**CCDC No.**
DT309	$C_{40}H_{31}N_3O$	1897654
DT320	$C_{41}H_{33}N_3O$	1897656
DT321	$C_{42}H_{35}N_3O$	1897657
DT313	$C_{43}H_{37}N_3O$	1897655

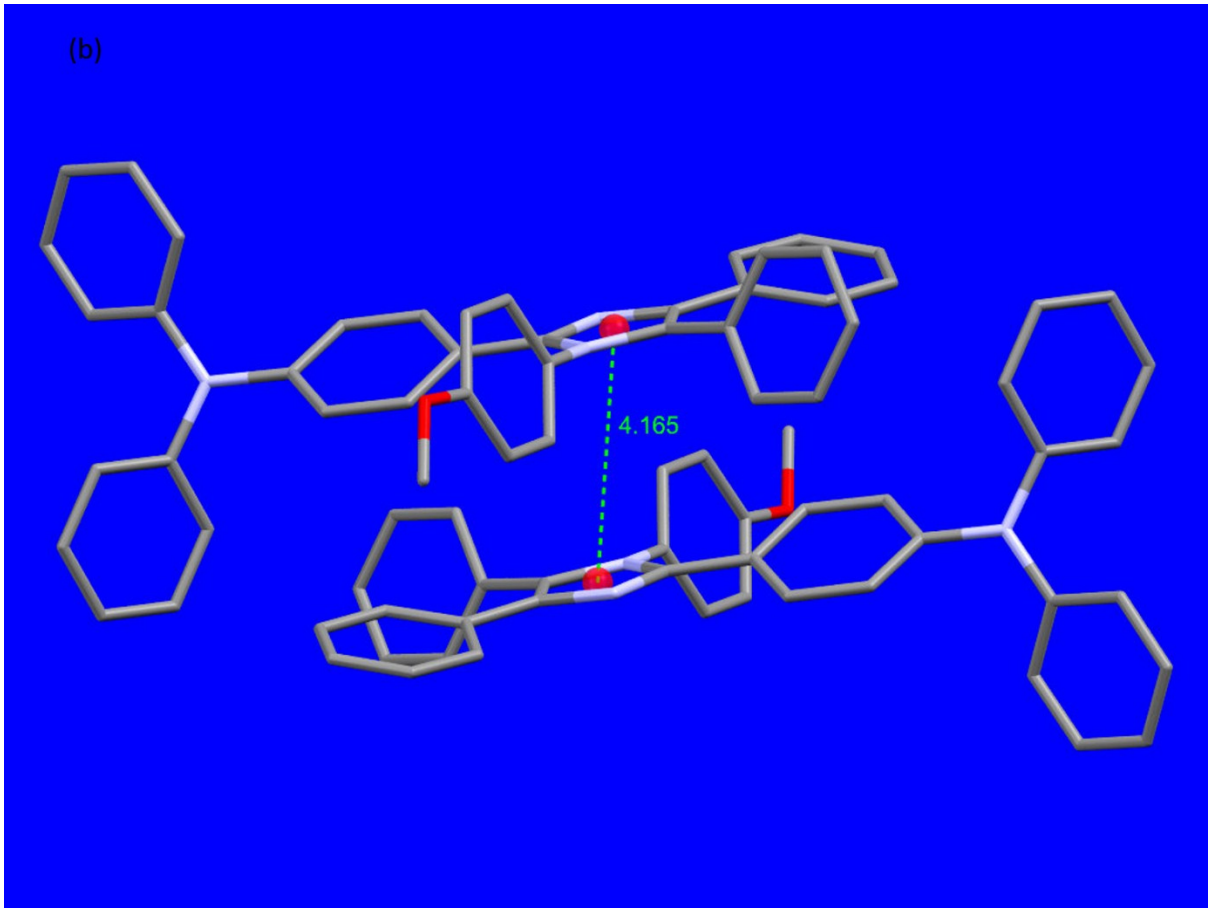

Figure S9. Distance between imidazole rings of two neighbouring molecules of **DT309**.

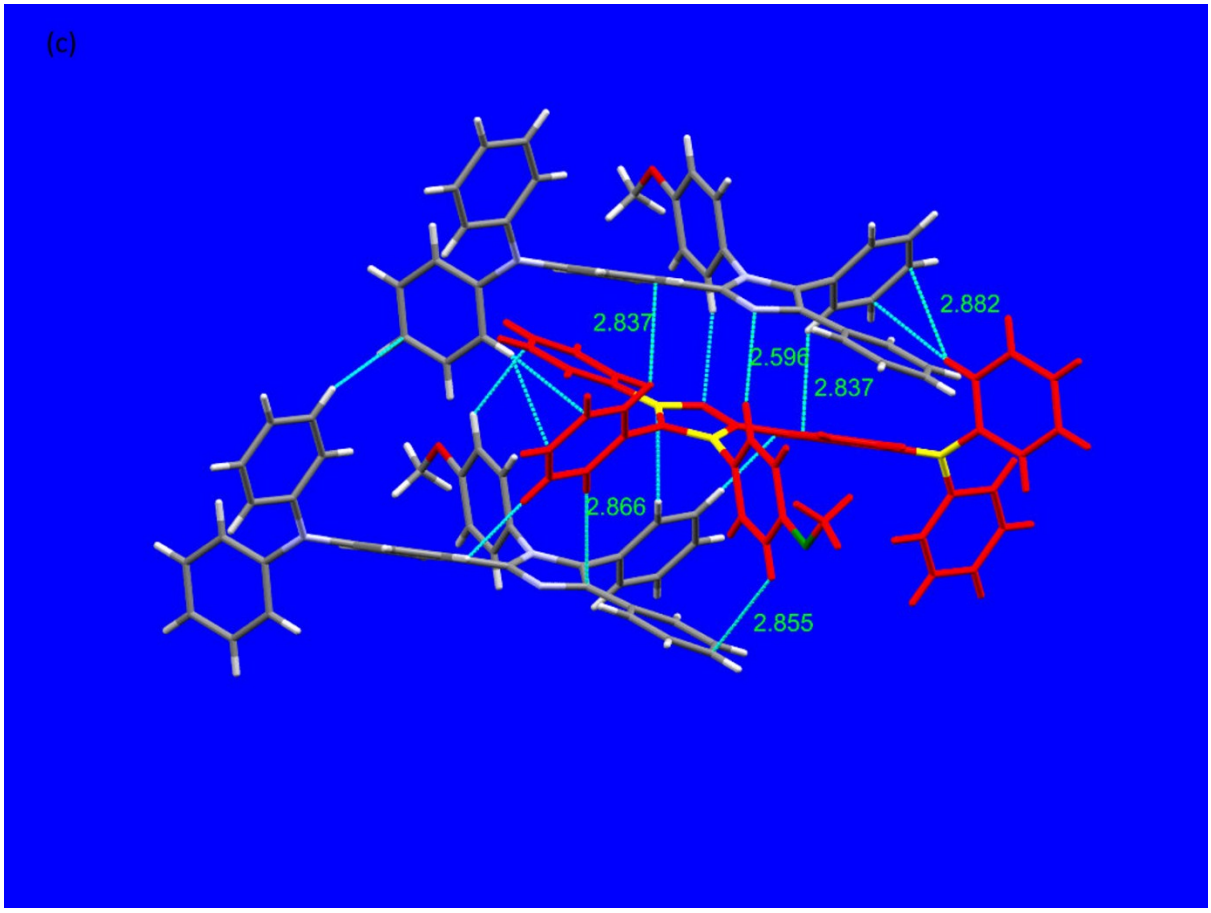

Figure S10. Existed short range interactions of **DT309** with the neighbouring molecules.

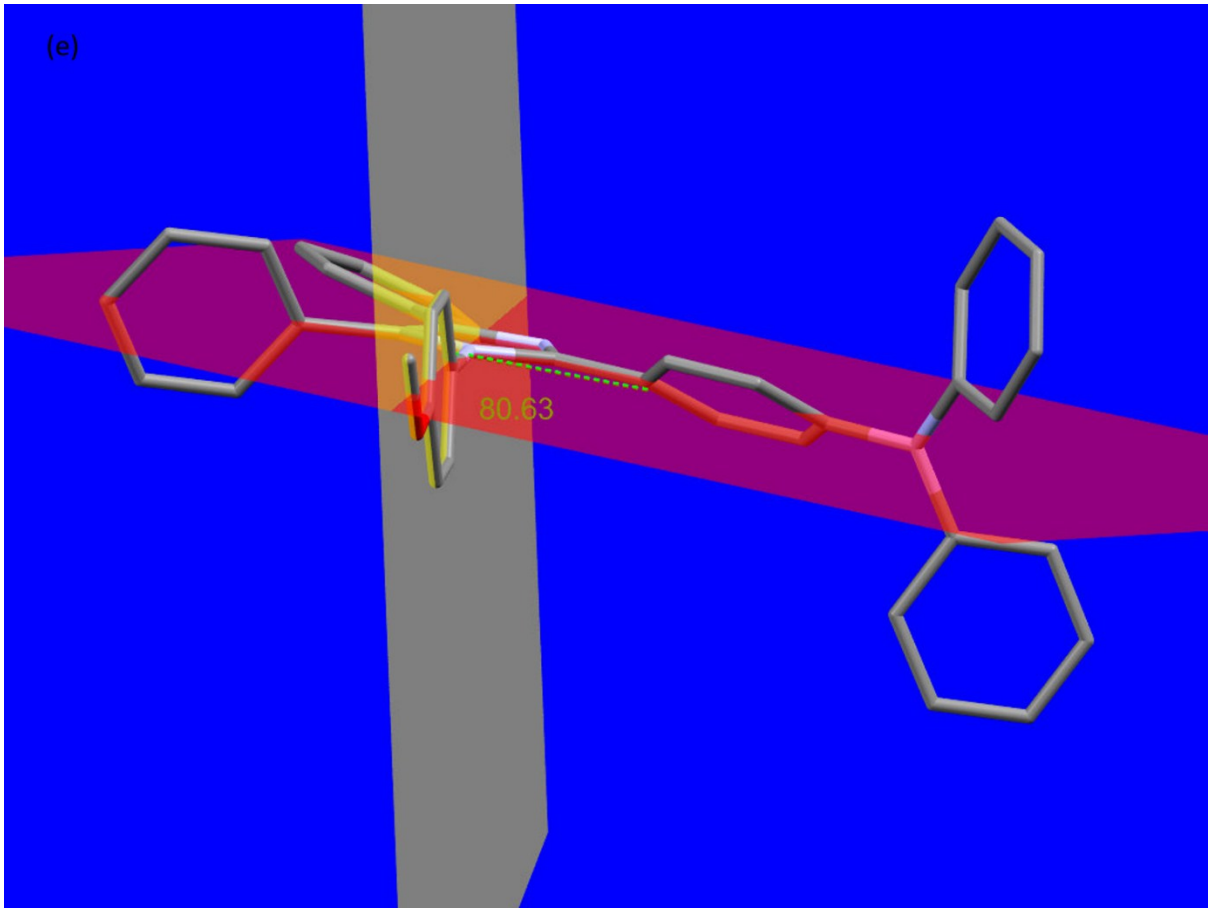

Figure S11. Angle between imidazole ring alkoxy substituted phenyl ring diagram of **DT309**.

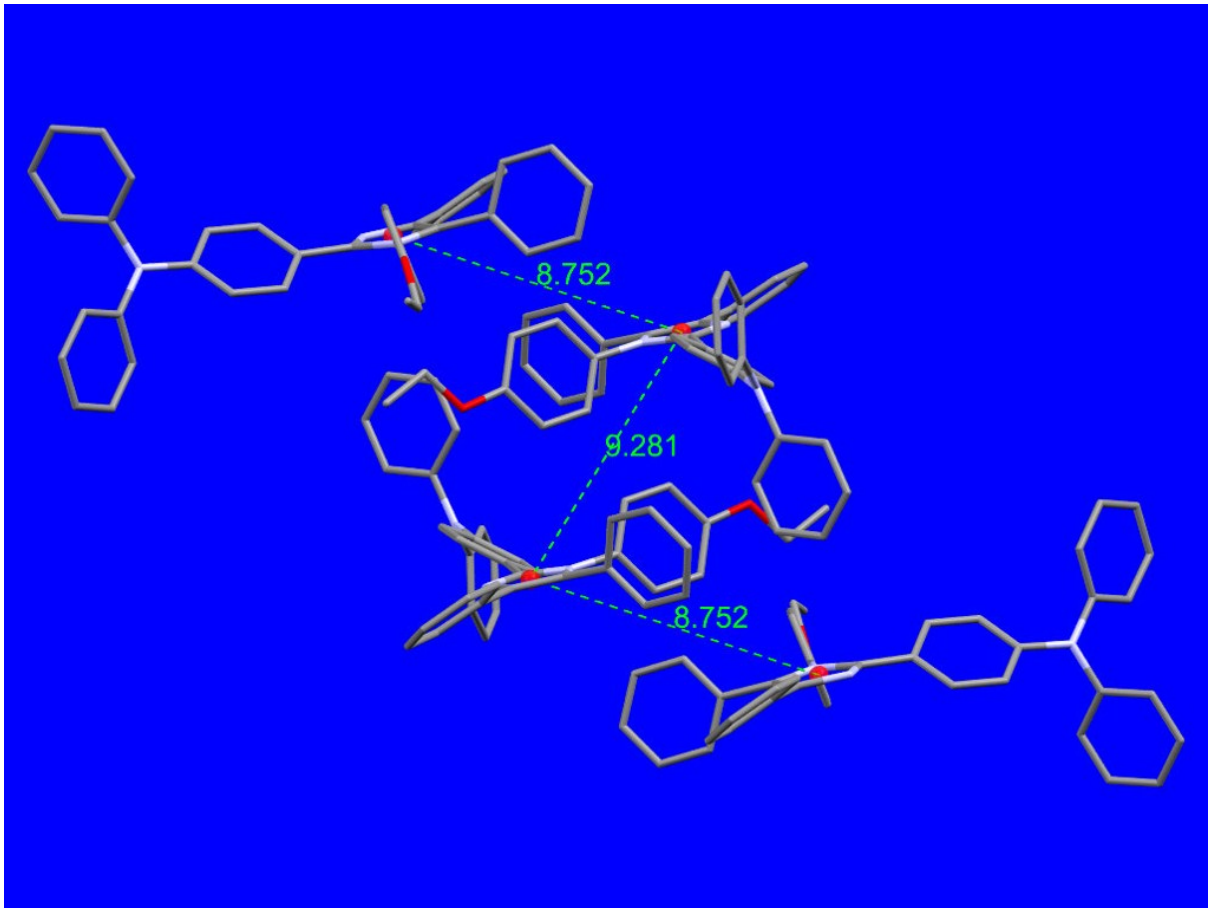

Figure S12. Distance between imidazole rings of two neighbouring molecules of **DT320**.

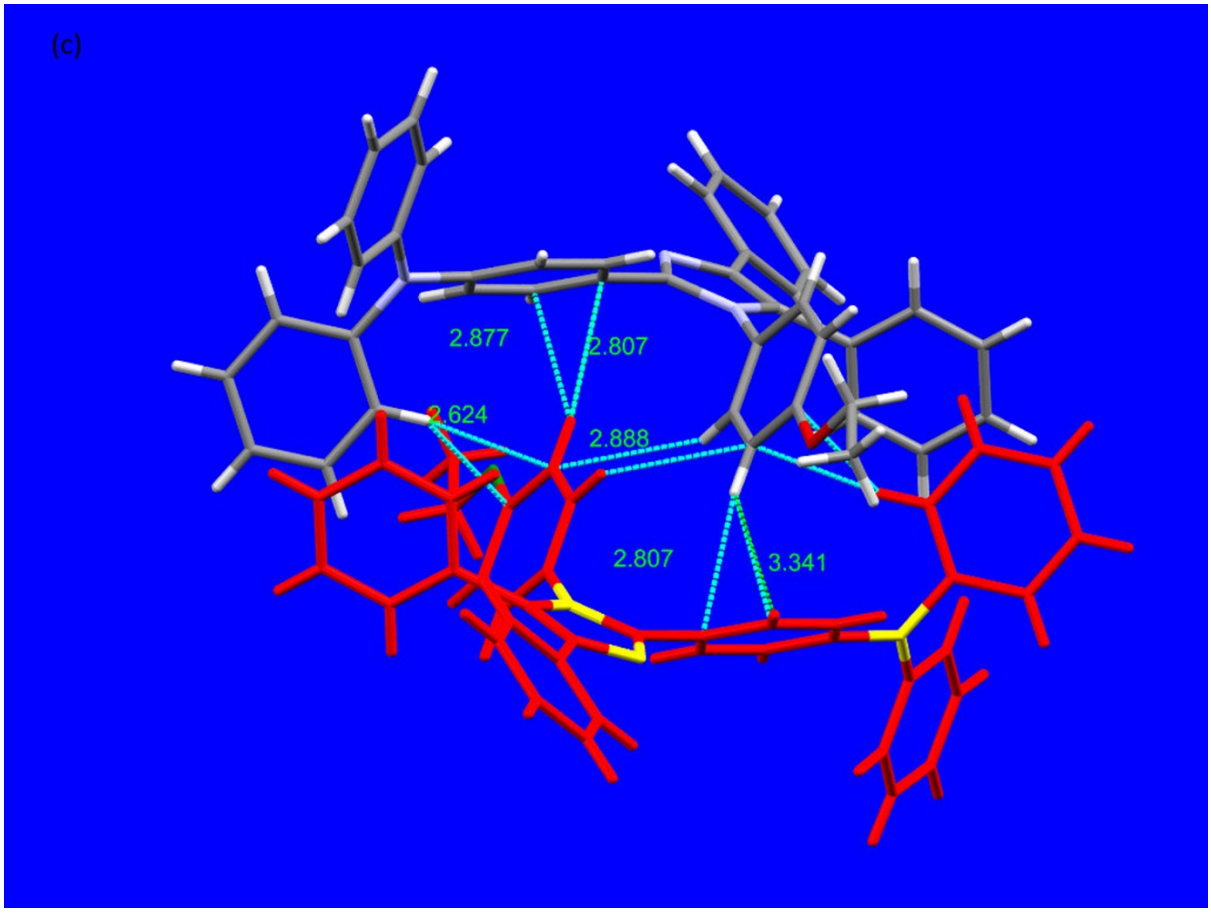

Figure S13. Existed short range interactions of **DT320** with the neighbouring molecules.

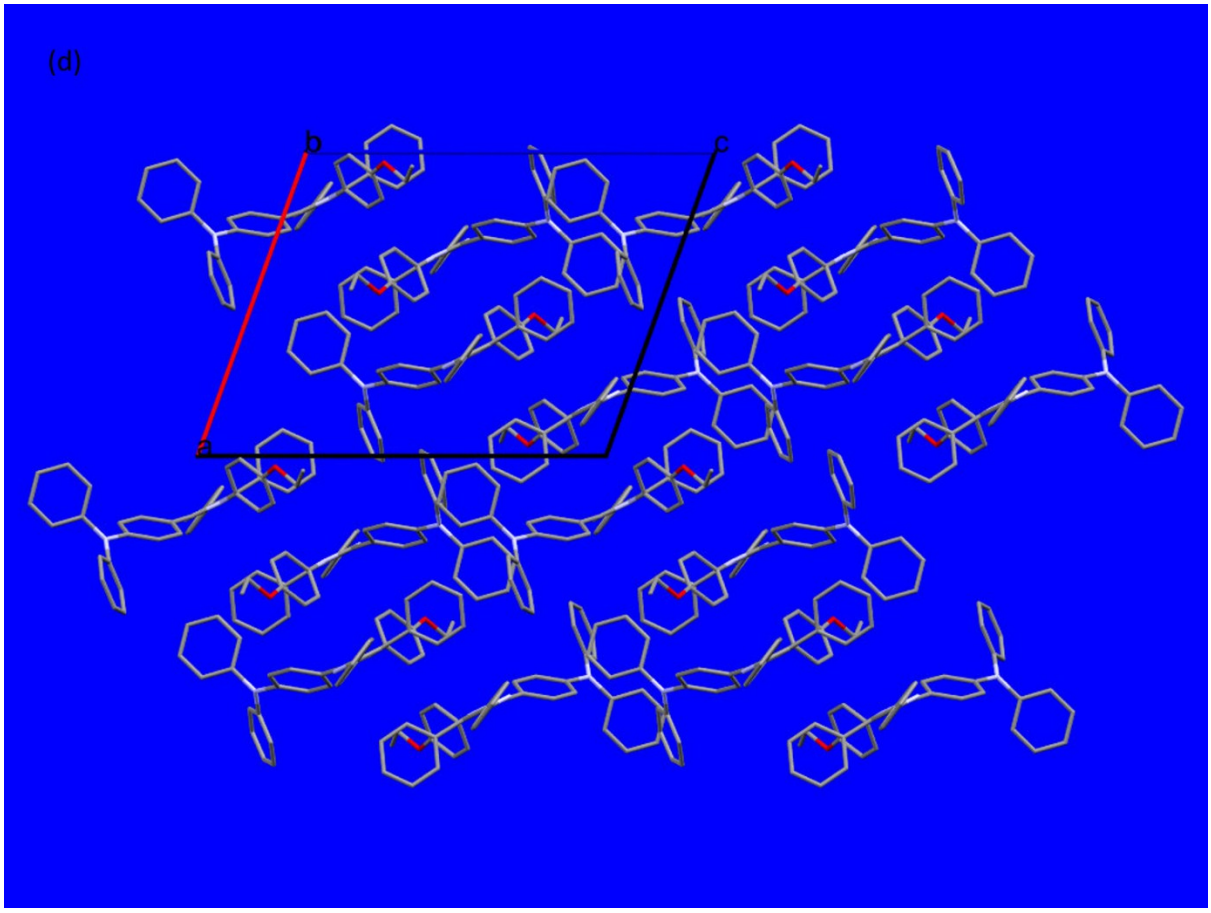

Figure S14. Crystal Packing diagram of **DT320** viewed along b axis.

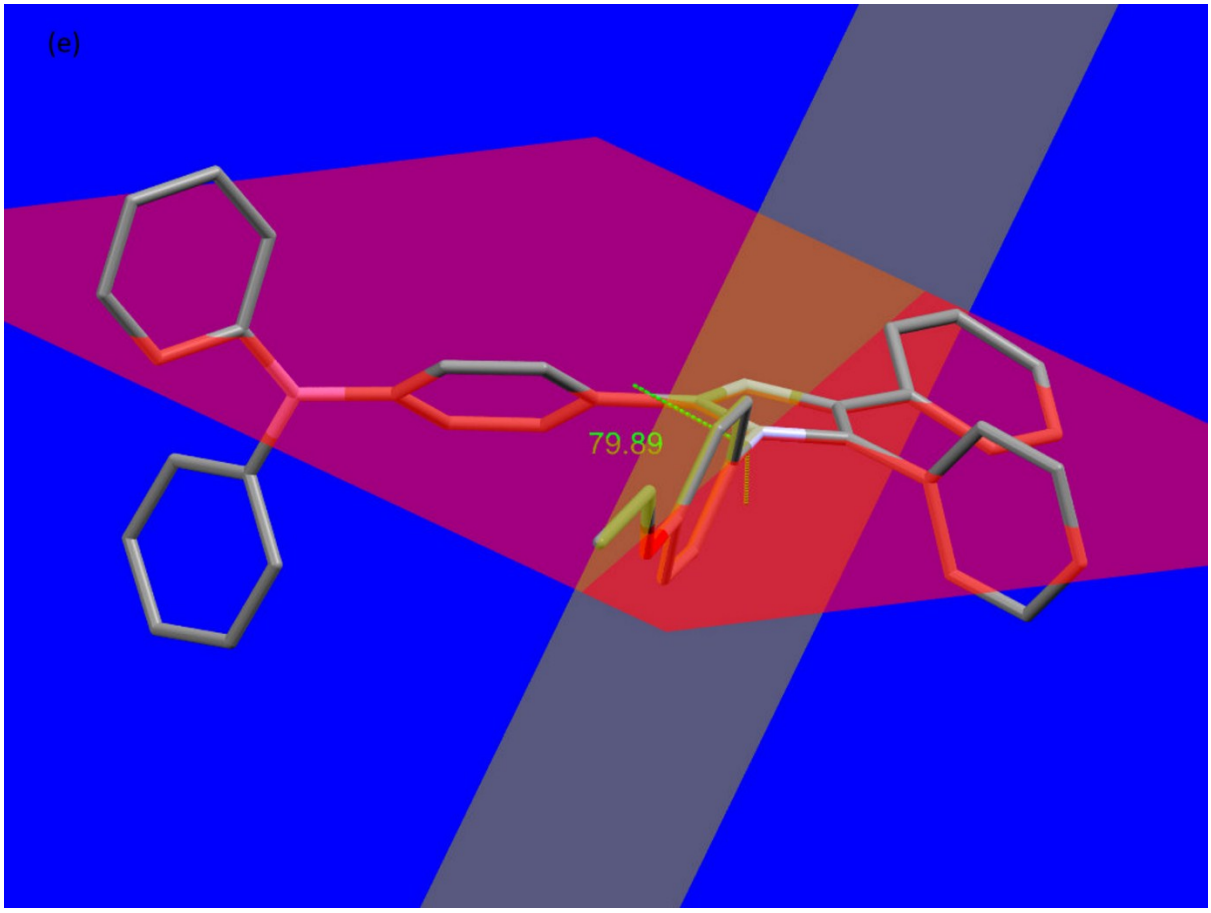

Figure S15. Angle between imidazole ring alkoxy substituted phenyl ring diagram of **DT320**.

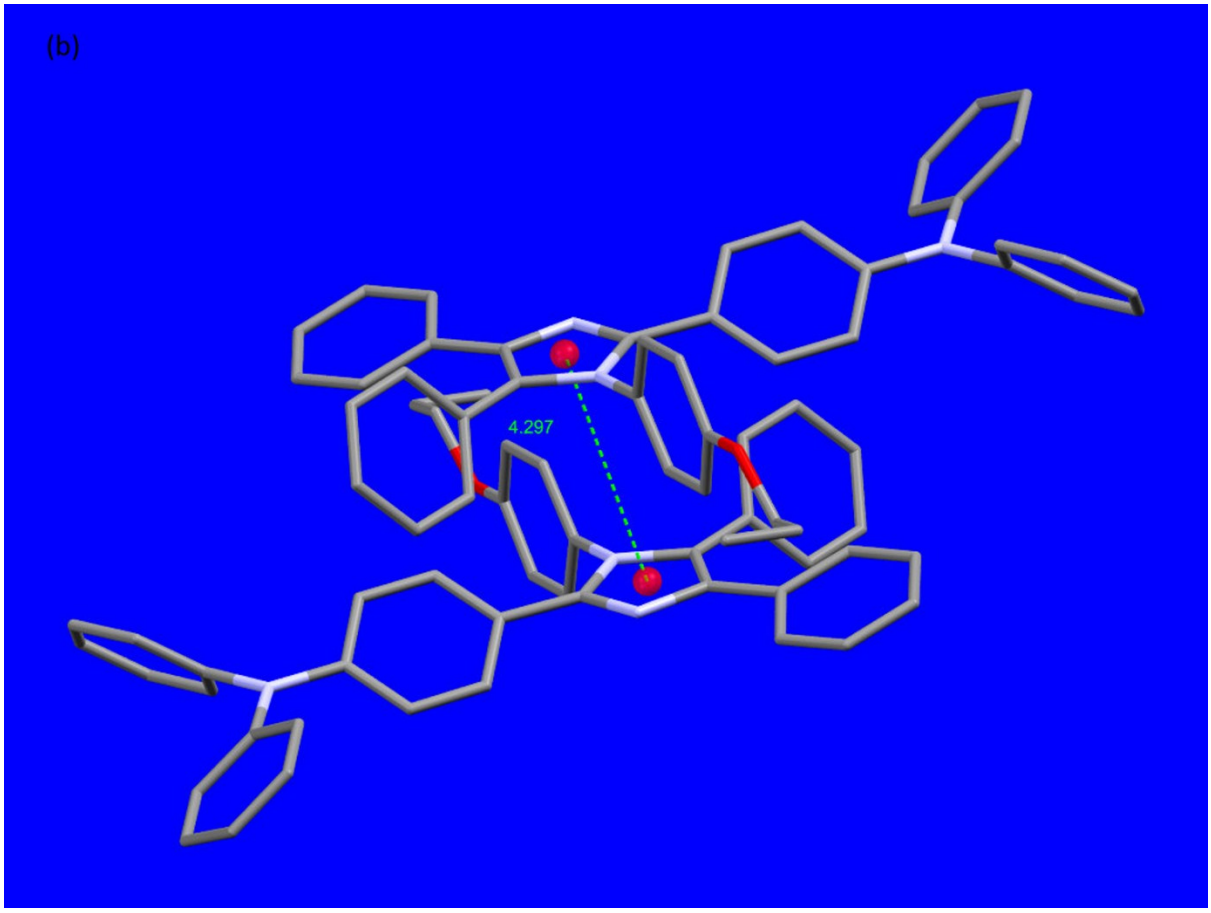

Figure S16. Distance between imidazole rings of two neighbouring molecules of **DT321**.

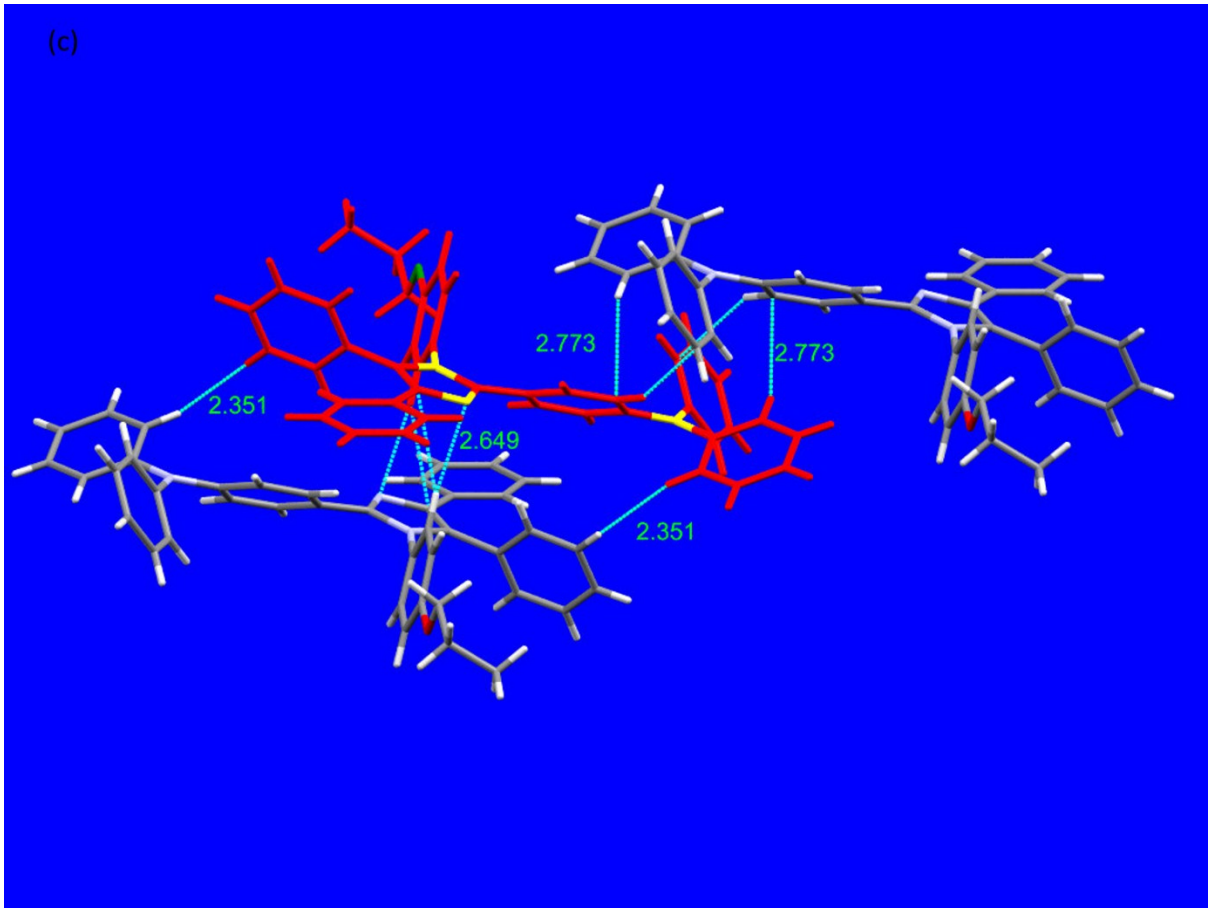

Figure S17. Existed short range interactions of **DT321**with the neighbouring molecules.

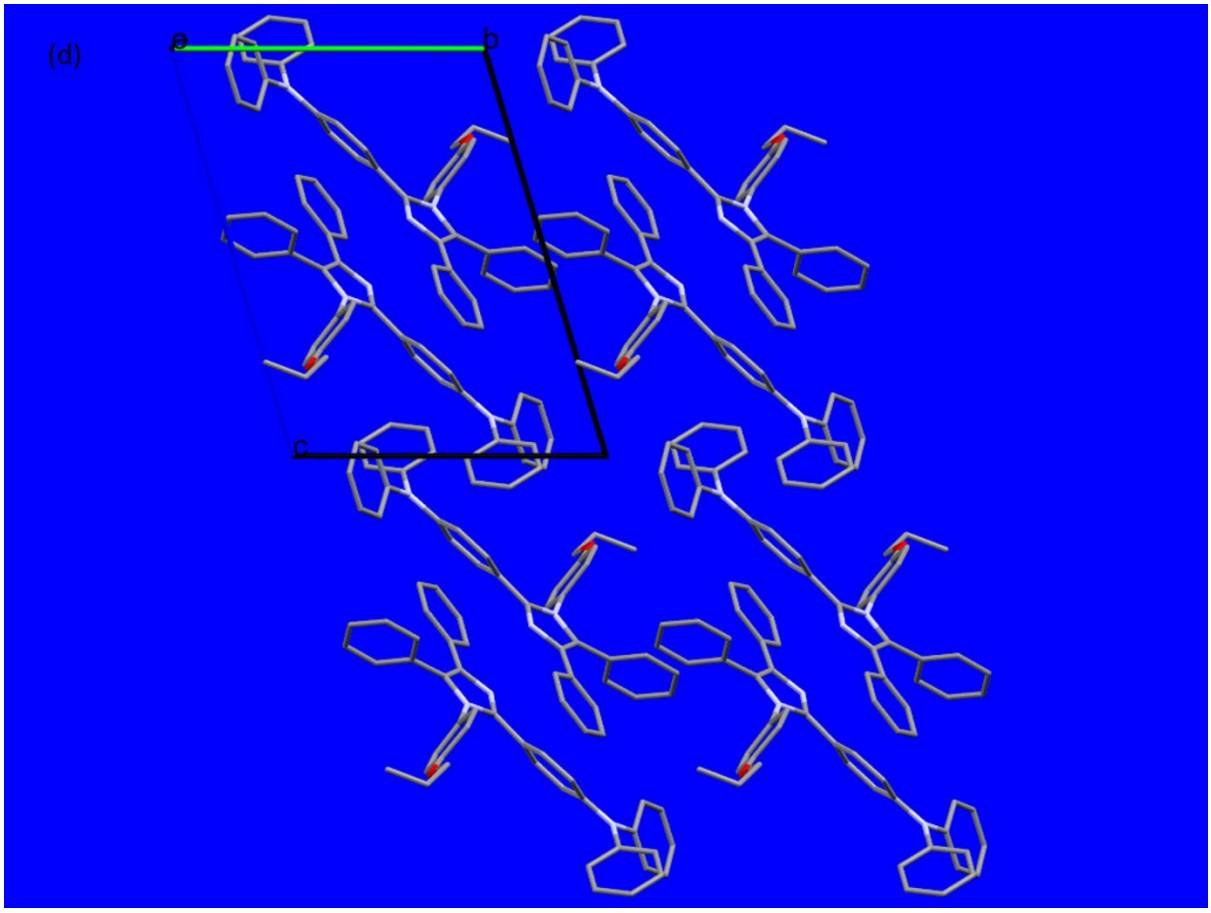

Figure S18. Crystal Packing diagram of **DT321** viewed along a axis.

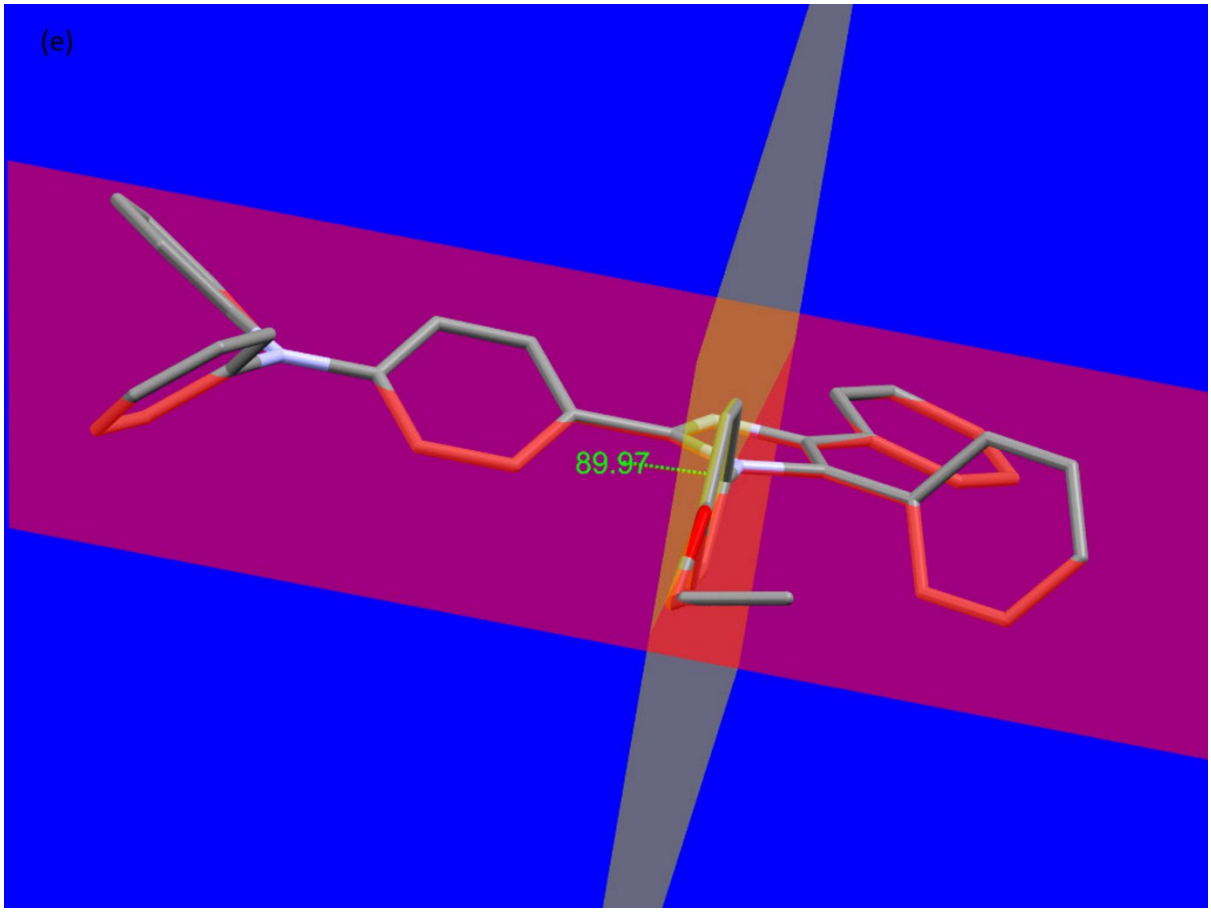

Figure S19. Angle between imidazole ring alkoxy substituted phenyl ring diagram of **DT321**.

.

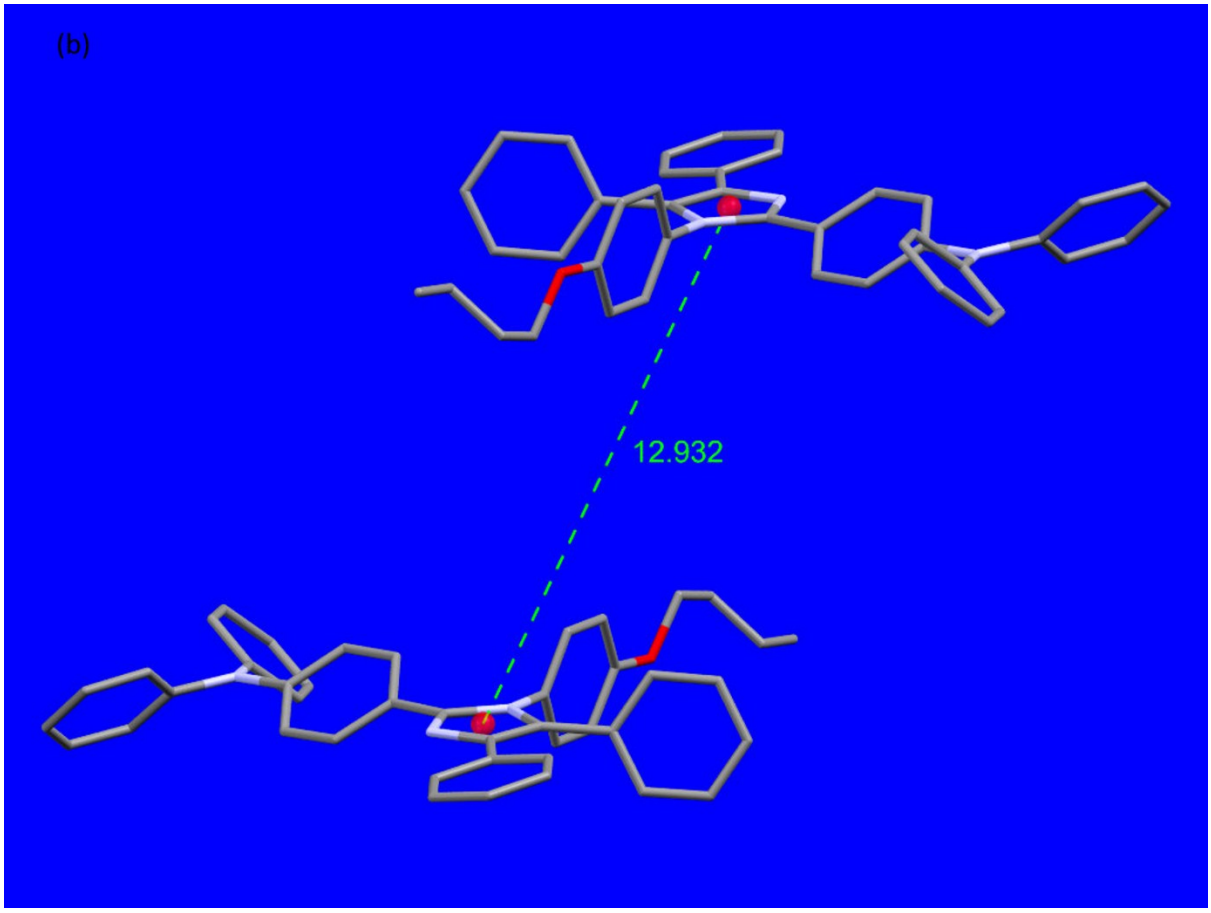

Figure S20. Distance between imidazole rings of two neighbouring molecules of **DT313**.

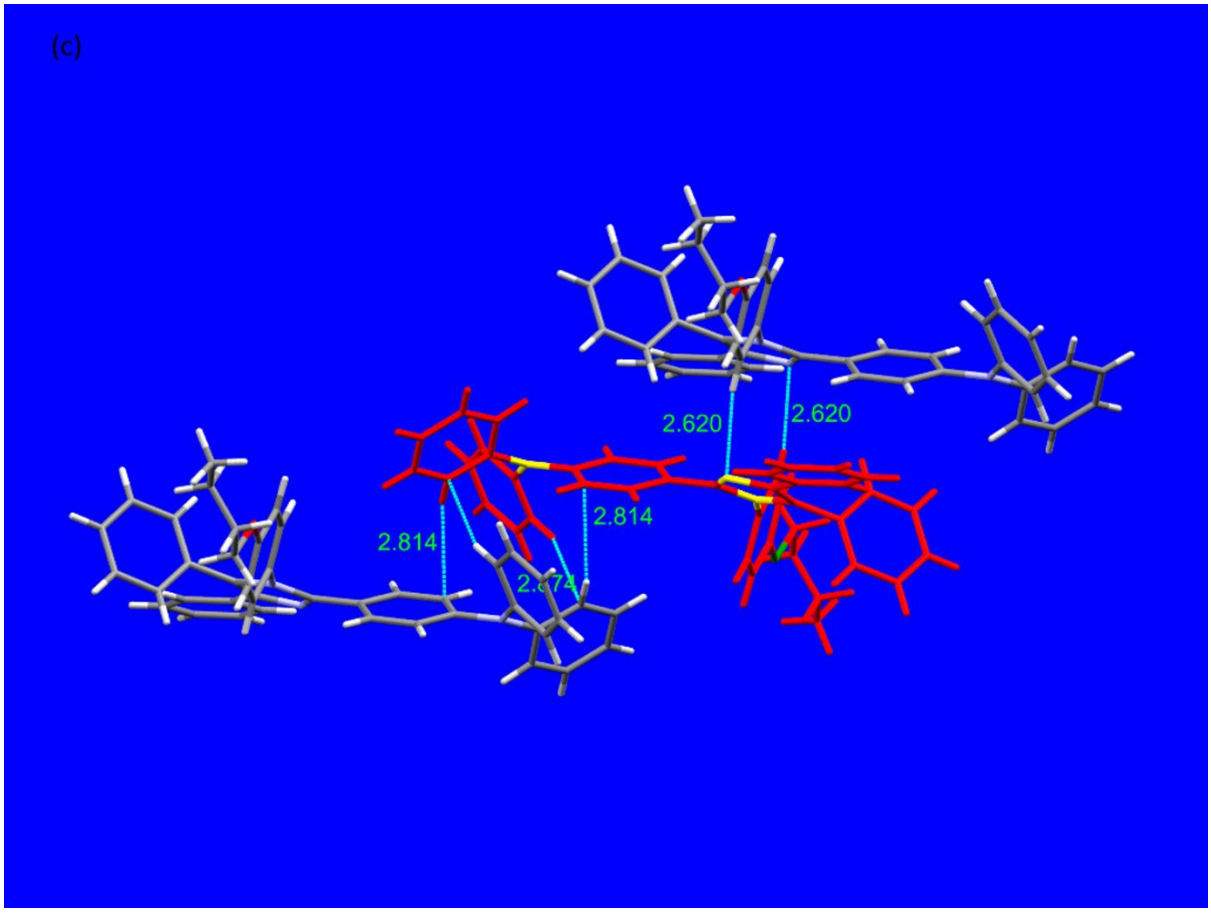

Figure S21. Existed short range interactions of **DT313** with the neighbouring molecules.

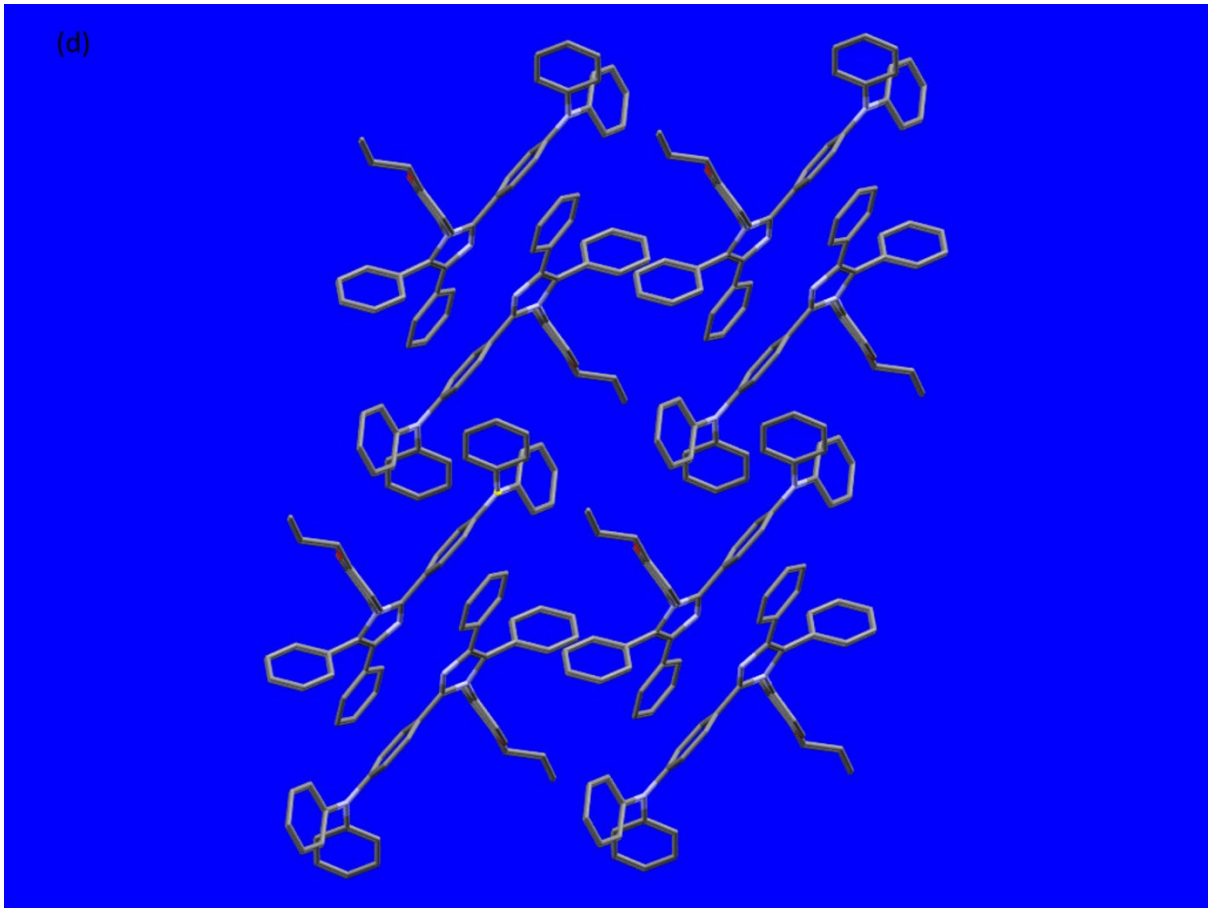

Figure S22. Crystal Packing diagram of **DT313**.

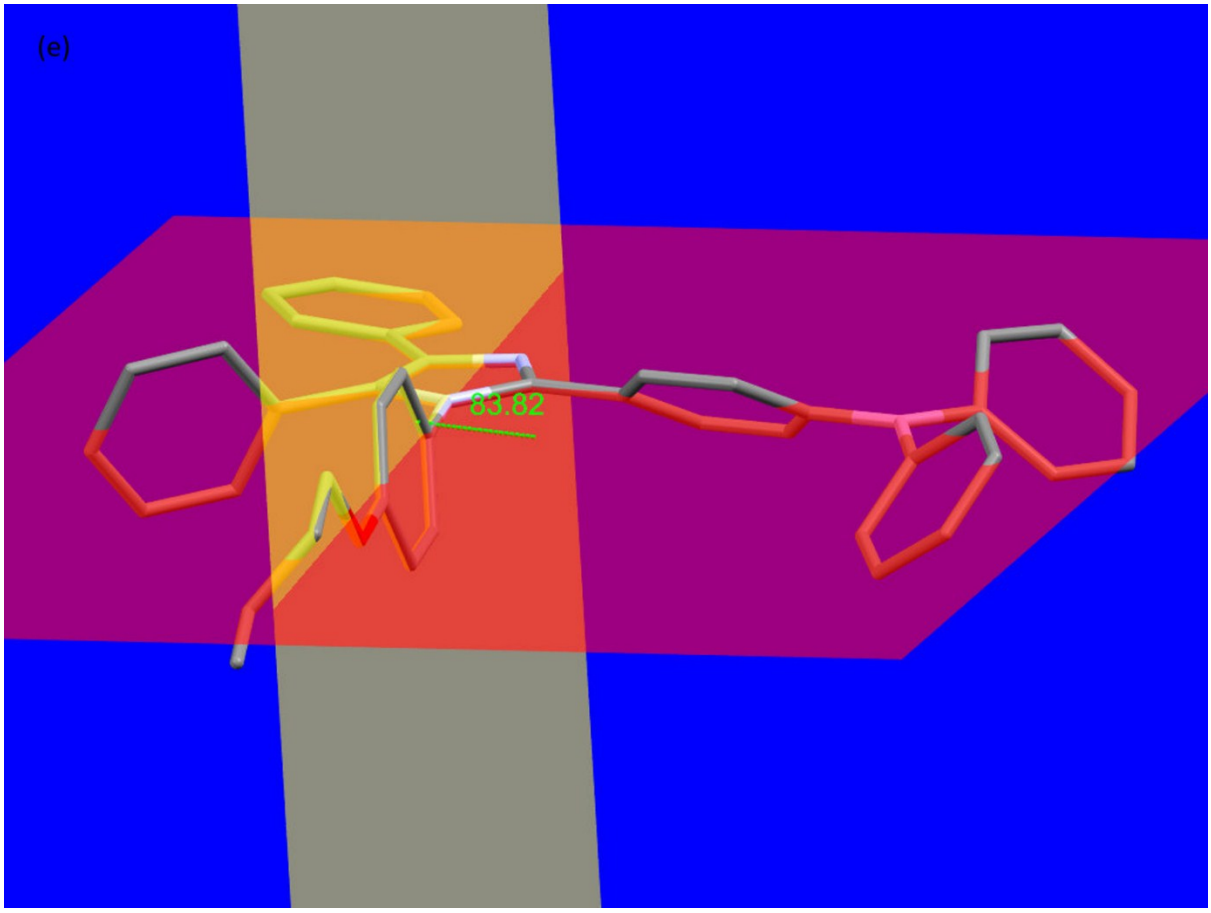

Figure S23. Angle between imidazole ring alkoxy substituted phenyl ring diagram of **DT313**.

Electroluminiscence Data

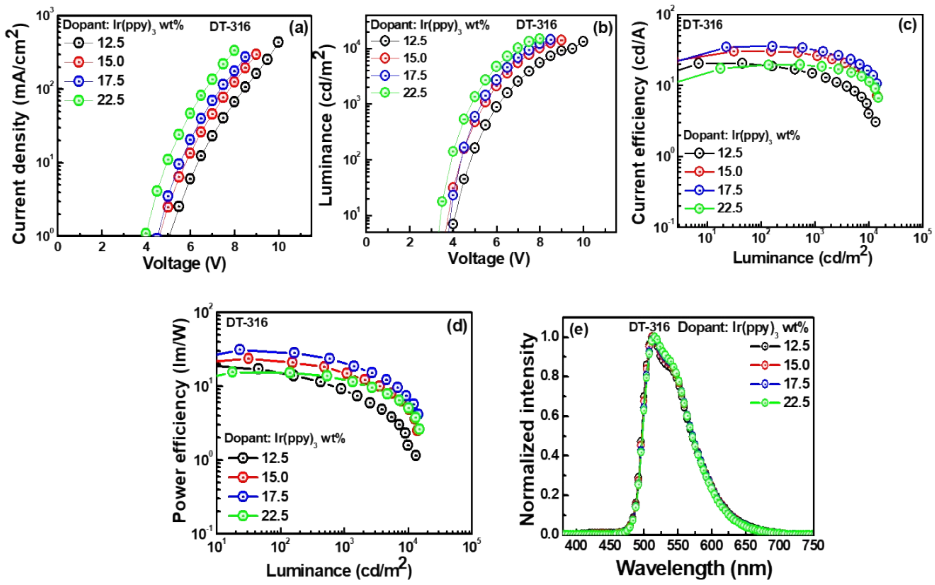

Figure S24. Electroluminscent properties of solution-processed green phosphorescent OLED consisting of $Ir(ppy)_3$ and **DT-316** as a guest and host, respectively.

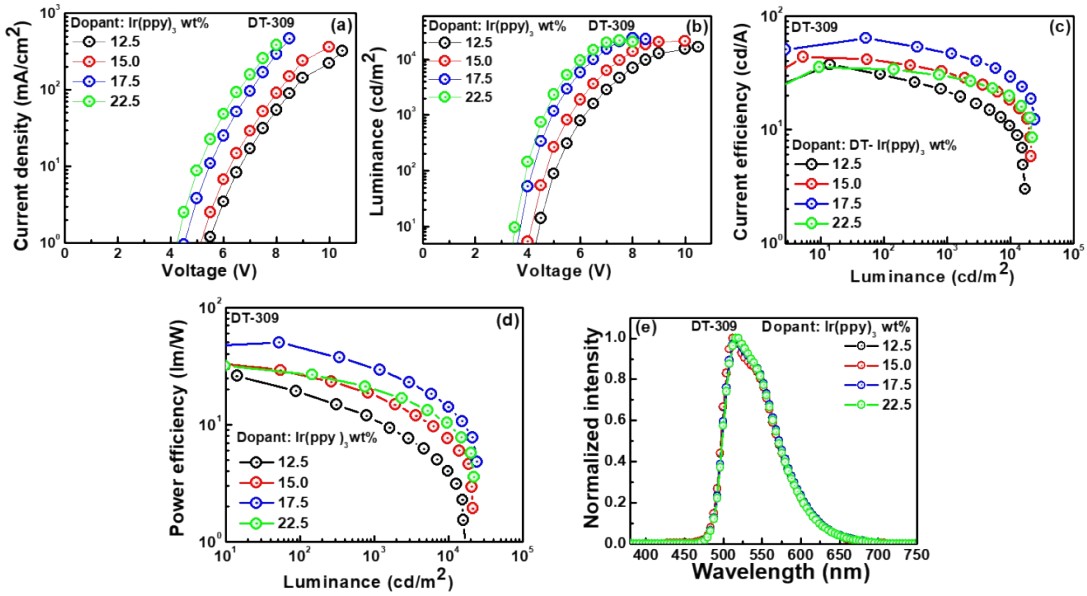

Figure S25. Electroluminscent properties of solution-processed green phosphorescent OLED consisting of $Ir(ppy)_3$ and **DT-309** as a guest and host, respectively.

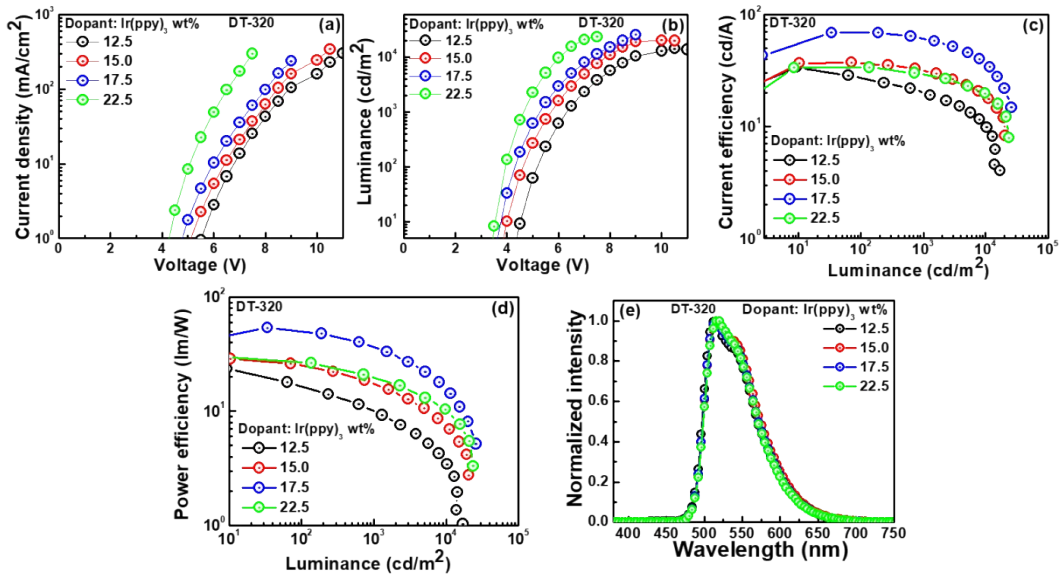

Figure S26. Electroluminscent properties of solution-processed green phosphorescent OLED consisting of Ir(ppy)$_3$ and **DT-320** as a guest and host, respectively.

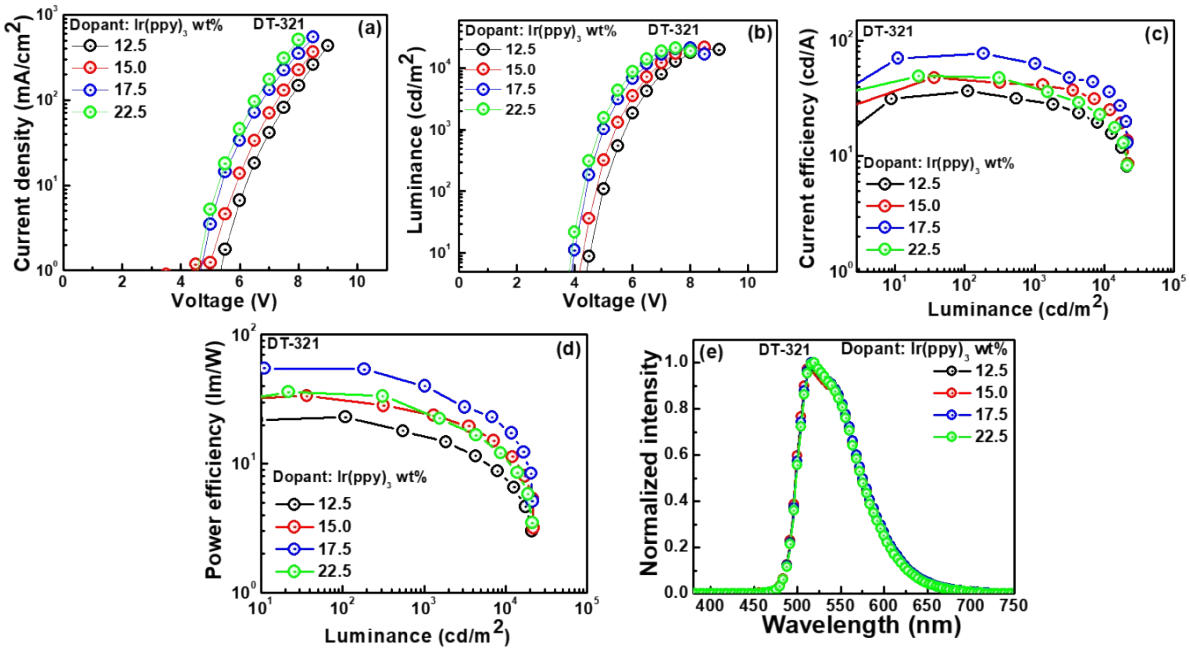

Figure S27. Electroluminscent properties of solution-processed green phosphorescent OLED consisting of Ir(ppy)$_3$ and **DT-321** as a guest and host, respectively.

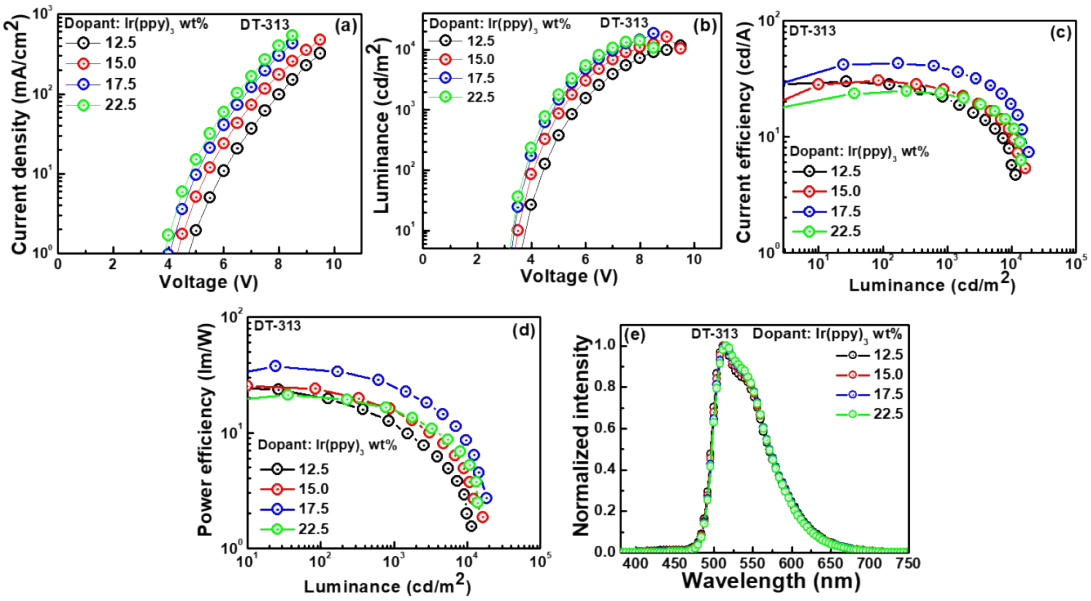

Figure S28. Electroluminscent properties of solution-processed green phosphorescent OLED consisting of $Ir(ppy)_3$and **DT-313** as a guest and host, respectively.

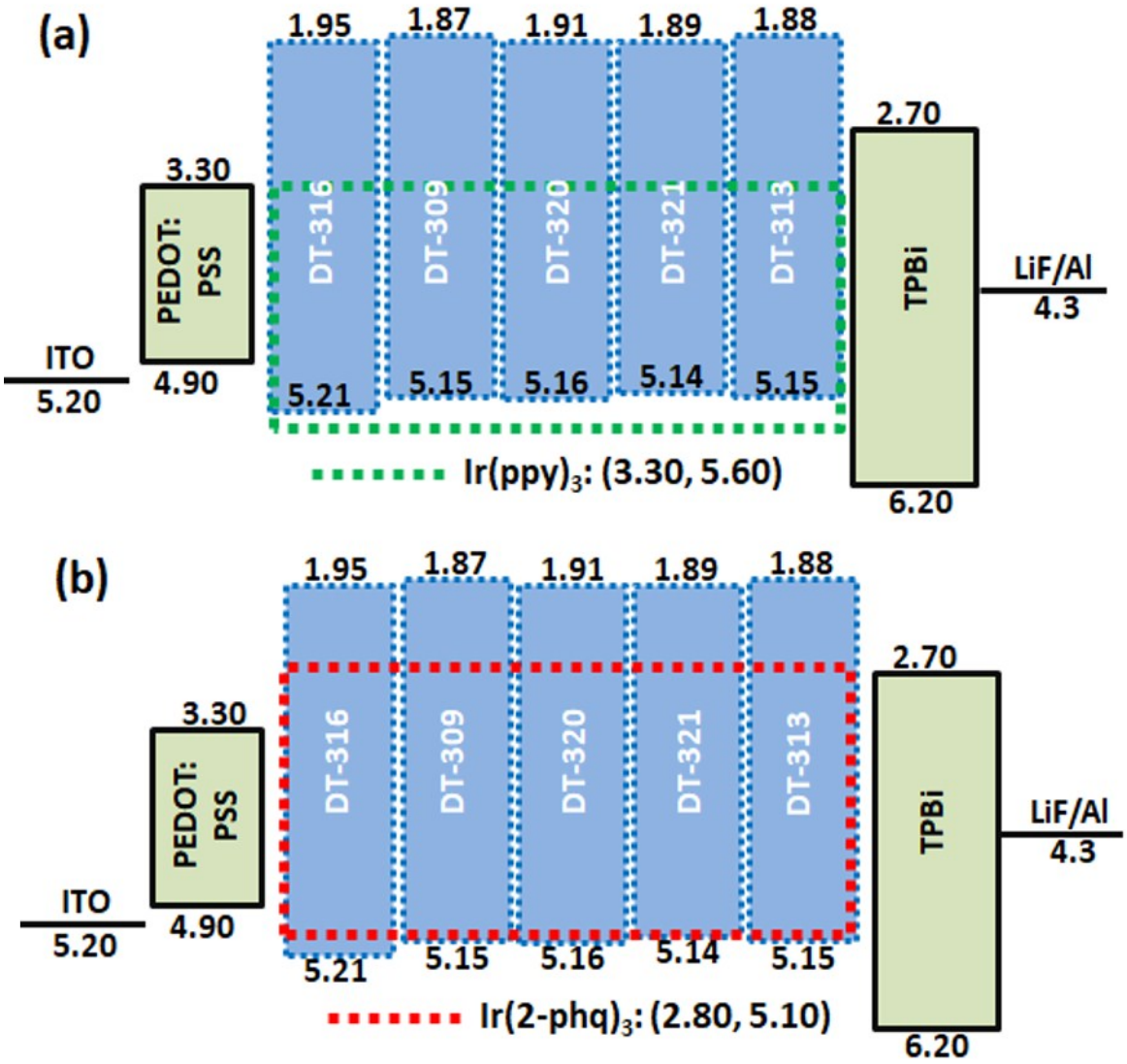

Figure S29. Schematic diagram of the energy levels of the (a) green and (b) red phosphorescent OLED devices containing the spin-coated films of five different newly synthesized host materials, namely, **DT316**, **DT309**, **DT320**, **DT321**, and **DT313**.

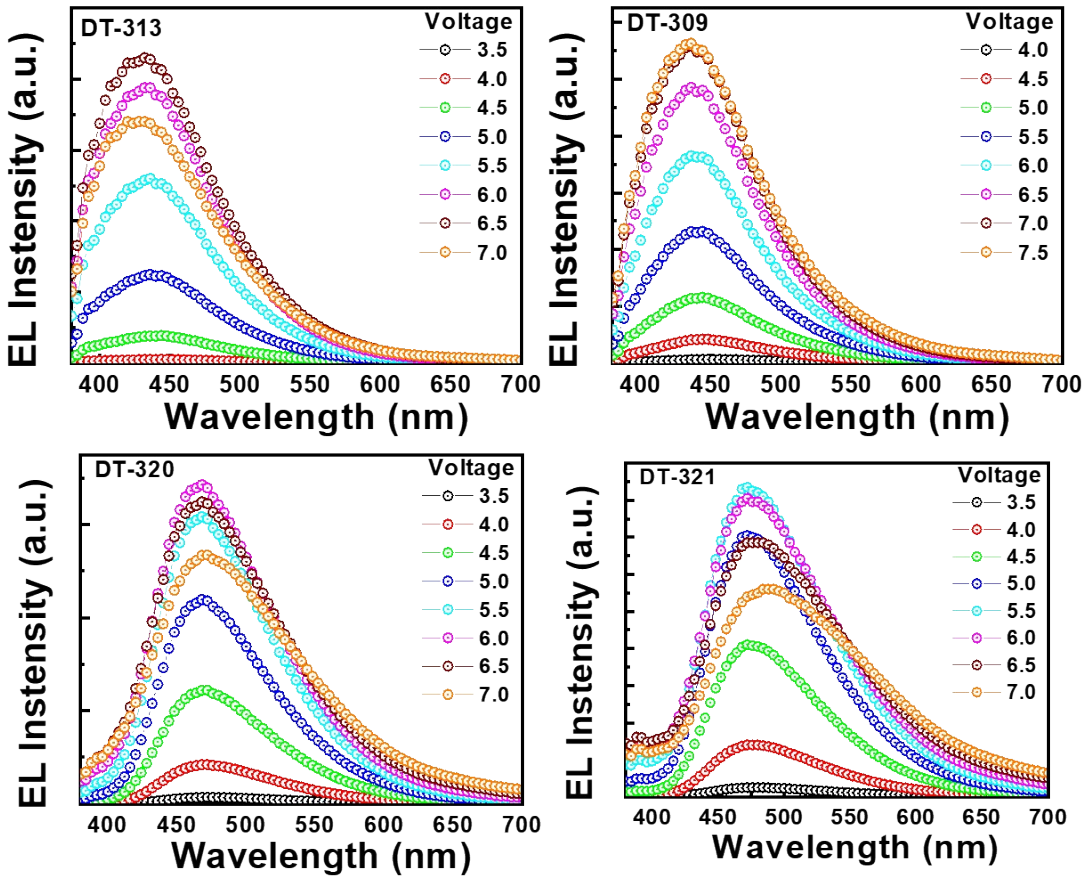

Figure S30. EL spectra of **DT309, DT320, DT321,** and **DT316** at different voltages.

Theoretical Analysis

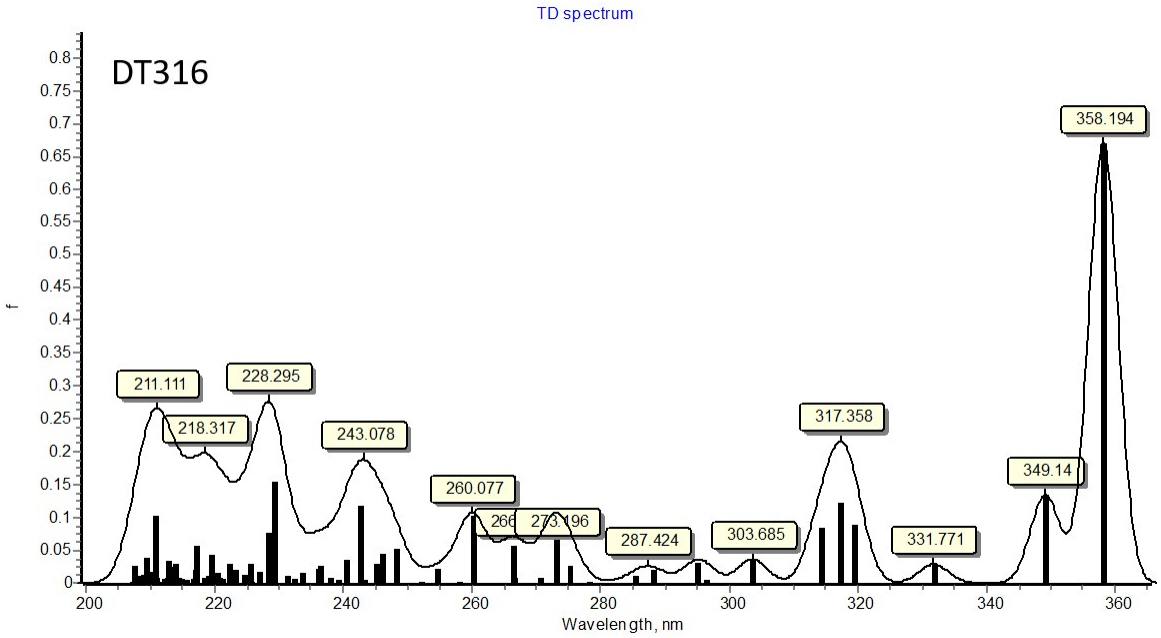

Figure S31. TD-DFT calculated UV-vis transitions profile for compound **DT316.**

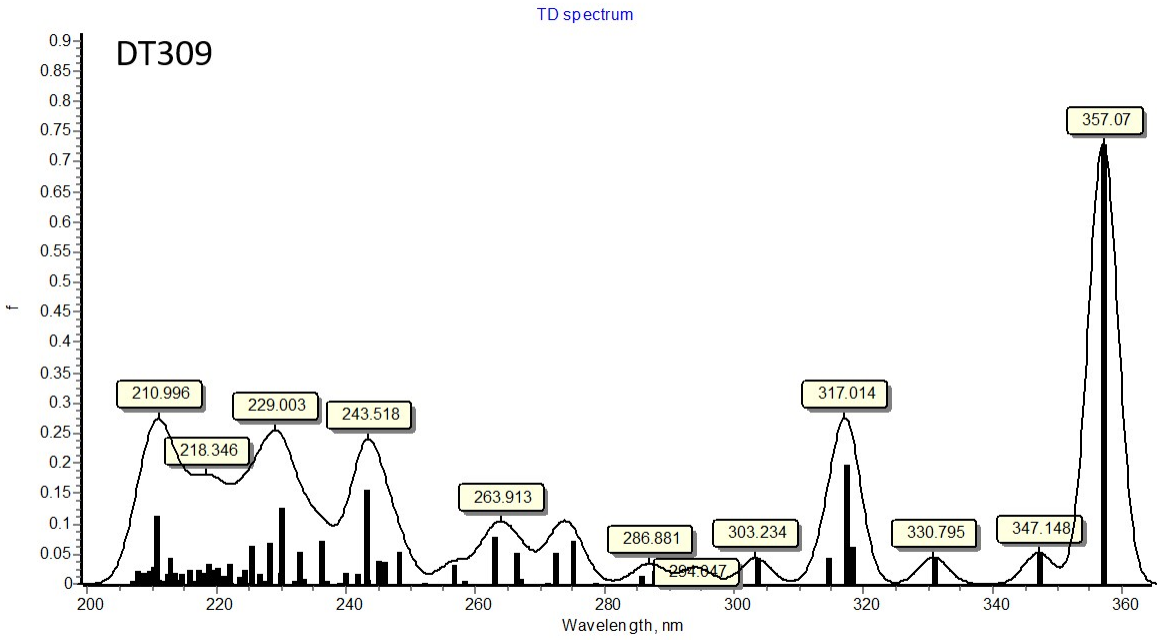

Figure S32. TD-DFT calculated UV-vis transitions profile for compound **DT309.**

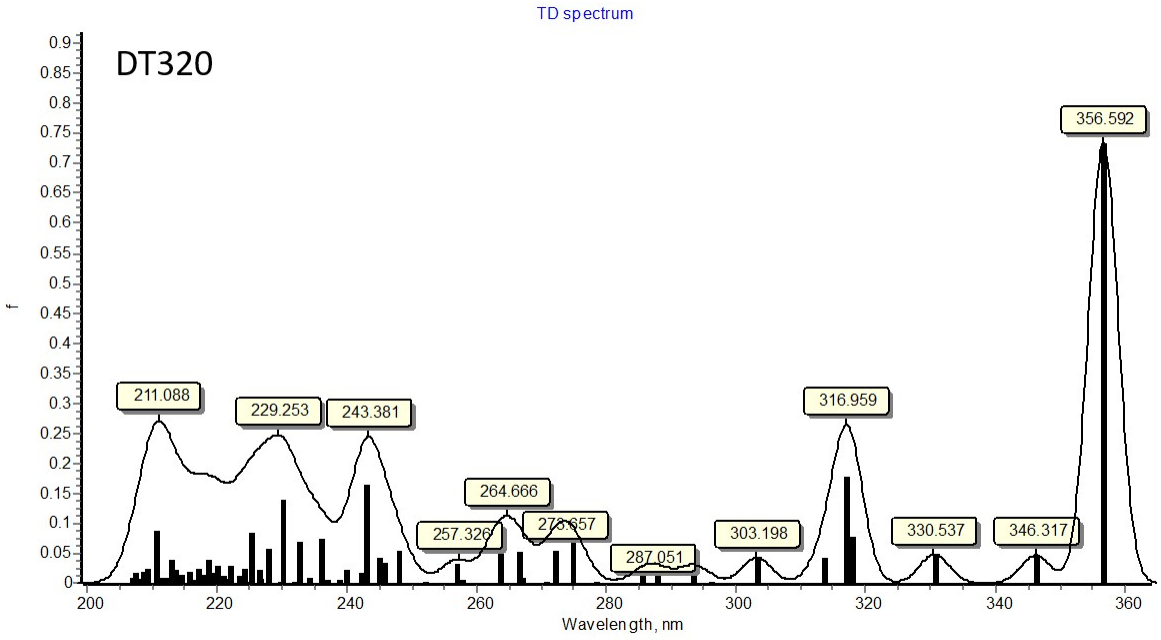

Figure S33. TD-DFT calculated UV-vis transitions profile for compound **DT320.**

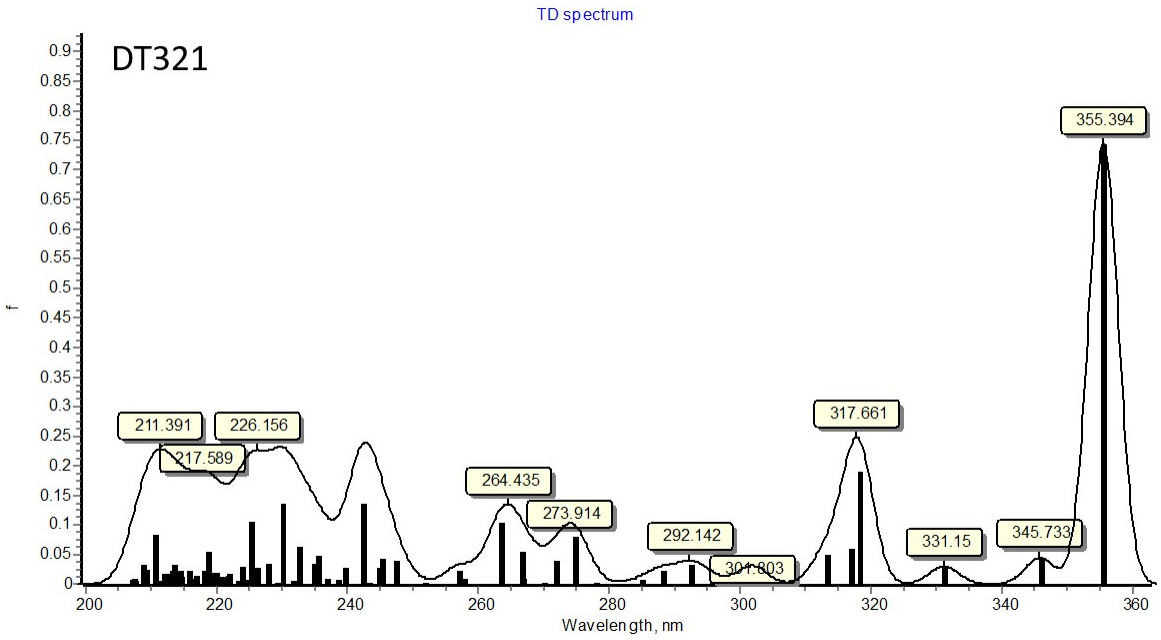

Figure S34. TD-DFT calculated UV-vis transitions profile for compound **DT321.**

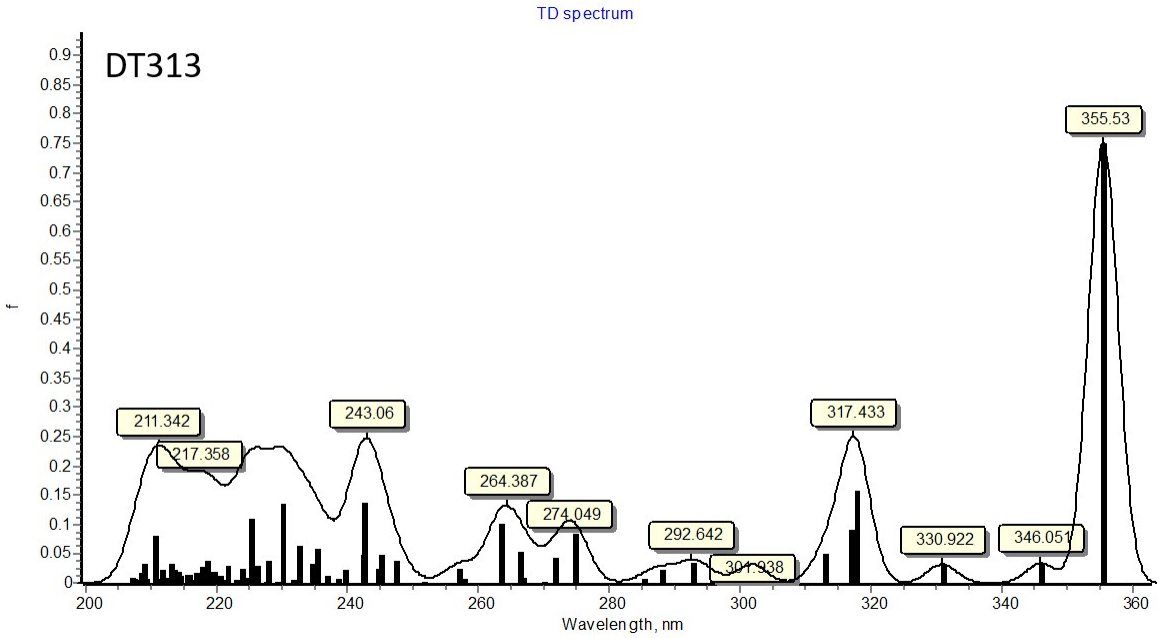

Figure S35. TD-DFT calculated UV-vis transitions profile for compound **DT313.**

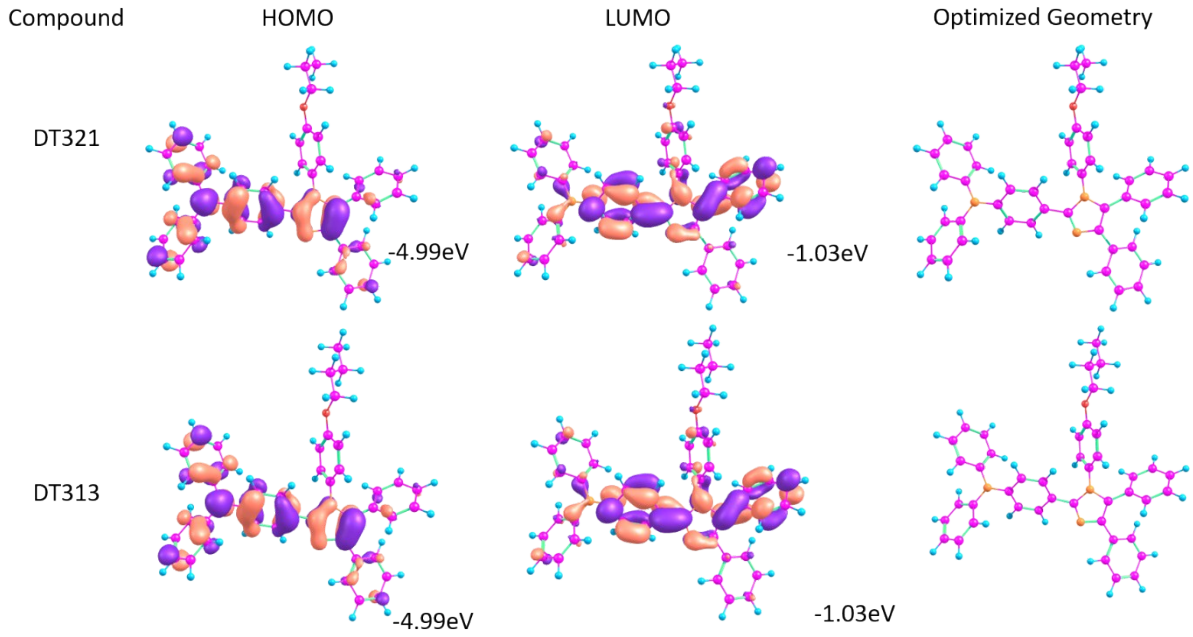

Figure S36. Optimized structures and HOMO LUMO distributions for **DT321** and **DT313.**

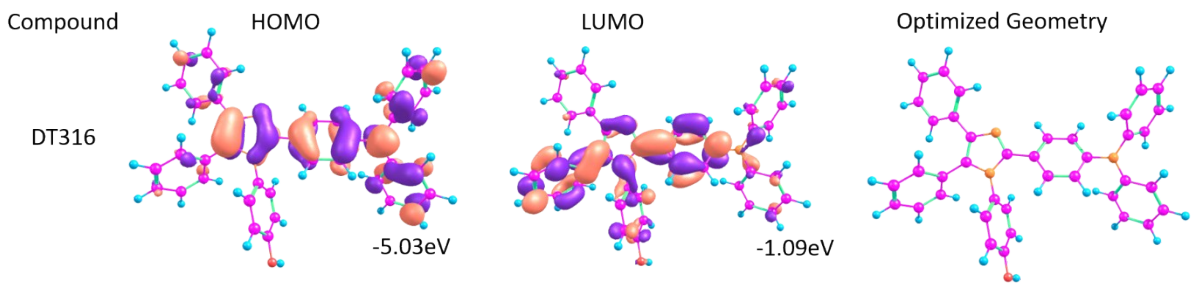

Figure S37. Optimized structures and HOMO LUMO distributions for **DT316**.

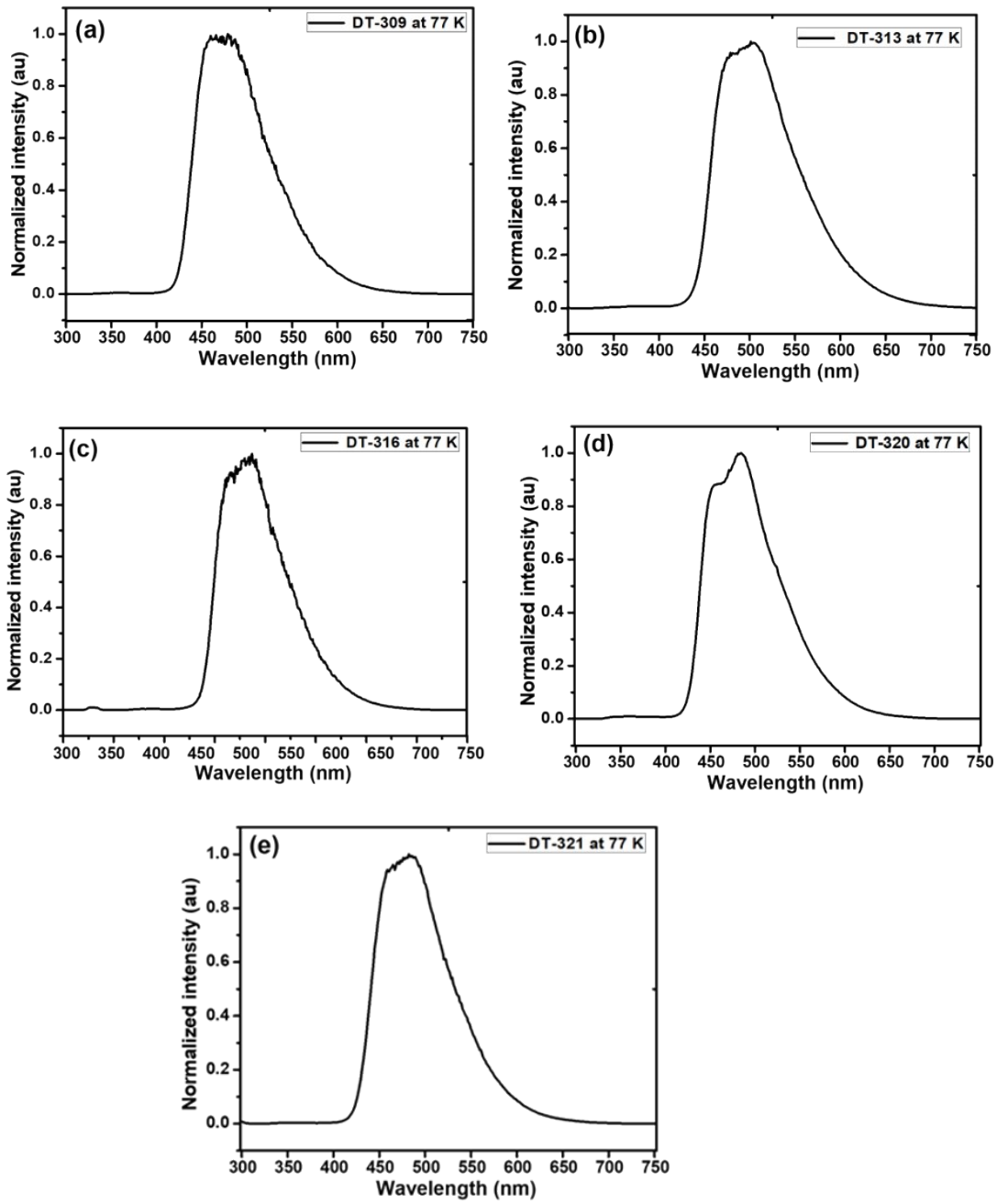

Figure S38. Normalized phosphorescence spectra of the compounds (a) **DT-309**, (b) **DT-313**, (c) **DT-320**, (d) **DT-316** and (e) **DT-321** RP-BP were recorded in THF solvent at 77K. The excitation wavelength was 335 nm for phosphorescence spectra.

NMR Spectra

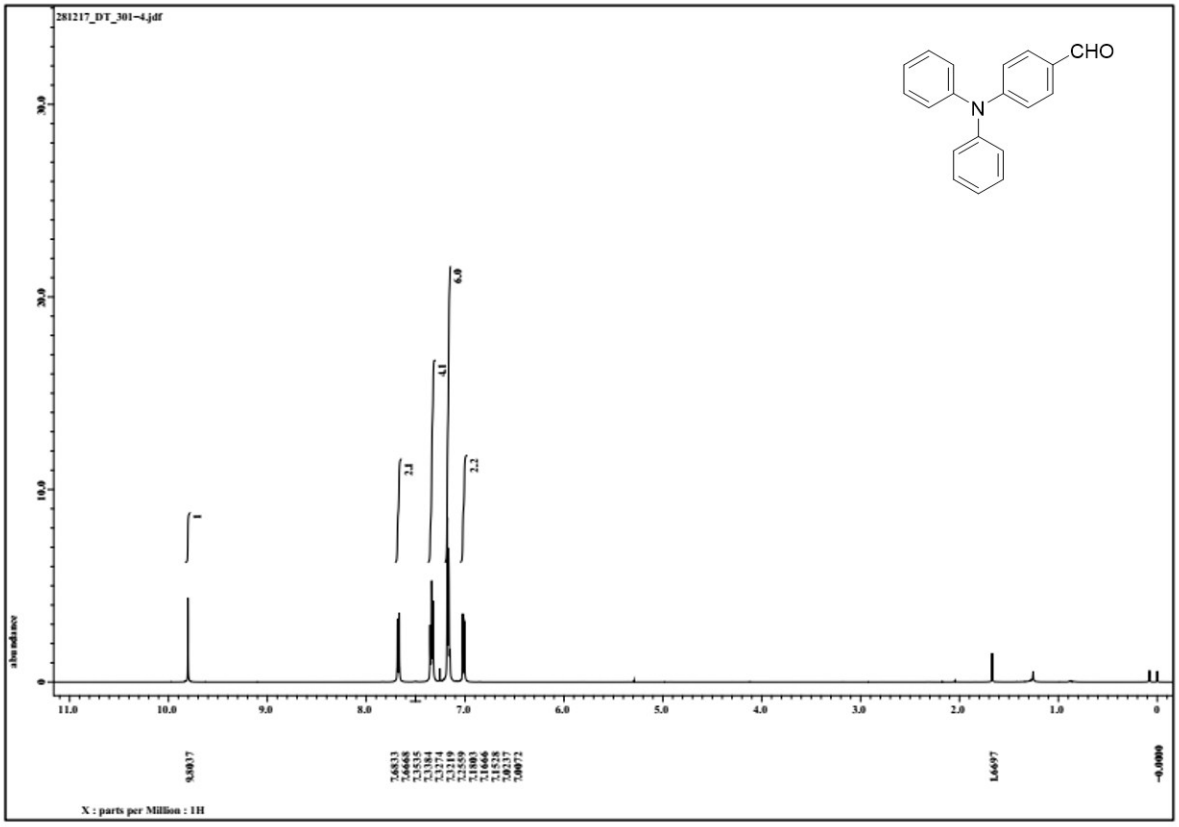

Figure S39. ^{1}H-NMR of **DT301.**

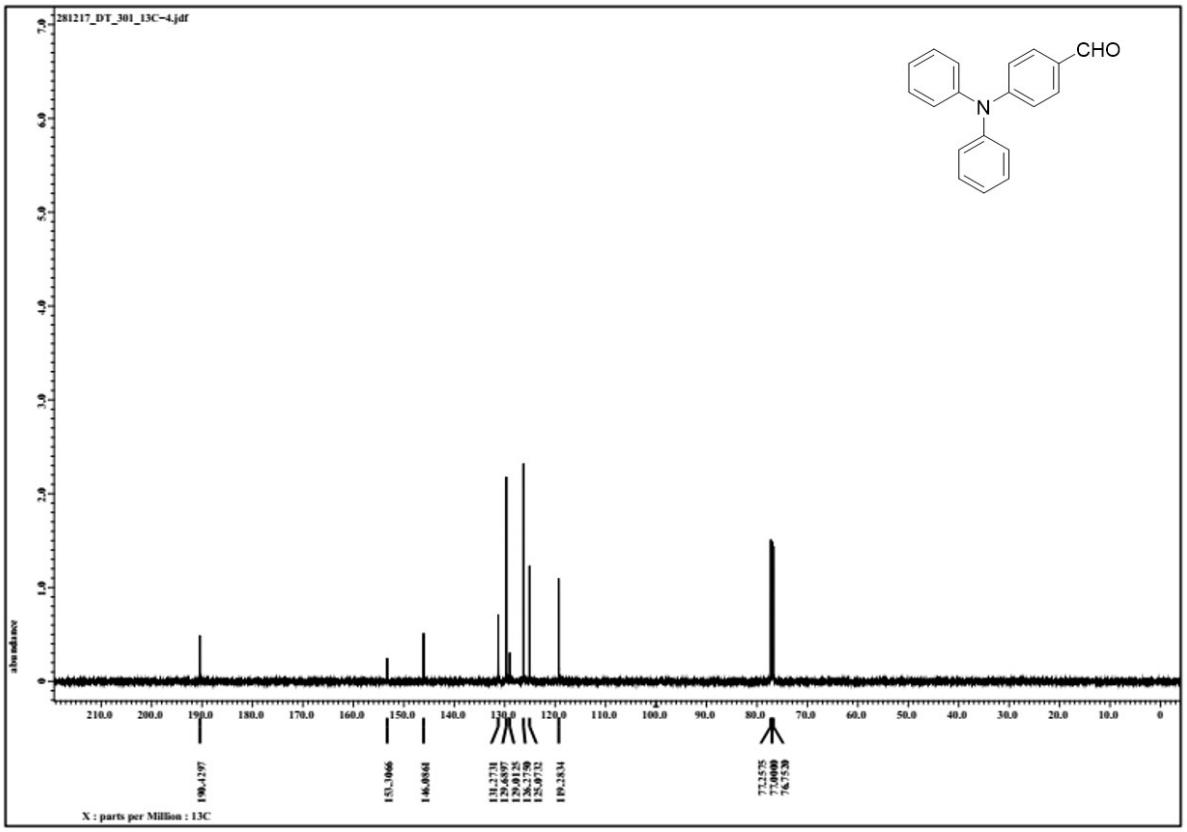

Figure S40. ^{13}C-NMR of **DT301.**

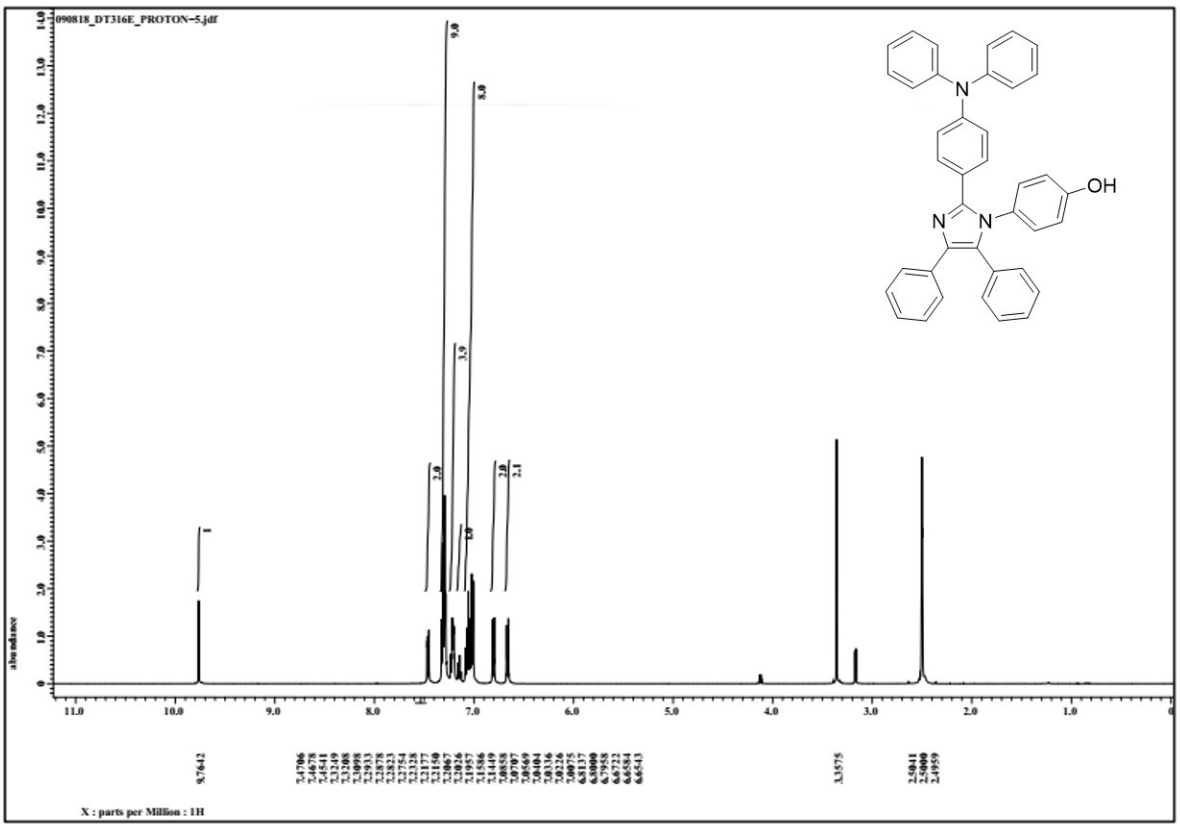

Figure S41. ^{1}H-NMR of **DT316.**

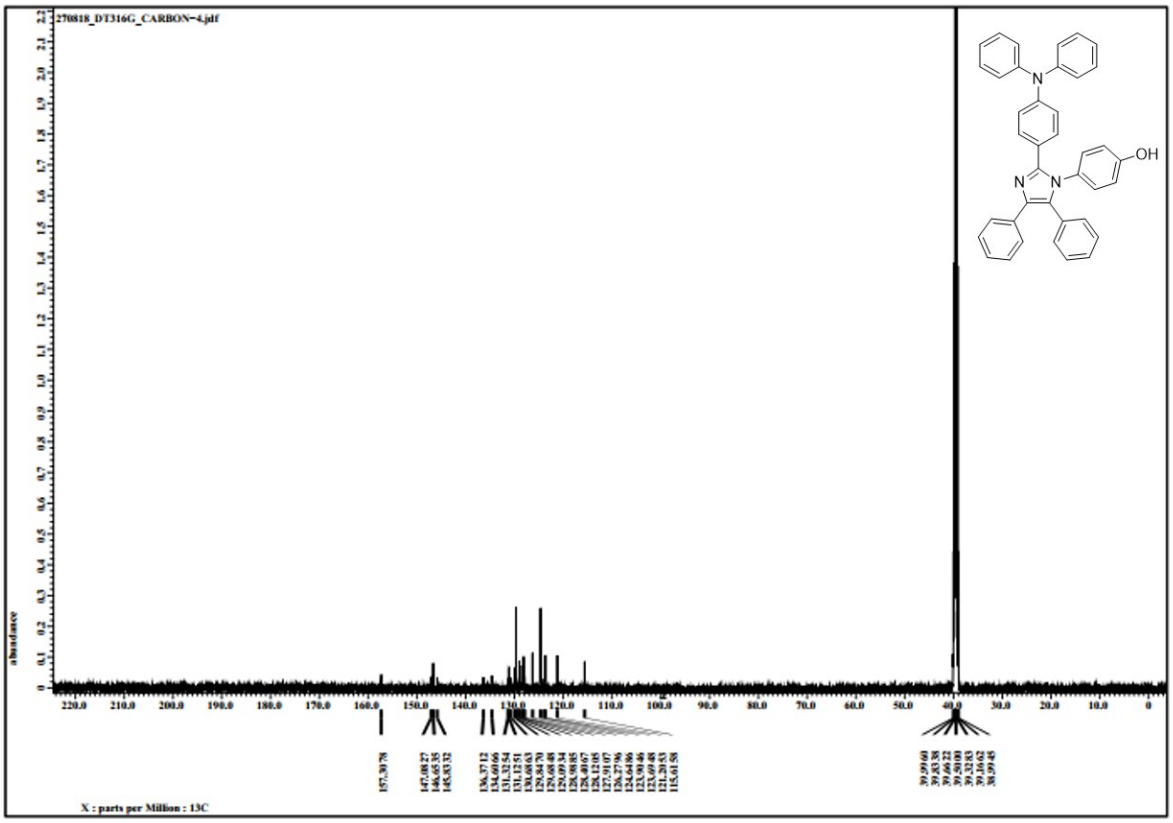

Figure S42. ^{13}C-NMR of **DT316.**

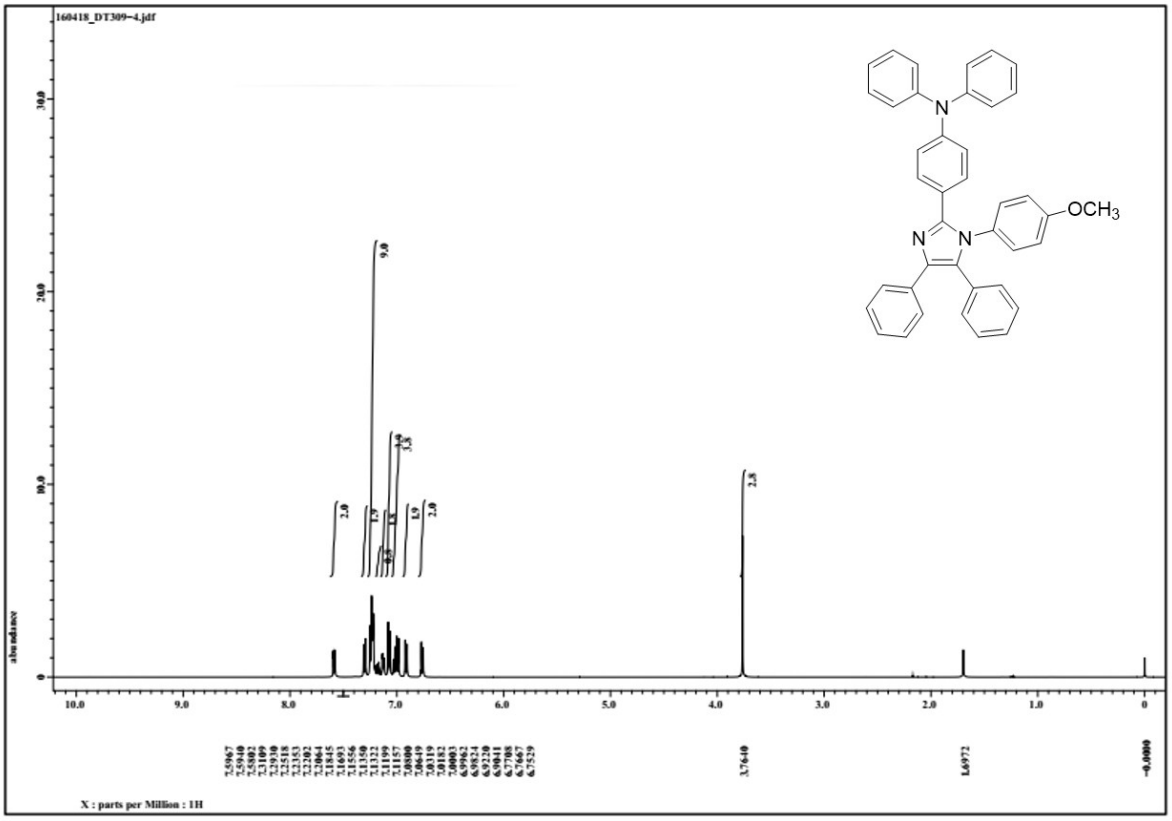

Figure S43. ^{1}H-NMR of **DT309.**

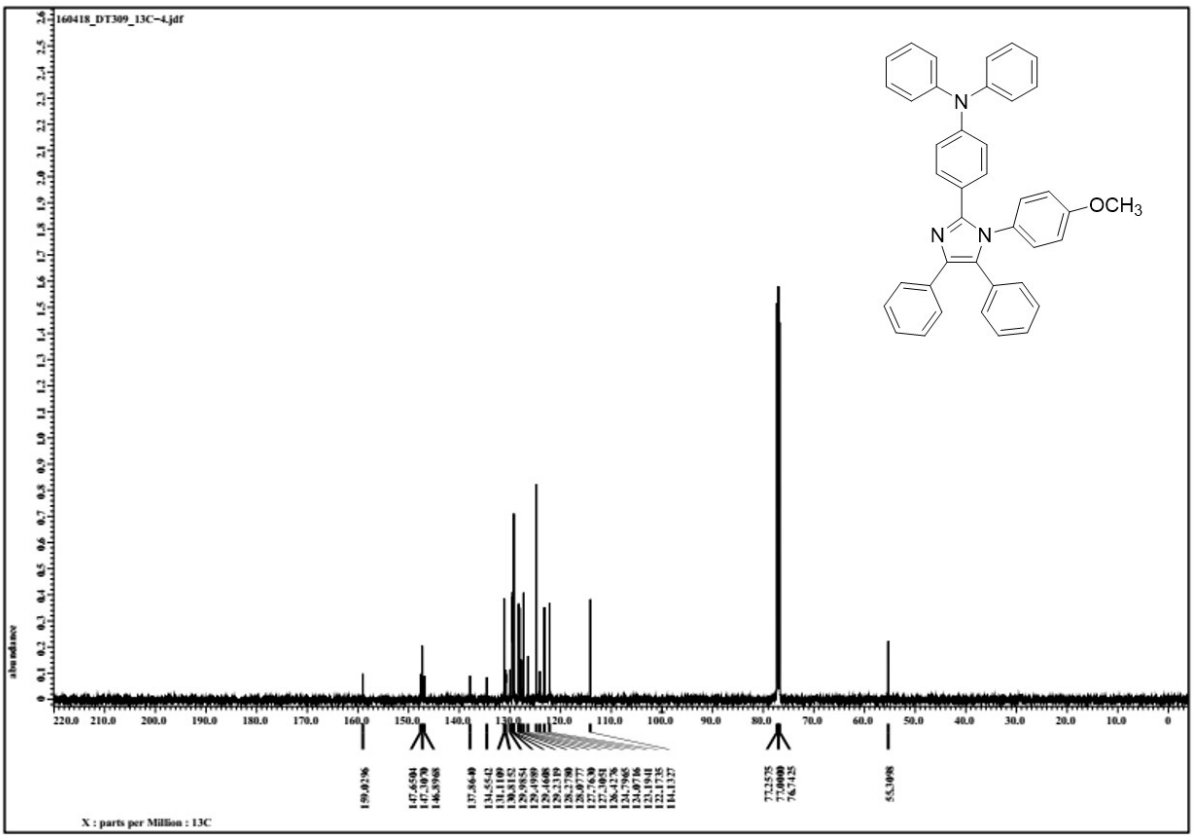

Figure S44. ^{13}C-NMR of **DT309.**

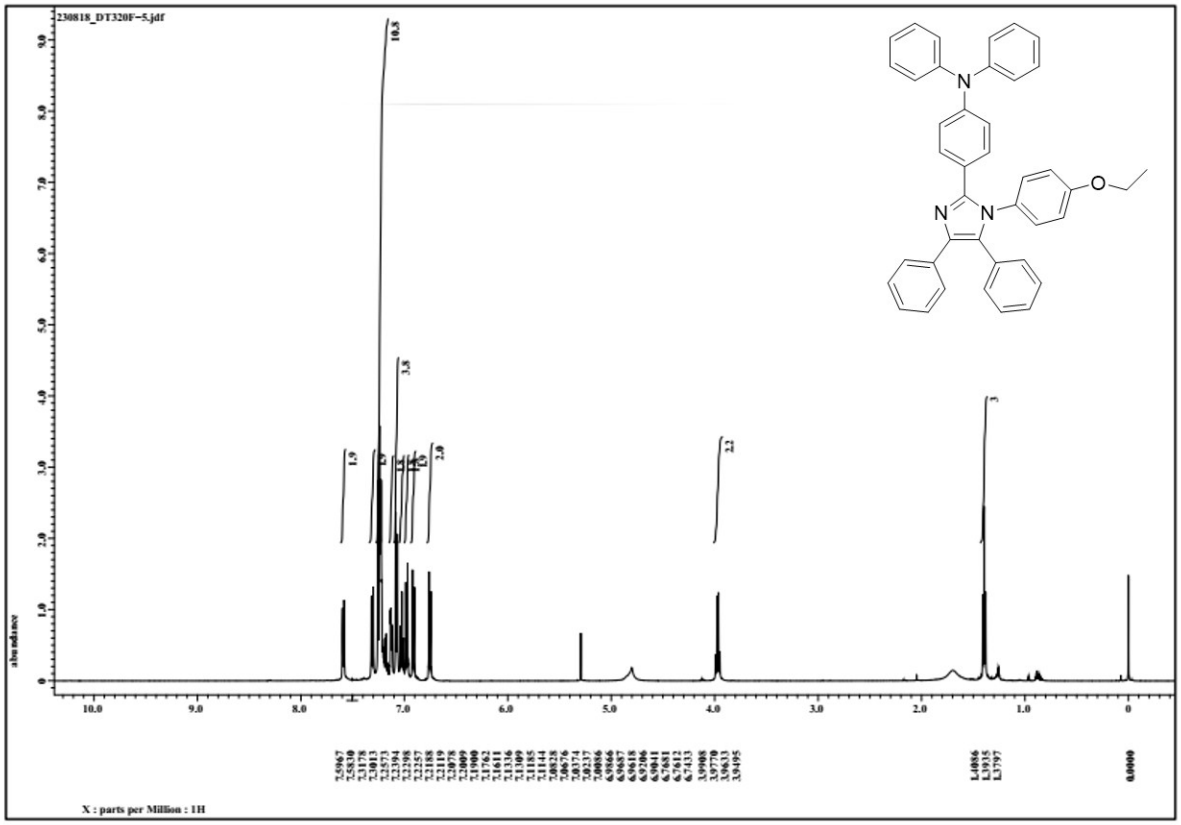

Figure S45. ^{1}H-NMR of **DT320.**

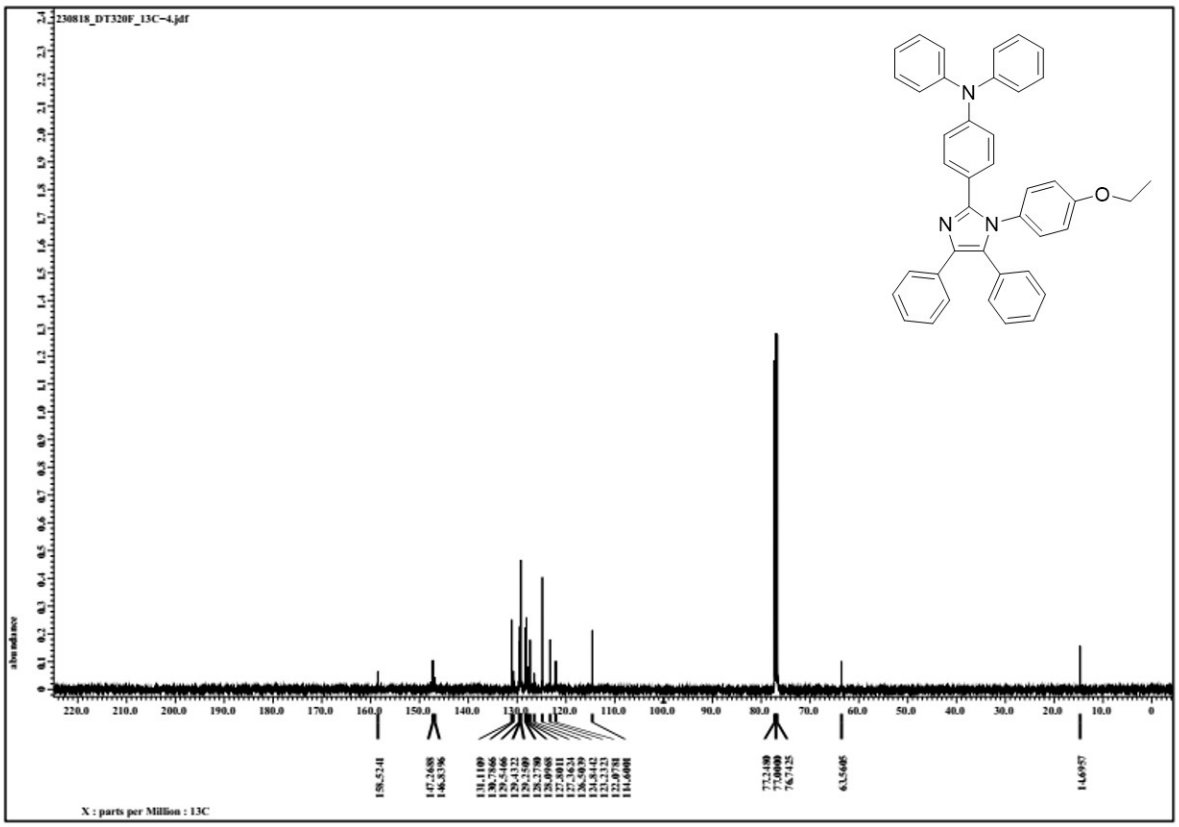

Figure S46. ^{13}C-NMR of **DT320.**

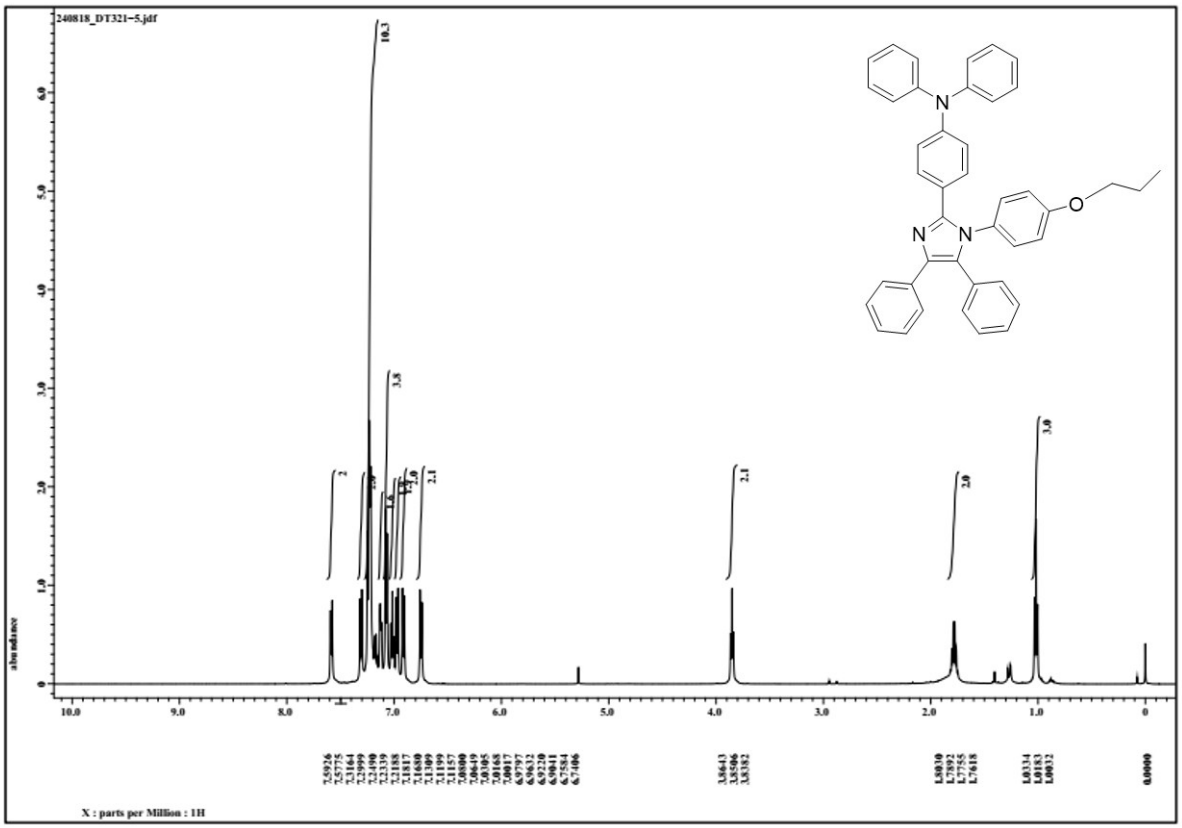

Figure S47.^{1}H-NMR of **DT321.**

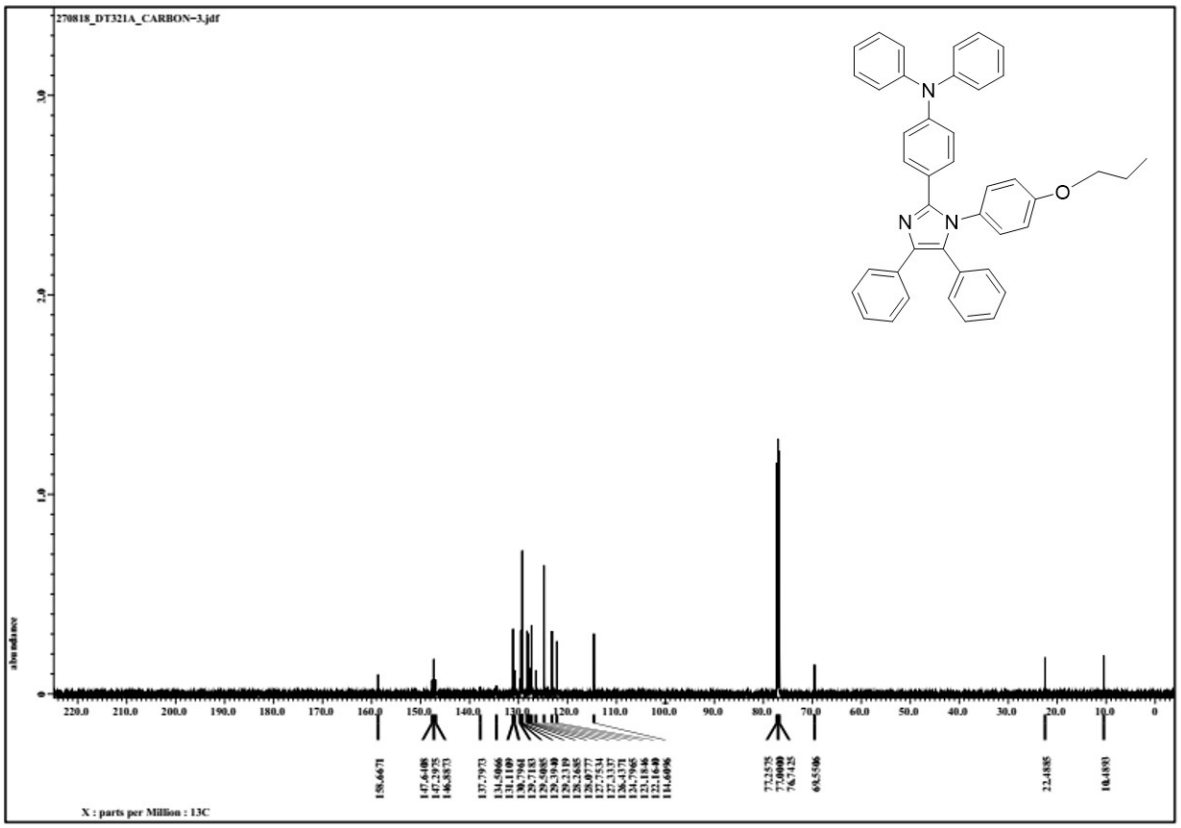

Figure S48. ^{13}C-NMR of **DT321.**

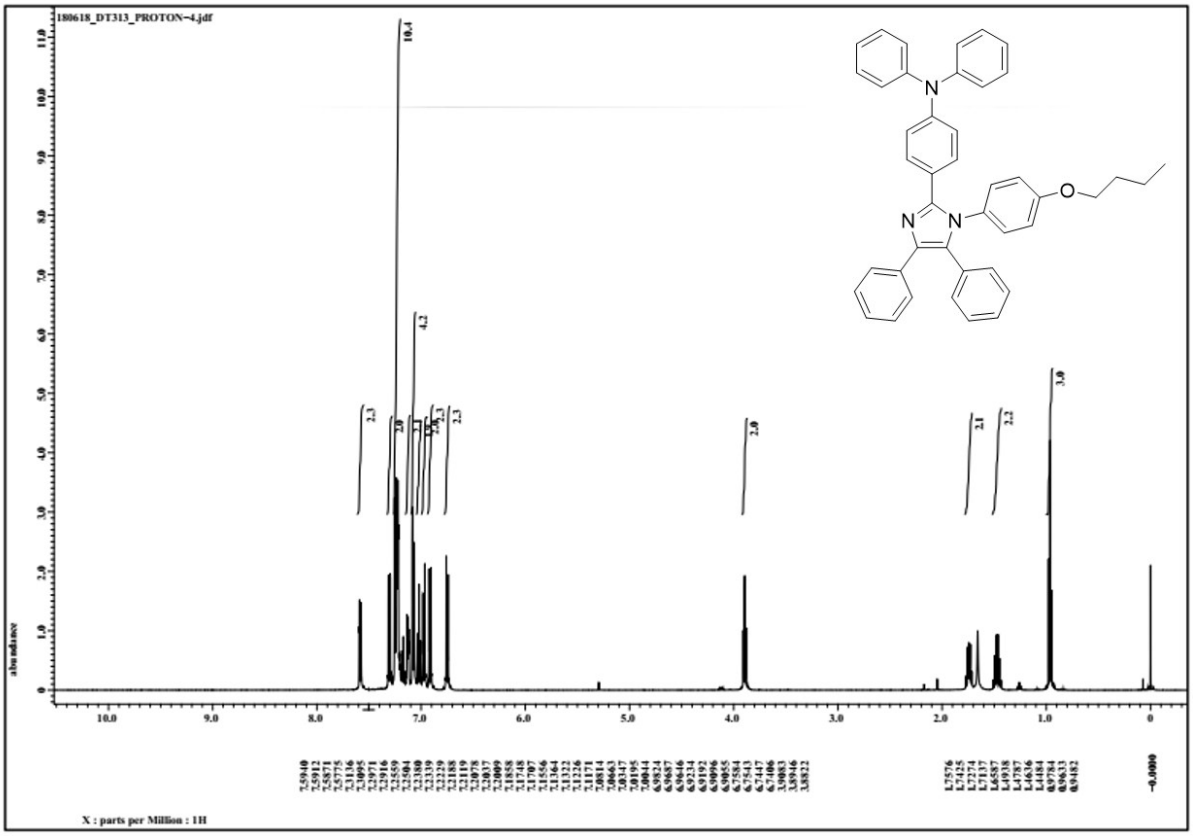

Figure S49.^{1}H-NMR of **DT313.**

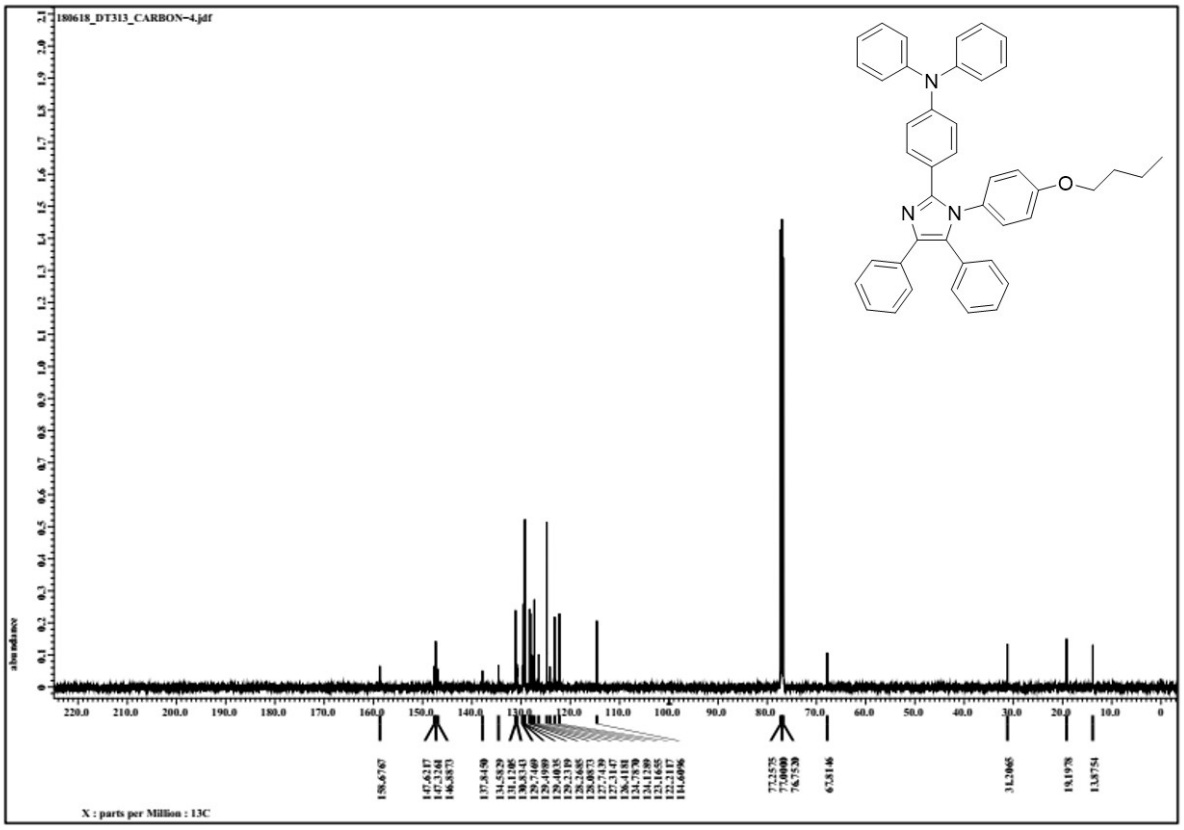

Figure S50. ^{13}C-NMR of **DT313.**

Mass Spectra

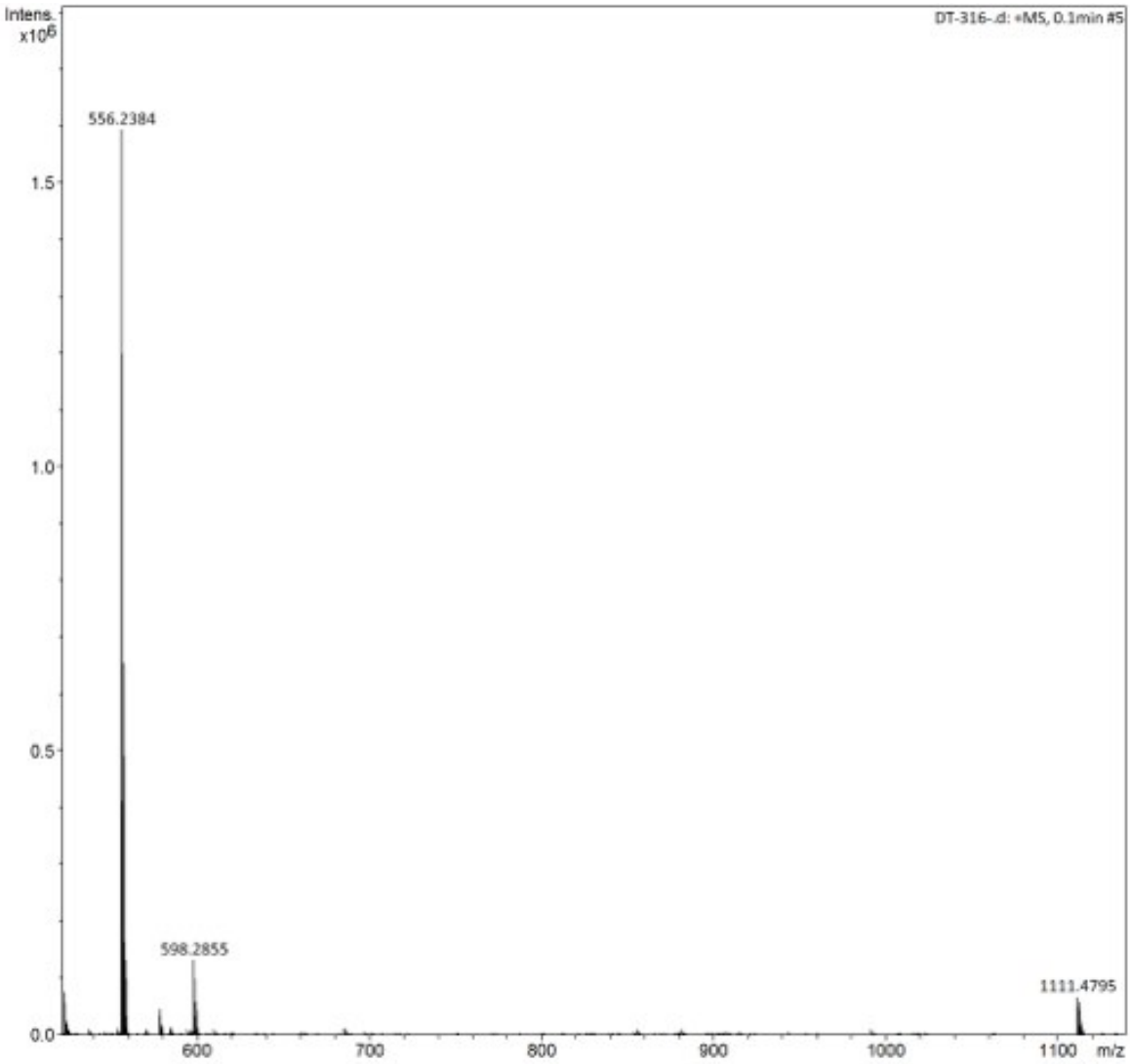

Figure S51. Mass Spectra of **DT316.**

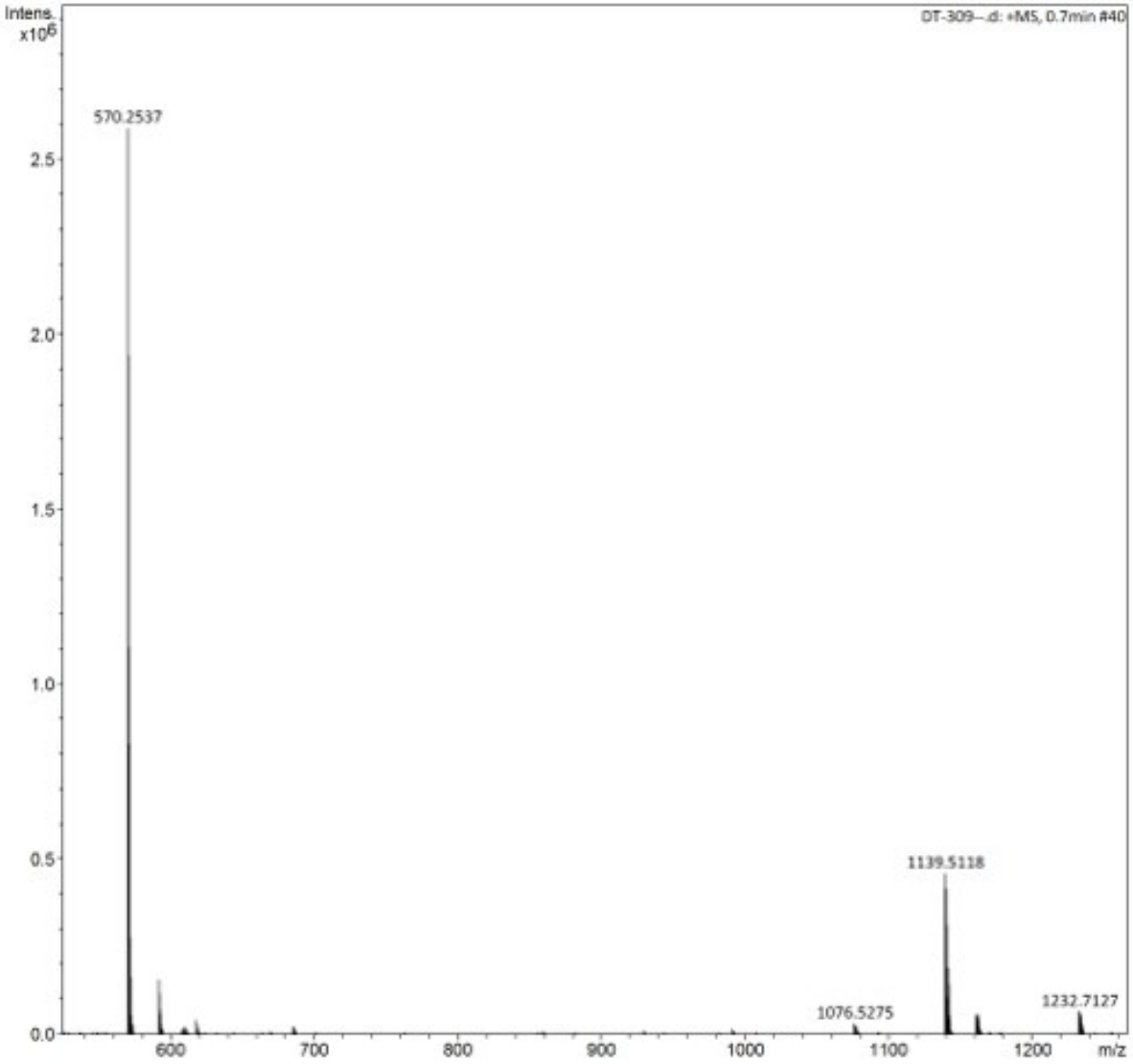

Figure S52. Mass Spectra of **DT309.**

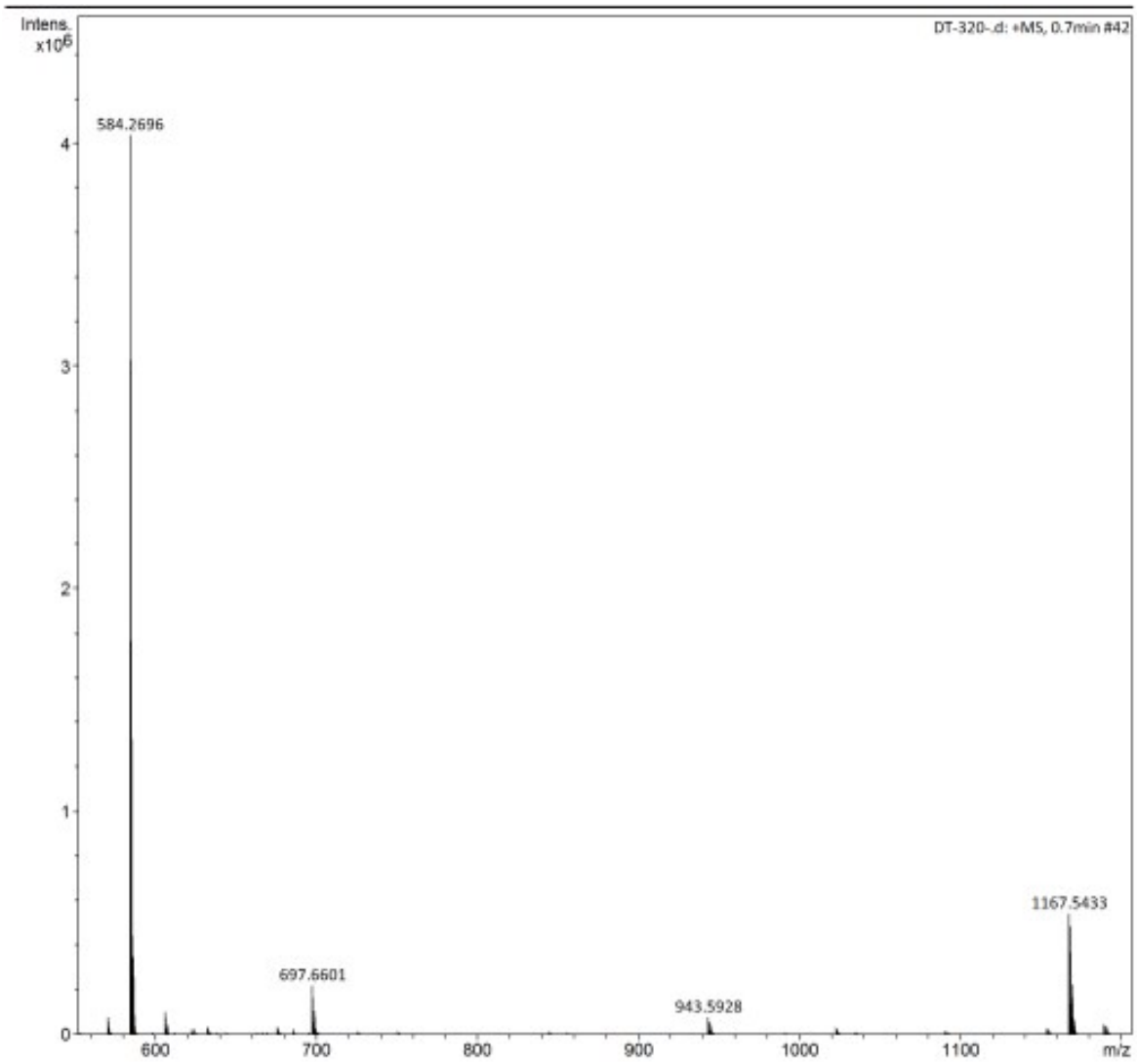

Figure S53. Mass Spectra of **DT320.**

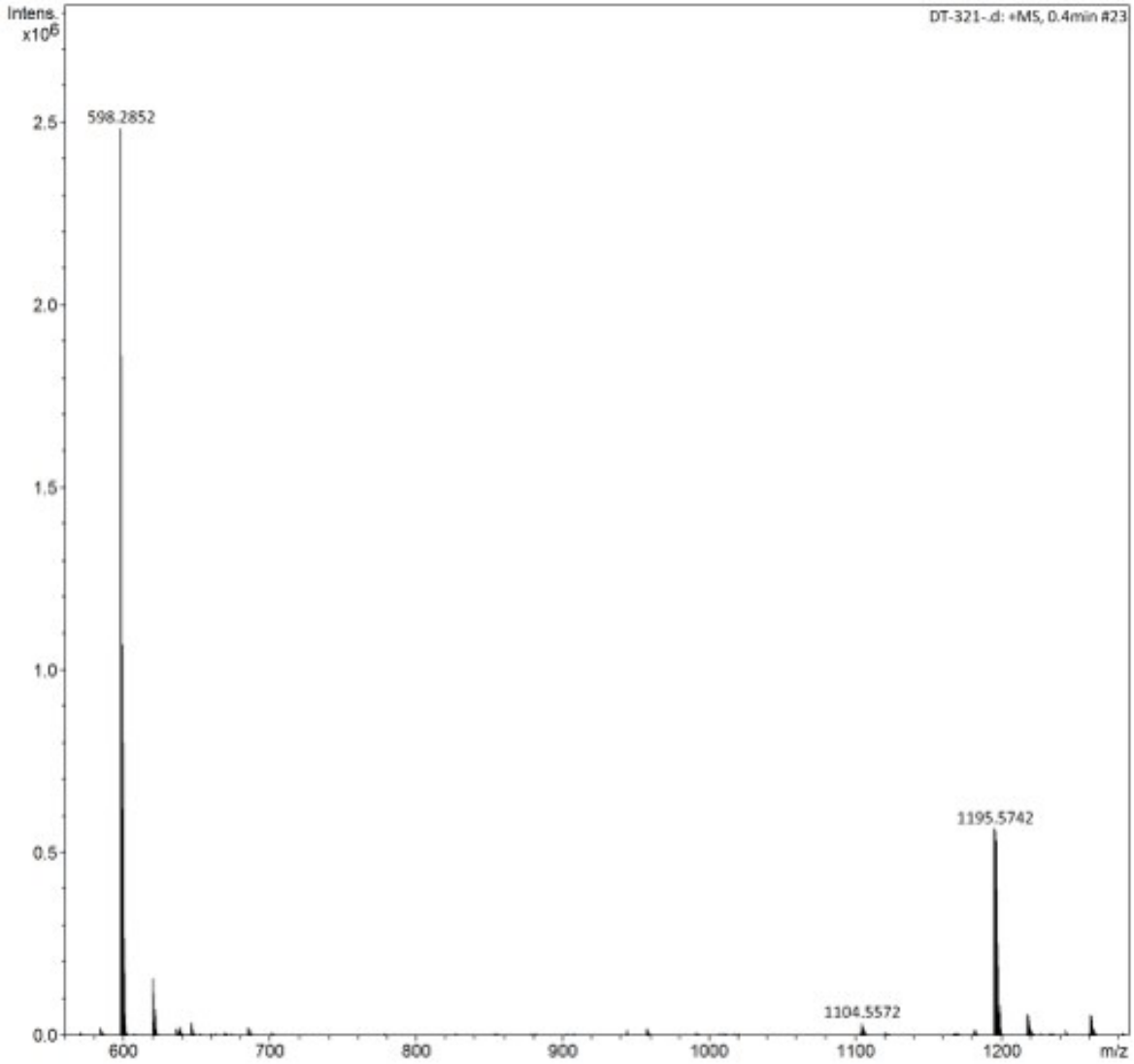

Figure S54. Mass Spectra of **DT321.**

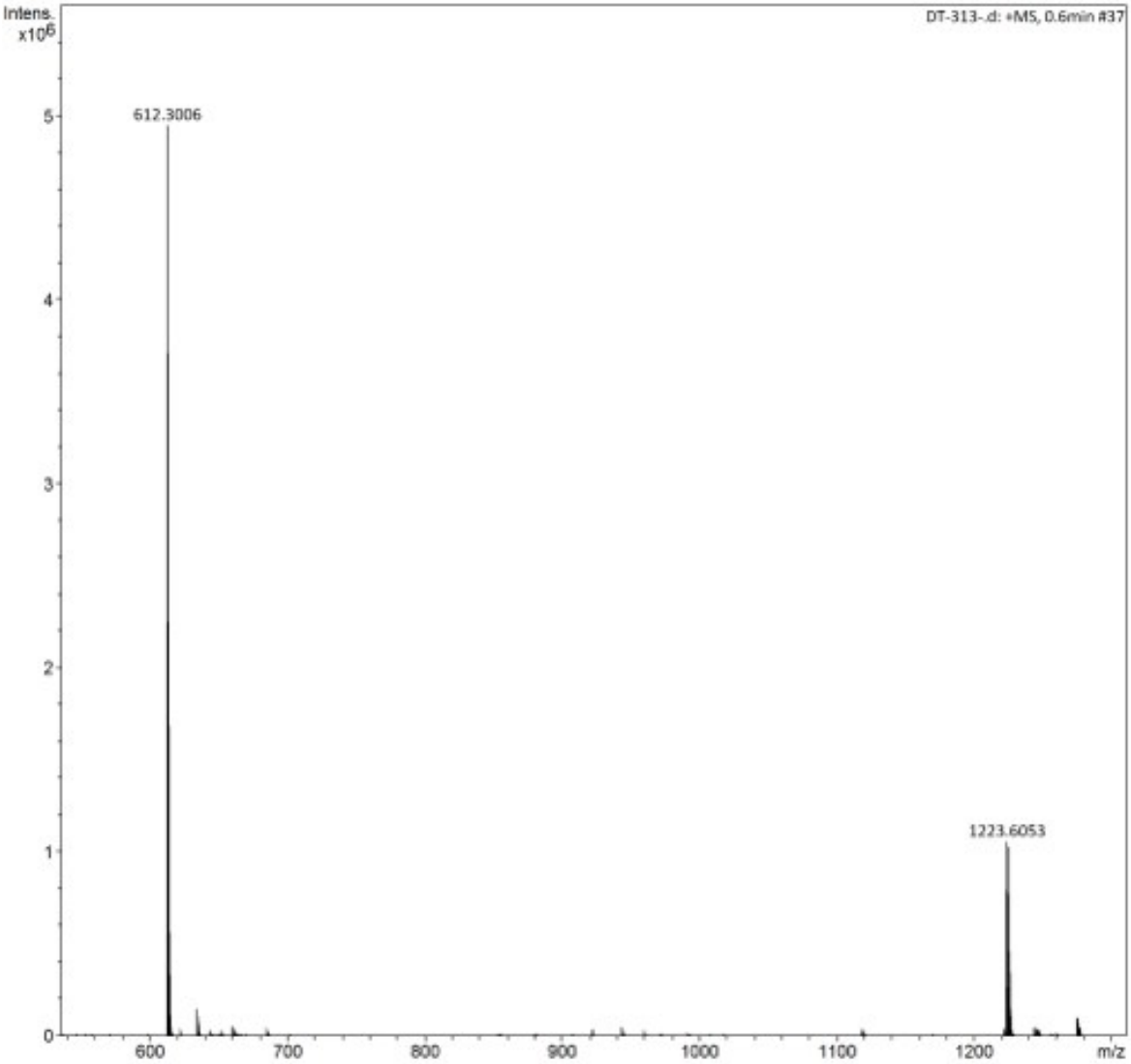

Figure S55. Mass Spectra of **DT313.**

Reference

1. C. Li, W. Yang, W. Zhou, M. Zhang, R. Xue, M. Li and Z. Cheng, *New Journal of Chemistry*, 2016, **40**, 8837-8845.
2. X. Du, S. Tao, Y. Huang, X. Yang, X. Ding and X. Zhang, *Applied Physics Letters*, 2015, **107**, 104_101.
3. T. Tsuboi, H. Murayama and A. Penzkofer, *Thin Solid Films*, 2006, **499**, 306-312.
4. J.-H. Jou, Y.-T. Su, S.-H. Liu, Z.-K. He, S. Sahoo, H.-H. Yu, S.-Z. Chen, C.-W. Wang and J.-R. Lee, *Journal of Materials Chemistry C*, 2016, **4**, 6070-6077.